Functional microfiber nonwoven fabric with adsorption site-immobilized polymer brush for capturing substances in the air

北九州市立大学

国際環境工学部

上江洲研究室

Kim Yung Yoon

(キムヨンユン)

—List of Contents—

Preface

This is a study on the application and method of functionalization via polymer brushes. We tried to adsorb and detect threat substances in the atmosphere using microfiber non-woven fabric with better physical properties than before. This paper presents the applications and possibilities of using polymer brushes.

Acknowledgment

So many people have helped me get to where I am today. I would like to take this opportunity to thank those who have helped.

First of all, I would like to thank Professor Kazuya Uezu of the University of Kitakyushu for his guidance and support for the publication of this thesis. Also, I would like to thank Professor Tomonari Kawano, Professor Takanori Kiahara, and Professor Takumi Sasaki of the University of Kitakyushu for reviewing my thesis, and Professor Muneharu Goto of the National Institute of Technology, Kitakyushu College for giving advice on my thesis.

And, I want to also express my gratitude to Professor Kazuo Sakurai, who helped measure and analyze FT-IR spectra in my research, and Professor Takanori Kihara again, who helped measure Lectin adsorption and produce fluorescent images. I would also like to express my gratitude to Shinichi Tatsumi and Hitomi Kuwahara of the University of Kitakyushu, who helped with GC analysis, and the staff members of Measurement and Analysis Center at the University of Kitakyushu for helping generate SEM images and ICP-OES data. Also, I thank Dr. Shota Fujii, who took the time to explain the organic chemical perspective of IDA-EDC.

I would also like to thank everyone at ENEOS Corporation for sponsoring and supporting the project in carrying out our research. I would also like to express my gratitude to all the students at Uezu Lab who have greatly helped my life in Japan.

Finally, I would like to express my gratitude to my father, mother, uncles, younger brother, and girlfriend Jinhee, who gave me a lot of support and advice whenever I was having a hard time.

Abstract

As indoor residence time increases, public interest in threatening substances in the atmosphere increases in modern society. We have pursued the development of adsorbents targeting volatile organic compounds (VOCs) and influenza viruses among these atmospheric threats. A polymer brush was decided to be used to develop an adsorbent, and radiation-induced graft polymerization was selected to introduce the polymer brush. Polymer brushes manufactured through radiation-induced graft polymerization have a significant advantage in determining the amount and quality of functions imparted through density control.

In the case of VOCs, it was attempted to detect and adsorb VOCs gas by introducing metal ions into a polymer brush, focusing on the fact that metal complexes are advantageous for sensing in the recent sensing field. A ligand capable of adsorbing VOCs gas in a state of being coupled to metal was selected through a "Cambridge Crystal Graphic Data Center (CCDC). In this experiment, 4-picolylamine (4-AMP) was determined as a ligand. And copper was selected as a metal ion to adsorb VOCs gas.

4-AMP was introduced with an average molar conversion rate of 63%, and copper ions were immobilized at a maximum of 0.51 mmol/g. The copper-immobilized 4-AMP-Copper microfiber nonwoven fabric showed a 50% removal rate out of 4L of 50ppm acetone gas at 170% degree of grafting. At this time, the acetone adsorbed by the 4-AMP-Copper microfiber nonwoven fabric was 0.04 mmol/g-4-AMP-Copper.

In the case of the influenza virus, hemagglutinin and sialic acid on the surface of influenza cells react specifically, so sialic acid was introduced into a polymer brush, and the adsorption of influenza virus was targeted. However, it was judged that it was difficult to handle the influenza virus directly, so an experiment was performed using WGA, a lectin that specifically reacts with sialic acids, such as hemagglutinin. IDA-EDC was introduced with an average molar conversion rate of 47%. In the case of N-acetylneuraminic acid microfiber nonwoven fabric (NANA MNWF) introduced with sialic acid, when the degree of grafting was 87%, 118.2μg of 200μg of lectin was adsorbed, showing a maximum adsorption amount of 59.1%. NANA MNWF showed a similar level of adsorption when dg was 40-100%, but a decrease was observed when dg was 100% or more.

In this experiment, an experiment was attempted in which the primary target was also meaningful in giving functionality, away from the typical process of adsorbing the target immediately after the ligand was introduced.

Keywords: polymer brush, VOCs, acetone, gas, influenza, virus, lectin, aerosol

List of tables

List of figures

Chapter 1 General Introduction

1.1. Background

People's efforts for clean air began in the past. In the case of the USA, since 1950, the Clean Air Act has been one of the most extensive regulatory bills passed in the United States. As a result, the Clean Air Act has successfully reduced pollutant concentrations, but very high costs have been paid to achieve this goal, and it is unclear whether this is a result of regulations. Still, the effects of pollution reduction have resonated with people in terms of health and well-being, and these benefits are significant results [1]. Although it is difficult to analyze precisely whether pollution reduction is due to regulation, the adoption and countermeasures of effective and evidence-based regulations are essential as political intervention is the only way to achieve significant improvements at high population levels [1,2].

The threat in the atmosphere does not distinguish between urban and rural areas. The primary sources of pollution from cities include energy production, transportation, residential cooking, fossil fuels for heating and waste incineration, and sources from rural areas include kerosene, biomass, coal combustion, agricultural waste incineration, and substances emitted from certain farming and forestry activities. This includes volatile organic compounds generated from the use or finishing of household goods and construction goods [3]. Also, atmospheric threats don't just depend on chemicals. Infectious viruses are a prime example of the recent problem in the atmosphere that has received the most attention. Representative infectious viruses include the influenza virus and Covid-19, which have recently emerged as the biggest problem. These two have in common that infection by droplets and infection by contact occur [4-6]. Many countries continue to implement regulations to prevent the spread of viruses and reduce the causes of air pollutants, which has raised public awareness of the threats posed by viruses and air pollutants.

Due to the recent epidemic of the infectious virus, people spend more time indoors. However, it is dangerous indoors because it is more affected by infectious viruses and volatile organic compounds [4, 7-11]. The public is trying to relieve the anxiety from these threats by purchasing air purifiers and masks. The purchasing trend of these items is continuously increasing, and studies on air cleaning methods that can purify these threats are constantly being actively conducted [12, 13].

Therefore, as part of a solution to the increasing atmospheric threat in this study, we attempted to develop a novel atmospheric threat substance adsorbent through a functional polymer brush of microfiber nonwoven fabric made using radiation-induced graft polymerization.

1.2. Polymer brush

Polymer brushes are soft material units that can be covalently bonded to the surface of a substrate to induce functional and structural modifications [14-18]. Substrates using polymer brushes are receiving special attention in various fields such as electronics, sensors, antifouling, biomimicry, catalysts, refining, medicine, and energy due to their flexibility in adjusting the length and density of polymer chains and the possibility of bonding additional functional molecules [14, 15].

The polymer brush approach can be divided as grafting-to and grafting-from techniques depending on the fabrication process. The grafting-to technique covalently anchors the polymer chain or polymer unit onto the reactive surface of the substrate, while the grafting-from technique forms a polymer chain or polymer unit via polymerization from polymeric initiating moiety on the substrate surface. The grafting-to technique generally forms a looser brush density than the grafting-from technique because of steric hindrance caused by the previously attached polymers in its coupling process at the interface [14, 17, 18]. In contrast to the grafting-to technique, the grafting-from approach is known to be more suitable for generating chains of high grafting density and thicker films. The immobilization of the initiating group on the surface significantly increases the grafting density of the chains. Polymer chains grow in situ on the surface of a dense initiating species and remain bound to the substrate. Because of these attractive properties, the “grafting from” approach is the preferred option for synthesizing polymer brushes with high grafting density [17, 18]. Graft copolymerization can be initiated by various methods, including chemical treatment, photochemical treatment, ionizing radiation (such as gamma radiation, electron beam radiation, etc.), photo-irradiation, plasma-induced techniques, enzymatic grafting, etc [16, 18].

We decided to use electron beam radiation-induced graft polymerization for the graft copolymer method among these methods. When the substrate is irradiated with an electron beam or gamma rays, a part of the substrate is destroyed, and a site to which a functional polymer can bind is generated, called a radical. When a functional polymer (monomer) reacts at the site where radicals are generated, a graft chain is created from the radical. Polymer chains grafted onto a substrate in which radicals have been generated during graft polymerization can generally be classified into two categories of polymer chains. The graft chains that occur inside the substrate are called polymer roots, and the graft chains that extend from the surface of the substrate are called polymer brushes [16].

In general, the substrate's hydrophobicity, roughness, stiffness/elasticity, and chemical composition into which the polymer brush is introduced are critical factors affecting performance. The observation of the entire surface is mainly confirmed by scanning electron microscopy (SEM), and atomic force microscopy (AFM) is used primarily to ensure the roughness of the surface quantitatively. To ensure that the polymer or biopolymer is properly attached to the surface, the chemical composition of the surface must be analyzed. Usually, Infrared (IR) and Raman spectrometry can be used to identify the functional material of the chemical/polymer. X-ray photoelectron spectroscopy (XPS) can analyze the electronic state and elemental composition of a surface [14]. In this experiment, to confirm the introduction of the polymer brush, we observed the surface through SEM and IR and identified the introduced functional material.

Figure 1- 1. Density control of polymer brushes.

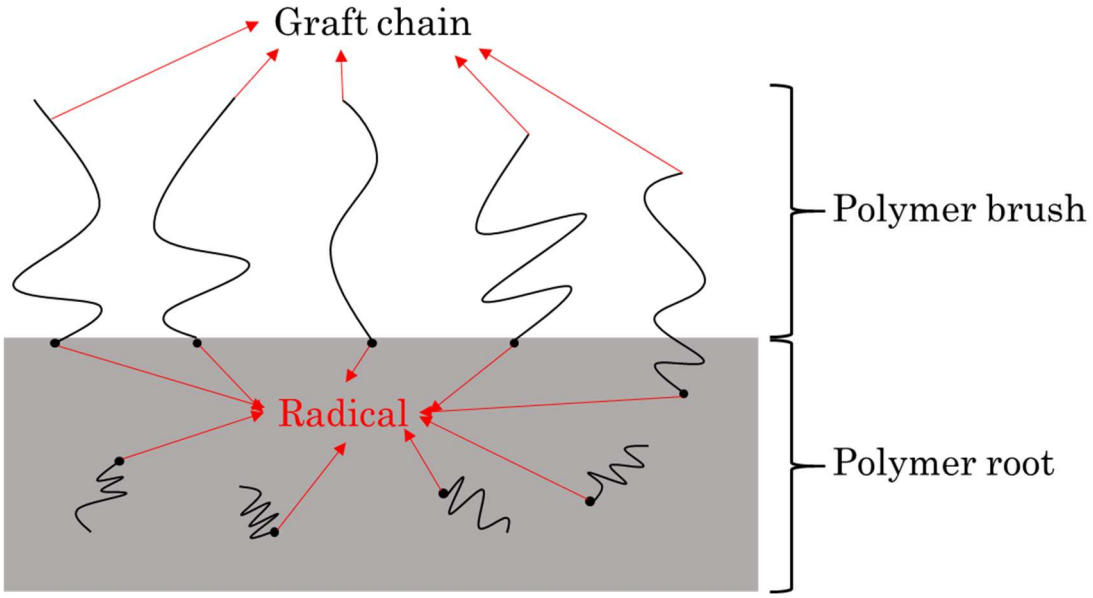

Figure 1- 2. Polymer brush and Polymer root.

1.2.1. Radiation Graft Polymerization

Radiation-induced graft polymerization is a method that utilizes radicals generated when a base substrate is irradiated with radiation, plasma, light, and chemicals in a way that introduces various functionalities. The substrate polymers primarily used include polyethylene, polypropylene, polytetrafluoroethylene, nylon 6, etc [16], and the shapes of the substrate polymers applied here vary, including porous hollow fiber membranes, nonwoven fabrics, films, and nanotubes [19-27]. Graft polymerization has several properties that can be introduced depending on the reacting monomer. In particular, In the case of a substrate polymer prepared by reaction with the vinyl monomer glycidyl methacrylate (GMA), the prepared substrate polymer has hydrophilicity and has the property of containing an epoxy group, so it was used in this experiment [19-23, 26, 27]. In general, when polymer brushes are fabricated using GMA as a monomer, the average length is known to be 35 nm [27]. However, it is reported that the length or density of the polymer brush produced can be controlled by controlling the radiation dose or monomer concentration and reaction time of the substrate made by the radiation graft polymerization method [14-18]. We highly valued these advantages of the radiation graft polymerization method and used them in this experiment.

The quantity and quality of the functional groups immobilized by reacting with the monomer determine the performance of the polymer adsorbent, and in particular, the density of the functional groups is a requirement directly related to the ability to bind to the target. Although the grafting degree of functional groups generally used is around 50% to 150%, it is also possible to prepare a base polymer having a grafting degree of 200 to 300% or more. However, the physical strength tends to be lowered when a base polymer has a grafting degree of 200~300% or more [16].

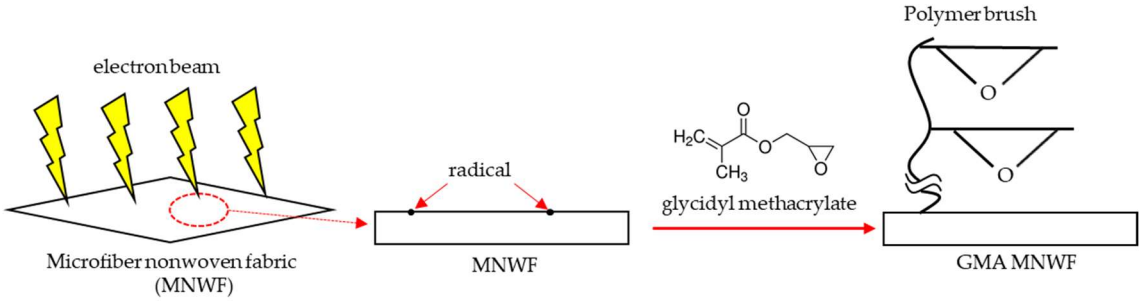

Figure 1- 3. Radiation-induced graft polymerization with GMA monomer

1.3. Hazardous substances in the air

1.3.1. Volatile Organic Compounds (VOCs)

Volatile organic compounds (VOCs) have recently become a hot topic as one of the biggest causes of indoor air pollution. VOC is a generic term for substances harmful to the human body among substances that have a low boiling point in a liquid or gaseous state and easily exist in the atmosphere [28]. Depending on their molecular structure, VOCs include alkanes, alkenes, aromatic hydrocarbons, alcohols, aldehydes, and ketones [28-30]. VOCs range from a variety of solvents used in industries to organic gases emitted during production, particularly in the chemical, petrochemical, pharmaceutical, food processing, pulp and paper, color printing and painting industries, pharmaceutical factories, insulation, and automotive industries [3, 29 -32]. We spend much of our daily life indoors in modern society, and indoor air pollution caused by VOCs is a severe problem. In particular, VOCs are known to be significantly affected by environmental factors such as confined spaces and humidity. Since the concentration of VOC may be higher indoors than outdoors, special attention is required [7-11].

The best-known term for indoor air pollution with VOCs is sick house syndrome (SBS). SBS was first defined by the World Health Organization (WHO) in 1982 and described a set of symptoms commonly found indoors [10]. VOCs considered the leading causes of SBS are formaldehyde, acetaldehyde, benzene, ethylbenzene, limonene, p-dichlorobenzene, styrene toluene, xylene, and acetone. They are mainly from building materials, paints, printing inks, or fumes from cooking [11]. Formaldehyde can burn your eyes or irritate your upper respiratory tract, even at low concentrations, depending on environmental conditions such as temperature and humidity. In addition to formaldehyde, exposure to VOCs increases the risk of respiratory diseases such as pneumoconiosis and lung cancer and may cause temporary irritation and inflammation of the skin, eyes, and nose [33, 34].

Exposure to VOCs can pose a significant threat to our safe indoor life. Therefore, we would like to try adsorption and detecting VOCs through a substrate with a polymer brush that gives various functionalities. Acetone, most commonly used as the first step in VOCs adsorption, was targeted.

1.3.1.1 Acetone

Acetone was previously included on the list of VOCs, but this is changing with the recent trend of exclusion. However, being excluded from the list does not mean that the risk does not exist. Acetone is mainly used in industrial sites and laboratories, and the general public can also purchase it in a diluted state. Acetone is one of the simplest ketones masquerading and affects human health when airborne concentrations exceed 173 ppm [35]. Short-term exposure to acetone irritates the central nervous system, aggravate the nose, throat, lungs, and eyes, and causes headaches and dizziness. It may also produce vomiting symptoms. If very high acetone levels are inhaled or exposed, one may lose consciousness and experience skin irritation [36]. Because of these risks, it is essential to control the concentration of acetone gas in the living environment or workplace [37]. In addition, acetone can function as a biomarker for diseases through the amount contained in the breath when a person exhale. It has been found that when the amount of acetone in the expiratory volume differs from that of ordinary people, it can indicate the risk of lung cancer, diabetes, dietary fat loss, congestive heart failure, and cerebral attack [38–41]. Research is being actively conducted to develop ultra-sensitive sensors that function as biomarkers for diseases. However, the effective high-sensitivity acetone detection sensor proposed by modern research has several problems, such as bulkiness and the need to operate at high temperatures. Therefore, there is a need for a sensor material that can efficiently detect acetone with high sensitivity at room temperature [41-45]. According to the danger of acetone and the need for detection, acetone was selected as the initial target for VOCs removal and adsorption experiments. If acetone, the simplest ketone, could be adsorbed, it would be considered applicable to various volatile organic compounds (VOCs) adsorption.

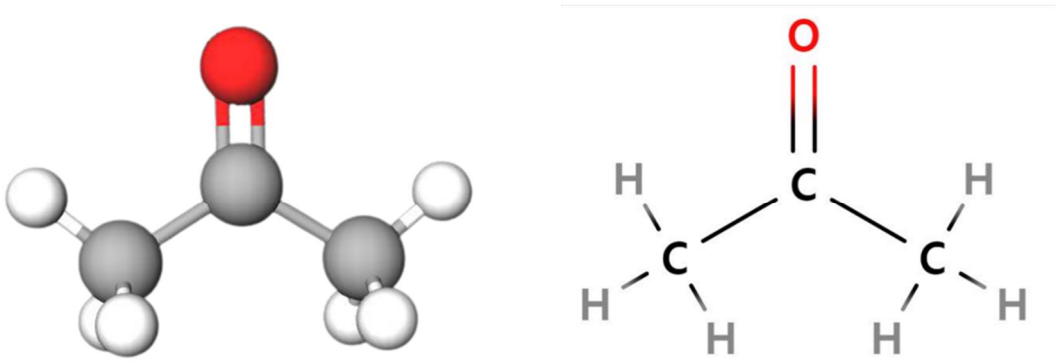

Figure 1- 4. 3D and 2D image of Acetone molecule (image from molview.org).

1.3.2. Influenza virus

1.3.2.1. Sugar chain cluster effect

Influenza virus hemagglutinin is known as a site that binds to human cells in the viral infection pathway [46-50]. In the case of hemagglutinin, it binds to sialic acid present in human cells through a specific reaction. Therefore, we aimed to develop a polymer brush containing sialic acid to absorb the influenza virus as the final target.

In general, sialic acid in human cells exists in the form of sugar chains. Monosaccharides that makeup sugar chains include glucose, mannose, galactose, fucose, xylose, N-acetylglucosamine, and sialic acid, and these sugar chains interact with a single protein. In general, the interaction between a single sugar chain and a single protein is weak because weak forces such as hydrogen bonding and hydrophobic interactions mainly occur. Compensating for these shortcomings is the sugar cluster effect or sugar chain polyvalent effect [51-55]. In other words, proteins or glycolipids do not spread into cells but concentrate in some areas as needed to form sugar clusters, increasing the binding force.

In the past, polyvalent N-acetylneuraminic acid-containing compounds were not used clinically to treat or prevent influenza. Despite intensive research on polyvalent inhibitors, the US FDA has not approved the use of polyvalent-based compounds as therapeutics due to inconsistencies and pharmacokinetic issues [52]. However, with the functional demonstration of this sugar cluster effect in recent studies, it has become a significant design guide for developing antibodies, antiviral agents, and toxin inhibitors in immunology [53-57].

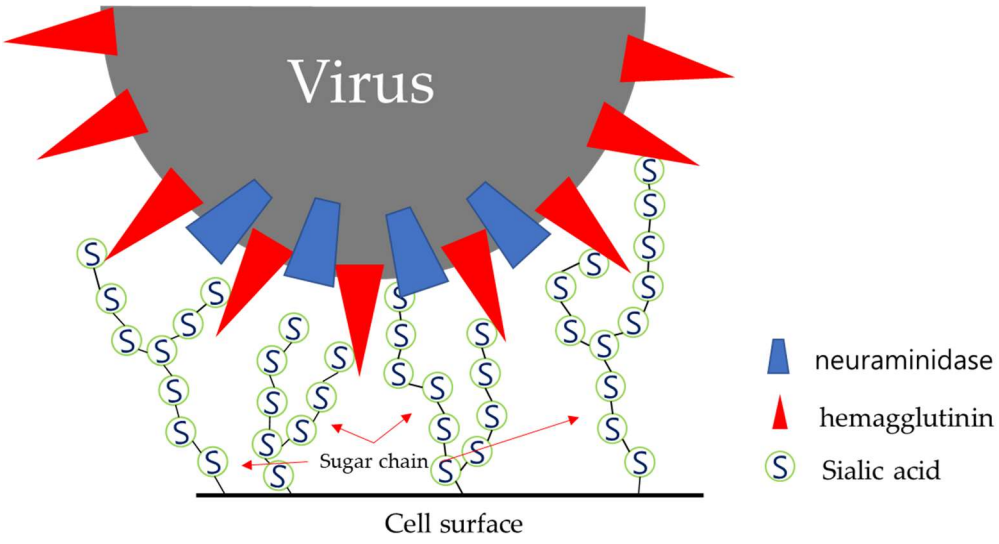

Figure 1- 5. Image of sialic acid sugar chain clusters bound to influenza virus.

1.3.2.2. Influenza virus hemagglutinins and lectins

The direct use of the influenza virus in adsorption experiments required other methods due to difficulties in handling. Therefore, the existence of a substance having properties similar to hemagglutinin of the influenza virus began to be searched for.

As an alternative to the influenza virus used in adsorption experiments, we considered targeting a lectin that can explicitly react with sialic acids, such as the hemagglutinin (HA) of the influenza virus. N-Acetylneuraminic acid (NANA), one of the sialic acids, is known to respond with H1-type hemagglutinin of influenza virus by specific recognition [58-64]. Similar to the specific recognition reactions of NANA with HA, Concanavalin A (ConA) [58, 63] and Wheat germ agglutinin (WGA) [58, 63, 64] are also capable of specific recognition reactions with NANA.

Since we are in the initial stage of developing a virus adsorbent, it was thought that the experiment using lectin does not require handling of influenza virus, so it is possible to experiment with a safe state. Therefore, rather than directly adsorbing the influenza virus in the design stage of the adsorption experiment, we tried to check whether the lectin, which is non-hazardous material, can be adsorbed on the newly developed adsorbent. Con A and WGA were candidates for the lectin to be used in the experiment. However, in our lab's previous experiments, WGA had better adsorption performance than Con A, so the adsorption target lectin was finally determined as WGA.

Although the crystal structure of the influenza virus and WGA is different, both can bind by NANA specific recognition and are considered helpful as alternatives to determining whether the influenza virus is adsorbed or not without infection risk during the experiment. WGA lectins are by-products of wheat processing, whose structure has been described since the 1970s [64, 65]. WGA lectins are composed of polypeptide chain homodimers [66] and are in the form of biaxial symmetry [68]. Polypeptides A, B, and C present in WGA are known to bind to N-Acetylglucosamine (GlcNAc) residues [65, 69]. Figure 6 shows the crystal structure of the influenza virus [70], which caused the worst pandemic in history in 1918, and the crystal structure of the WGA lectin. Although the structures of these two proteins are different, in common, both have the property of binding to NANA through specific recognition.

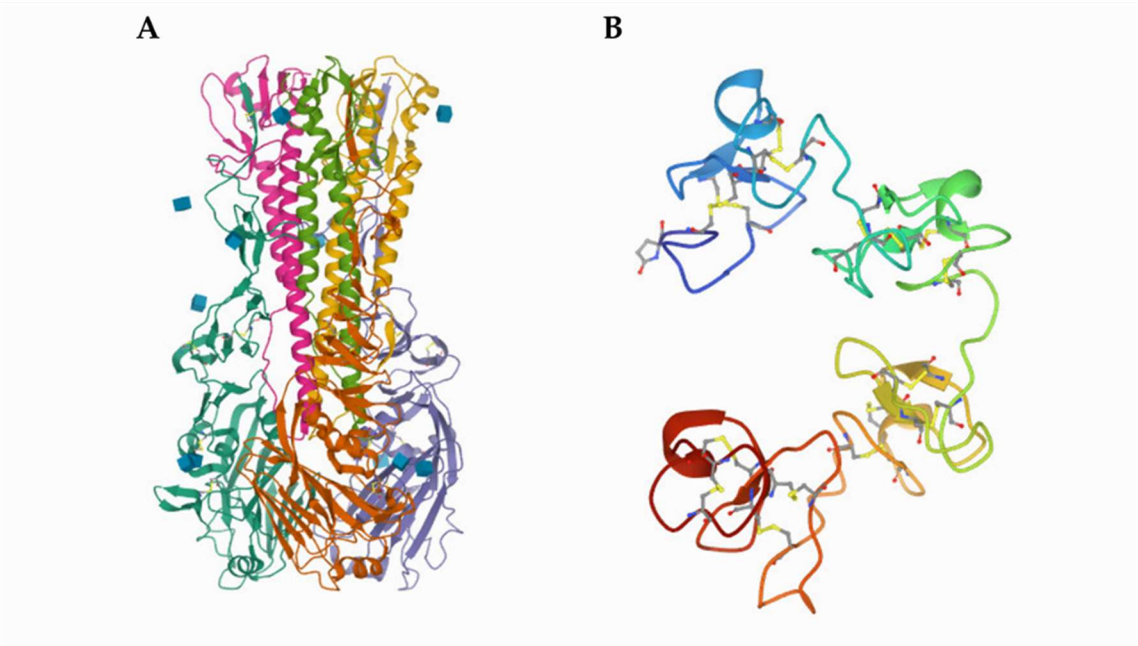

Figure 1- 6. Protein database biological assembly (A: 1ruz, 1918 H1 Hemagglutinin, B: 1WGC_1, Wheat germ agglutinin, from Protein data base).

1.4. Objectives and Outline of the Thesis

Experiments on imparting functionality through polymer brushes have been recognized for their utility from the past and are being studied to develop better materials through various materials and functional groups in many fields. In the past, adsorption and removal experiments of primary targets such as heavy metals and proteins contained in liquids were mainly performed using membranes, non-woven fabrics, films, etc.

In the case of substrates manufactured with the technology at that time, substrates with a high degree of graft or more had too much surface change, so functionality was not well imparted or destroyed in some cases. However, with the development of science, there have been many changes in the method of manufacturing and preparing substrates, and materials in which the unit of the substrate structure is made of micro or nano units are frequently used in recent materials. Even with the same type of substrate, the smaller the structural unit, the more surface area can be used for adsorption with the target, which significantly affects the adsorption and sensing results.

We selected nonwoven fabric, one of the most common substrates, as the base material for this study. In general, the advantage of non-woven fabrics is that they have large pores compared to other substrates, so they are not easily clogged and have strong durability [21]. As a disadvantage, since the pores are vast, the surface area in which the functional group bonded to the nonwoven comes into contact with the adsorption target is smaller than that of other substrates, giving the impression that it is disadvantageous for adsorption or sensing. However, in modern experiments, various attempts such as shape transformation and coating are being made to supplement the characteristics of the nonwoven fabric. The non-woven fabric we used is a non-woven fabric manufactured by ENEOS Corporation. It is woven with microfibers and overcomes the disadvantage of wide pore size while maintaining the advantages of general non-woven fabrics. I want to discuss the method and experiment of introducing a functional group using this microfiber nonwoven fabric and selecting the primary target for adsorption of the secondary target.

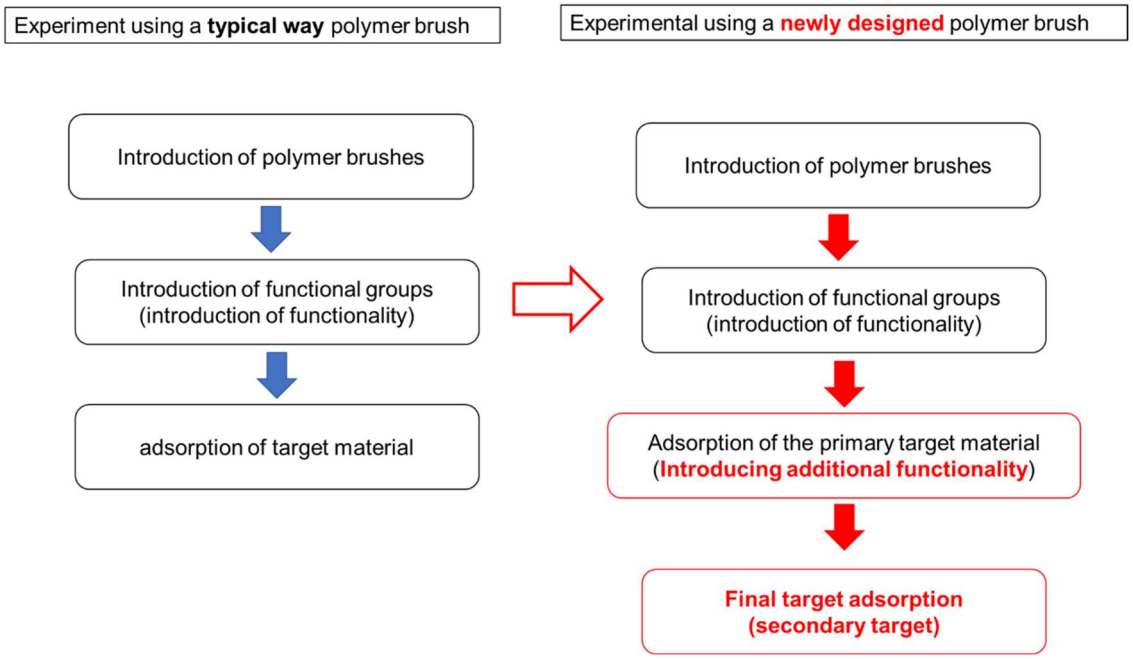

Scheme 1-1. Schematic diagram of secondary target adsorption using the primary target material introduced into the polymer brush.

1.5. References

1. Currie J; Walker R. What Do Economists Have to Say about the Clean Air Act 50 Years after the Establishment of the Environmental Protection Agency?. Journal of Economic Perspectives **2019**, 33, 4, pp. 3-26
2. Eguiluz-Gracia I; Mathioudakis AG; Bartel S; Vijverberg SJH; Fuertes E; Comberiati P; Cai YS; Tomazic PV; Diamant Z; Vestbo J; Galan C; Hoffmann B. The need for clean air: The way air pollution and climate change affect allergic rhinitis and asthma. Allergy **2020**, 75, 9, pp. 2170-2184
3. Air pollution and child health: prescribing clean air. WHO (World Health Organization) **2018**
4. Scheuch G. Breathing Is Enough: For the Spread of Influenza Virus and SARS-CoV-2 by Breathing Only. Journal of Aerosol Medicine And Pulmonary Drug Delivery **2020**, 33, 4, pp. 230-234
5. Brankston G; Gitterman L; Hirji Z; Lemieux C; Gardam M. Transmission of influenza A in human beings. The Lancet. Infectious diseases **2007**, 7, 4, 257-265
6. Chilamakuri R; Agarwal S. COVID-19: Characteristics and Therapeutics. Cells **2021**, 10, 2, 206
7. Enesca, A.; Cazan, C. Volatile Organic Compounds (VOCs) Removal from Indoor Air by Heterostructures/Composites/Doped Photocatalysts: A Mini-Review. Nanomaterials **2020**, 10, 1965.
8. Shah, K.W.; Li, W. A Review on Catalytic Nanomaterials for Volatile Organic Compounds VOC Removal and Their Applications for Healthy Buildings. Nanomaterials **2019**, 9, 910.
9. Chi, C.; Chen, W.; Guo, M.; Weng, M.; Yan, G.; Shen, X. Law and features of TVOC and Formaldehyde pollution in urban indoor air. Atmos. Environ. **2016**, 132, 85–90.
10. Mølhave, L. Organic compounds as indicators of air pollution. Indoor AIR **2003**, 13, 12–19.
11. Araki, A; Ketema, R.M; Ait Bamai, Y; Kishi, R. Aldehydes, Volatile Organic Compounds (VOCs), and Health, Indoor Environmental Quality and Health Risk toward Healthier Environment for All, Current Topics in Environmental Health and Preventive Medicine. Springer: Singapore **2020**, pp. 129–158.
12. Ito, K.; Zhang, S. Willingness to Pay for Clean Air: Evidence from Air Purifier Markets in China, Journal of Political Economy **2020**, 128, 5

13. Bhatti, A; Akram, H; Basit, H; Khan, A; Mahwish, S; Naqvi, R; Bilal, M. E-commerce trends during COVID-19 Pandemic. International Journal of Future Generation Communication and Networking **2020**, 13, 2, pp.1449-1452.
14. Kim, W; & Jung, J. Polymer brush: a promising grafting approach to scaffolds for tissue engineering. BMB reports **2016**, 49, 12, pp. 655–661.
15. Higaki, Y; Kobayashi, M; Murakami, D. et al. Anti-fouling behavior of polymer brush immobilized surfaces. *Polym J* **2016**, 48, pp. 325–331
16. Saito, K.; Fujiwara, K.; Sugo, T. Fundamentals of Radiation-Induced Graft Polymerization. In Innovative Polymeric Adsorbents. Springer: Singapore **2018**, pp. 1–22.
17. Lilge, Inga. Introduction to Polymer Brushes. In Polymer Brush Films with Varied Grafting and Cross-Linking Density via SI-ATRP: Analysis of the Mechanical Properties by AFM. Springer Fachmedien Wiesbaden **2017**, pp. 27-36
18. Sherazi, Tauqir A. Graft Polymerization. In Encyclopedia of Membranes. Springer Berlin Heidelberg **2015**, pp. 1-2
19. Kiyohara, S.; Kim, M.; Toida, Y.; Saito, K.; Sugita, K.; Sugo, T. Selection of a precursor monomer for the introduction of af-finity ligands onto a porous membrane by radiation-induced graft polymerization. *J. Chromatogr. A* **1997**, 758, pp. 209–215
20. Ogawa, H.; Sugita, K.; Saito, K.; Kim, M.; Tamada, M.; Katakai, A.; Sugo, T. Binding of ionic surfactants to charged polymer brushes grafted onto porous substrates. *J. Chromatogr. A* **2002**, 954, pp. 89–97
21. Kim, M.; Saito, K. Preparation of silver-ion-loaded nonwoven fabric by radiation-induced graft polymerization. *React. Funct. Polym.* **1999**, 40, pp. 275–279
22. Sunaga, K.; Kim, M.; Saito, A.K.; Sugita, K.; Sugo, T. Characteristics of Porous Anion-Exchange Membranes Prepared by Cografting of Glycidyl Methacrylate with Divinylbenzene. *Chem. Mater.* **1999**, 11, pp. 1986–1989
23. Fujiwara, K. Separation functional fibers by radiation induced graft polymerization and application. *Nucl. Instrum. Methods Phys. Res. Sect. B Beam Interact. Mater. At.* **2007**, 265, pp. 150–155

24. Chen, S.; Wu, G.; Liu, Y.; Long, D. Preparation of Poly(acrylic acid) Grafted Multiwalled Carbon Nanotubes by a Two-Step Irradiation Technique. *ACS Appl. Macromol.* **2006**, 39, pp. 330–334
25. Hasegawa, S.; Takahashi, S.; Iwase, H.; Koizumi, S.; Morishita, N.; Sato, K.; Narita, T.; Ohnuma, M.; Maekawa, Y. Radia-tion-induced graft polymerization of functional monomer into poly(ether ether ketone) film and structure-property analy-sis of the grafted membrane. *Polymer* **2011**, 52, pp. 98–106
26. Dong, Z.; Liu, J.; Yuan, W.; Yi, Y.; Zhao, L. Recovery of Au(III) by radiation synthesized aminomethyl pyridine functional-ized adsorbents based on cellulose. *Chem. Eng. J.* **2016**, 283, pp. 504–513
27. Okobira T; Matsuo A; Matsumoto H;Tanaka T; Kai K; Minari C; Goto M; Kawakita H; Uezu K. Enhancement of immobi-lized lipase activity by design of polymer brushes on a hollow fiber membrane.
28. Zhu, L.; Shen, D.; Luo, K.H. A critical review on VOCs adsorption by different porous materials: Species, mechanisms and modification methods. *J. Hazard. Mater.* **2020**, 389, 122102
29. Li, X.; Zhang, L.; Yang, Z.; Wang, P.; Yan, Y.; Ran, J. Adsorption materials for volatile organic compounds (VOCs) and the key factors for VOCs adsorption process: A review. *Sep. Purif. Technol.* **2020**, 235, 116213
30. He, C.; Cheng, J.; Zhang, X.; Douthwaite, M.; Pattisson, S.; Hao, Z. Recent Advances in the Catalytic Oxidation of Volatile Organic Compounds: A Review Based on Pollutant Sorts and Sources. *Chem. Rev.* **2019**, 119, 4471–4568
31. Rene, E.R.; Murthy, D.; Swaminathan, T. Performance evaluation of a compost biofilter treating toluene vapours. *Process Biochem.* **2005**, 40, pp. 2771–2779
32. Li, Y.; Chang, H.; Yan, H.; Tian, S.; Jessop, P.G. Reversible Absorption of Volatile Organic Compounds by Switcha-ble-Hydrophilicity Solvents: A Case Study of Toluene with N, N-Dimethylcyclohexylamine. *ACS Omega* **2020**, 6, pp. 253–264
33. Gaikwadd A; Shivhare N. Inddor air pollution – A threat. International journal of scientific research and review **2019**, 7, 5, pp. 1463-1467
34. Araviiskaia E; Berardesca E; Bieber T; Gontijo G; Sanchez Viera M; Marrot L; Chuberre B; Dreno B. The impact of airborne pollution on skin.

Journal of the European Academy of Dermatology and Venereology: JEADV **2019**, 33, 8, pp. 1496-1505

35. Zhang, Y.; Zhao, J.; Du, T.; Zhu, Z.; Zhang, J.; Liu, Q. A gas sensor array for the simultaneous detection of multiple VOCs. *Sci. Rep.* **2017**, 7, 1960
36. Kalapos, M.P. Acetone, Encyclopedia of Toxicology, 3rd ed.; Academic Press: Cambridge, MA, USA, 2014; pp. 36–39
37. Xu, X.; Chen, Y.; Zhang, G.; Ma, S.; Lu, Y.; Bian, H.; Chen, Q. Highly sensitive VOCs-acetone sensor based on Ag-decorated SnO2 hollow nanofibers. J. Alloy. Compd. 2017, 703, 572–579.
38. Galassetti, P.R.; Novak, B.; Nemet, D.; Rose-Gottron, C.; Cooper, D.M.; Meinardi, S.; Newcomb, R.; Zaldivar, F.; Blake, D.R. Breath ethanol and acetone as indicators of serum glucose levels: An initial report. *Diabetes Technol. Ther.* **2005**, 7, pp. 115–123
39. Wang, Z.; Wang, C. Is breath acetone a biomarker of diabetes? A historical review on breath acetone measurements. *J. Breath Res.* **2013**, 7, 037109
40. Wang, C.; Sahay, P. Breath analysis using laser spectroscopic techniques: Breath biomarkers, spectral fingerprints, and detection limits. *Sensors* **2009**, 9, pp. 8230–8262
41. Marcondes-Braga, F.G.; Gutz, I.G.R.; Batista, G.L.; Saldiva, P.H.N.; Ayub-Ferreira, S.M.; Issa, V.S.; Mangini, S.; Bocchi, E.A.; Bacal, F. Exhaled acetone as a new biomarker of heart failure severity. *Chest* **2012**, 142, pp. 457–466
42. Obeidat, Y. The Most Common Methods for Breath Acetone Concentration Detection: A Review. *IEEE Sens. J.* **2021**, 21, 14540–14558
43. Kalidoss, R.; Umapathy, S. An overview on the exponential growth of non-invasive diagnosis of diabetes mellitus from exhaled breath by nanostructured metal oxide Chemi-resistive gas sensors and μ-preconcentrator. *Biomed. Microdevices* **2020**, 22, 2
44. Lekha. S.; M. Suchetha. Recent Advancements and Future Prospects on E-Nose Sensors Technology and Machine Learning Approaches for Non-Invasive Diabetes Diagnosis: A Review. *IEEE Rev. Biomed. Eng.* **2021**, 14, pp. 127–138
45. Martinez, E.P.A.; Osuna, V.; Dominguez, R.B.; Márquez-Lucero, A.; Zaragoza-Contreras, E.A.; Vega-Rios, A. Room Temper-ature Detection

of Acetone by a PANI/Cellulose/WO3 Electrochemical Sensor. *J. Nanomater.* **2018**, 2018, 6519694

46. Chilamakuri, R.; Agarwal, S. COVID-19: Characteristics and Therapeutics. Cells **2021**, 10, 206
47. Brankston, G.; Gitterman, L.; Hirji, Z.; Lemieux, C.; Gardam, M. Transmission of influenza A in human beings. Lancet. Infect. Dis. **2007**, 7, pp. 257–265
48. Webster, R.G.; Laver, W.G. The origin of pandemic influenza. Bull World Health Organ. **1972**, 47, pp. 449–452
49. Boonstra, S.; Blijleven, J.S.; Roos, W.H.; Onck, P.R.; van der Giessen, E.; van Oijen, A.M. Hemagglutinin-Mediated Membrane Fusion: A Biophysical Perspective. Annu. Rev. Biophys. **2018**, 47, pp. 153–173
50. Kuchipudi, S.; Nelli, R.; Gontu, A.; Satyakumar, R.; Nair, M.S.; Subbiah, M. Sialic Acid Receptors: The Key to Solving the Enigma of Zoonotic Virus Spillover. Viruses **2021**, 13, 262
51. Monsigny, M.; Mayer, R.; Roche, A.C. Sugar-lectin interactions: Sugar clusters, lectin multivalency and avidity. Carbohydr. Lett. **2000**, 4, pp. 33–52
52. Carlescu, Irina; Scutaru, Dan; Popa, Marcel; Uglea, Constantin V. Synthetic sialic-acid-containing polyvalent antiviral inhibitors. Medicinal Chemistry Research **2008**, 18, 6, pp. 477-494
53. Nagao M; Fujiwara Y; Matsubara T; Hoshino Y; Sato T;Miura Y. Design of Glycopolymers Carrying Sialyl Oligosaccharides for Controlling the Interaction with the Influenza Virus. Biomacromolecules **2017**, 18, 12, pp. 4385-4392
54. Hai-Peng Liu; Xin Meng; Qun Yu; Yun-Chang Tao; Fei Xu; Yun He; Peng Yu; Yang Yang. Synthesis of S-sialyl polymers as efficient polyvalent influenza inhibitors and capturers. Journal of carbohydrate chemistry **2018**, 37, 1, pp. 18-29
55. Nagao, Masanori; Kurebayashi, Yuuki; Seto, Hirokazu; Tanaka, Tomonari; Takahashi, Tadanobu; Suzuki, Takashi; Hoshino, Yu; Miura, Yoshiko. Synthesis of well-controlled glycopolymers bearing oligosaccharides and their interactions with influenza viruses. Polymer Journal **2016**, 48, pp. 745-749
56. Harding CM; Nasr MA; Scott NE; Goyette-Desjardins G; Nothaft H; Mayer AE; Chavez SM; Huynh JP; Kinsella RL; Szymanski CM;

Stallings CL; Segura M; Feldman MF. A platform for glycoengineering a polyvalent pneumococcal bioconjugate vaccine using E. coli as a host. Nature communications **2019**, 10, 1, 891

57. Shinchi H; Yuki N; Ishida H; Hirata K; Wakao M; Suda Y. Visual Detection of Human Antibodies Using Sugar Chain-Immobilized Fluorescent Nanoparticles: Application as a Point of Care Diagnostic Tool for Guillain-Barré Syndrome. PloS one **2015**, 10, 9, e0137966
58. Wright, C.S. 2·2 Å resolution structure analysis of two refined N-acetylneuraminyl-lactose—Wheat germ agglutinin isolec-tin complexes. J. Mol. Biol. **1990**, 215, 635–651. Doi:10.1016/s0022-2836(05)80174-3.
59. Bondioli, L.; Costantino, L.; Ballestrazzi, A.; Lucchesi, D.; Boraschi, D.; Pellati, F.; Benvenuti, S.; Tosi, G.; Vandelli, M.A. PLGA nanoparticles surfacecorated with the sialic acid, N-acetylneuraminic acid. Biomaterials **2010**, 31, 3395–3403.
60. Boons, G.J.; Wong, C.H. The Chemistry of Sialic Acid. In Carbohydrate-Based Drug Discovery; Wong, C.H., Ed.; John Wiley and Sons: Hoboken, NJ, USA, **2003**; pp. 55–101.
61. El-Deeb, I.M.; Guillon, P.; Winger, M.; Eveno, T.; Haselhorst, T.; Dyason, J.C.; von Itzstein, M. Exploring Human Parainflu-enza Virus Type-1 Hemagglutinin–Neuraminidase as a Target for Inhibitor Discovery. J. Med. Chem. **2014**, 57, 7613–7623. Doi:10.1021/jm500759v.
62. Tulin, E.K.C.; Nakazawa, C.; Nakamura, T.; Saito, S.; Ohzono, N.; Hiemori, K.; Nakakita, S.I.; Tateno, H.; Tonozuka, T.; Nishikawa, A. Glycan detecting tooleveloped from the Clostridium botulinum whole hemagglutinin complex. Sci. Rep. **2021**, 11, 21973.
63. Mandenius, C.F.; Wang, R.; Aldén, A.; Bergström, G.; Thébault, S.; Lutsch, C.; Ohlson, S. Monitoring of influenza virus he-magglutinin in process samplesing weak affinity ligands and surface plasmon resonance. Anal. Chim. Acta **2008**, 623, 66–75.
64. Matsubara, T.; Onishi, A.; Saito, T.; Shimada, A.; Inoue, H.; Taki, T.; Nagata, K.; Okahata, Y.; Sato, T. Sialic acid-mimic pep-tides as hemagglutinin inhibitors for anti-influenza therapy. J. Oedicinal Chem. **2010**, 53, 4441–4449.
65. Murziene, G.B.; Dzikaras, M. Wheat Germ Agglutinin—From Toxicity to Biomedical Applications. Appl. Sci. **2021**, 11, 884.

66. Urtasun, N.; Baieli, M.F.; Cascone, O.; Wolman, F.J.; Miranda, M.V. High-level expression and purification of recombinant wheat germ agglutinin in Rachiplusia nu larvae. Process Biochem. **2015**, 50, 40–47.
67. Peumans, W.J.; Stinissen, H.M.; Carlier, A.R. Isolation and partial characterization of wheat-germ-agglutinin-like lectins from rye (Secale cereale) and barley (Hordeum vulgare) embryos. Biochem. J. **1982**, 203, 239–243. Doi:10.1042/bj2030239.
68. Rice, R.H.; Etzler, M.E. Subunit structure of wheat germ agglutinin. Biochem. Biophys. Res. Commun. **1974**, 59, 414–419.
69. Allen, A.K.; Neuberger, A.; Sharon, N. The purification, composition and specificity of wheat-germ agglutinin. Biochem. J. **1973**, 131, 155–162. Doi:10.1042/bj1310155.
70. Salzberger, B.; Mohr, A.; Hitzenbichler, F.B. The Pandemic Influenza 1918. In Die Influenza 1918; Georg Thieme Verlag: Stuttgart, Germany, **2018**; pp. 1858–1863. Doi: 10.1055/a-0666-1962

Chapter 2 Metal Ion Immobilized Polymer Brush for VOCs Gas

2.1. Introduction

As air pollution is of worldwide concern, interest in indoor air quality increases in industry and general households. There are various causes of indoor air pollution, however, volatile organic compounds (VOCs) are one of the biggest problems. VOCs are a generic term for materials having a low boiling point in a liquid or gas state and easily present in the atmosphere [1], and according to a molecular structure, VOCs include alkane, alkene, aromatic hydrocarbon, alcohol, aldehyde, and ketone [1-3]. VOCs-producing industries include organic gas, chemicals, petrochemicals, pharmaceuticals, food processing, pulp and paper, color printing and painting, pharmaceutical factories, insulation, and automobile industries [2-5]. In particular, VOCs, an indoor air pollutant, can cause dangerous conditions for the human body as their concentration may be higher indoors than outdoors because they are highly affected by the environment such as enclosed places and humidity [6-8]. We are currently spending most of our daily and working times indoors because of the risk of virus infection. Therefore, it is challenging to be completely free from VOCs in everyday life and industrial sites, and this is a severe problem, so we aimed to detect and adsorb VOCs.

We set our target as acetone as the first attempt at adsorbing VOCs. Acetone, one of the simplest ketones, used to be treated as VOCs in many countries in the past, however, In modern society, it is a trend that acetone is excluded from the VOCs list. Still, this does not mean that acetone is not dangerous. Acetone is mainly used in industrial sites and laboratories, and the general public can also purchase it in a diluted state. Short-term exposure to acetone irritates the central nervous system, aggravate the nose, throat, lungs, and eyes, and causes headaches and dizziness. It may also produce vomiting symptoms. If very high acetone levels are inhaled or exposed, one may lose consciousness and experience skin irritation [9]. Therefore, it is necessary to control acetone concentration in the living environment or workplace [10]. In addition, acetone can function as a biomarker for diseases through the amount contained in the breath when a person exhales. It has been found that when the amount of acetone in the expiratory volume differs from that of ordinary people, it can indicate the risk of lung cancer, diabetes, dietary fat loss, congestive heart failure, and cerebral attack [11–14]. Although research to develop a very high-sensitivity sensor to function as a biomarker of a disease is being actively conducted, the effective high-sensitivity acetone detection sensor proposed in the modern study is bulky and has several significant technical problems, such as

limited operation at high temperatures. Therefore, there is a need for a sensor that can detect ace-tone with high sensitivity at room temperature and at a low cost [15–18].

As a recent trend in gas sensing research, research on VOCs sensors using metal oxides has proven fruitful. However, Gas sensing using metal oxides also has some disadvantages. It is challenging to use only a single metal oxide material, and when used in an un-doped state, there is increased resistance [19–21]. We were inspired by the latest trends in gas sensing using metal oxides, we devised a method to develop materials that can be used for sensing using metal ions.

Since the past, experiments aimed at high-efficiency metal ion adsorption have been attempted through the functional groups introduced in polymer brushes. Therefore, it was expected that the produced substrate could detect or adsorb acetone gas if functional groups and an appropriate amount of metal ions could be immobilized on a high-density polymer brush. Unlike the previous metal adsorption experiments, this experiment does not matter the maximum amount of metal ion adsorption. We predict that the vacant coordination site of metal ions can detect VOCs gas. Therefore, the key to this experiment is to introduce an appropriate amount of metal ions. If the metal ions bind too much and firmly to the functional groups, it is expected that no coordination sites remain available for binding with the acetone gas. In this experiment, the immobilization of metal ions is only a part of the functionalization process, and the ultimate goal is to try the adsorption of acetone gas, one of the VOCs. Scheme 2-1 shows an expected image of a material that could try to immobilize a metal ion with an appropriate bonding level using a functional group introduced in a polymer brush in the final step and adsorb acetone gas on an immobilized metal ion.

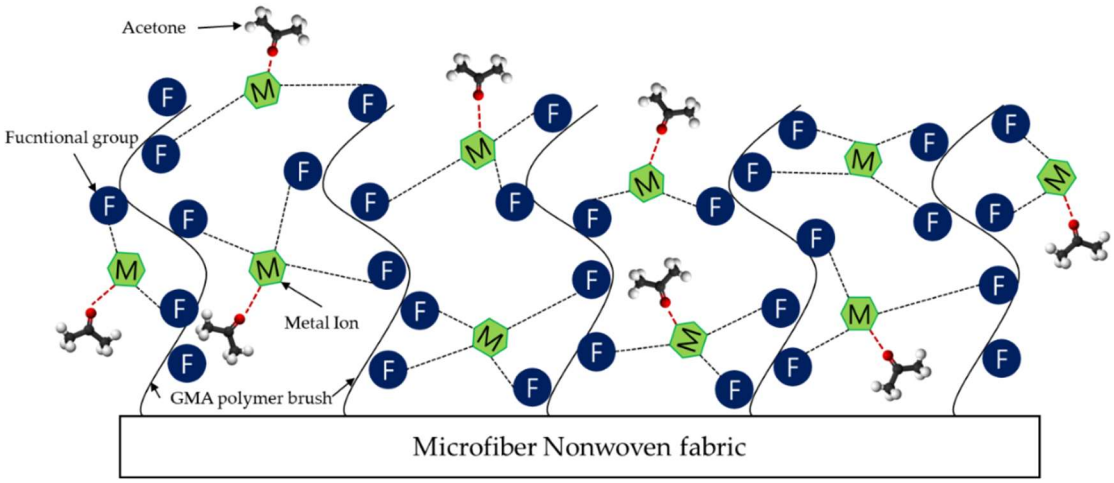

Scheme 2- 1. The design concept of a new material in which acetone molecules coordinate to metal ions immobilized on functional microfiber nonwoven fabric.

2.2. Experimental

2.2.1. Materials

4-picolylamine (98%, Tokyo chemical industry Co., Ltd., Tokyo, Japan, 97.5%, Alfa Aesar Chemical Co., ltd., Haverhill, USA), Sulfuric acid (0.5 mol/L, KANTO CHEMICAL Co., INC., Tokyo, Japan), Hydrochloric acid (1 mol/L, Tokyo Chemical Industry Co., Ltd., Tokyo, Japan), GASTEC GV-100, GASTEC No.151L, Polypropylene microfiber nonwoven fabric (dg 30~520%, ENEOS Corporation, Tokyo, Japan), Acetone (99.5%, Wako Chemical Co. Ltd., Odawara, Japan), ICP-OES (Model-9820, SHIMADZU, Kyoto, Japan), FE-SEM-EDS (JSM-7800f, Jeol, Tokyo, Japan), Gas chromatography (GC-2014, SHIMADZU, Kyoto, Japan), Tedlar bag (5L & 50L, AS ONE Corporation, Osaka, Japan), Digital micro scope(VHX-8000, Keyence, Osaka, Japan)

2.2.2. Selection of functional group

2.2.2.1. Cambridge Crystallographic Data Center (CCDC)

First, we searched using a program called Cambridge Crystallographic Data Center (CCDC) to find functional groups capable of adsorbing target VOCs (acetone and formaldehyde). CCDC is the world's first numerical science database system launched by the University of Cambridge. This system collected and covered all small-molecule chemicals and crystal structures studied by X-ray and neutron diffraction in studies published since 1965. Through CCDC, a ligand that can bind to VOCs while the metal ion is immobilized on the functional group was searched. The formaldehyde search yielded few results, and the acetone search yielded approximately 7,000 results from the CCDC. The results of the ligand search through CCDC are shown in Figure 3. Although many metal ions are theoretically presumed to be capable of binding to acetone, the list of substances that are likely to bind acetone in the state in which the metal ions discovered through CCDC are bound to ligands include copper, nickel, manganese, zirconium, lanthanum, etc. Some examples of these results are shown in Figure 4. Since many studies on the immobilization of copper ions to polymer brushes have been conducted previously, it was judged that using copper ions for immobilization was preferable for comparison of the amount of immobilization. Also, since our theory is to adsorb VOCs gas through the vacant coordination site of copper, we need a target for comparison. Therefore, we confirmed the introduction characteristics of zinc metal ions with different amounts of coordination sites and the VOCs gas adsorption characteristics. In the VOCs adsorption experiment, the selection of the ion exchanger (functional

group) was determined by CCDC, and the combined result of acetone and metal ions through CCDC was derived from the range applicable to the experiments, therefore, the focus was mainly on acetone. Ligands capable of binding to copper ions were classified at CCDC results, and among them, ligands that were applied to experiments and had the potential to exhibit high metal immobilization properties were selected. Among the search results, CCDC Refcode HECYUJ [22] was chosen because it was estimated that metal ions (copper) were fixed to the ligand and bound to acetone stably. Figure 6 shows the molecular structure of CCDC Refcode HECYUJ. The final functional group was selected as 4-Picolylamine (4-AMP), which was pyridine-based chemicals with a structured structure similar to that of CCDC Refcode HECYUJ. The process of selecting 4-AMP using the results of the CCDC database is shown in Figure 7. 4-AMP possesses the characteristics of the amine group, and it seemed that it would facilitate the immobilization of metal ions. In addition, it was expected to show high introduction capability in the GMA with an epoxy group-grafted MNWF because it has an amino group [23]. The method of introducing functional groups was determined based on research data on the bonding of metal ions with 4-AMP or 2-picolylamine, similar to 4-AMP's molecular structure [24-27]. The introduction of 4-AMP was performed by reacting at a concentration of 1M at a temperature of 80 °C for 24 hours.

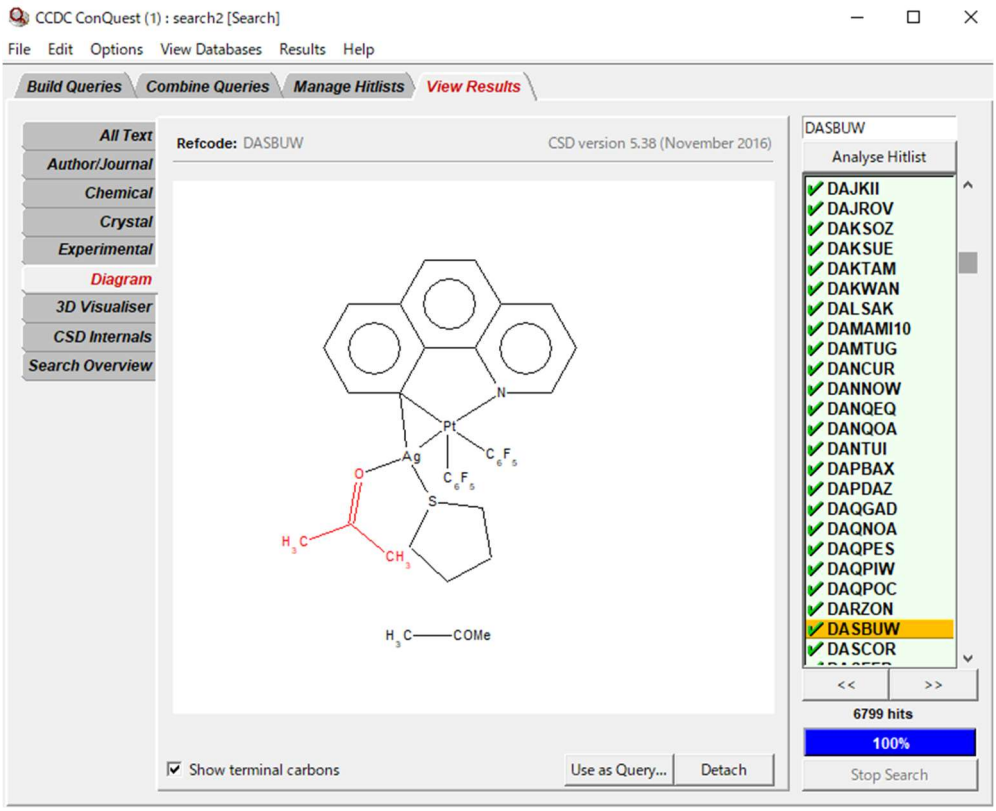

Figure 2- 1. Cambridge Crystallographic Data Center (CCDC).

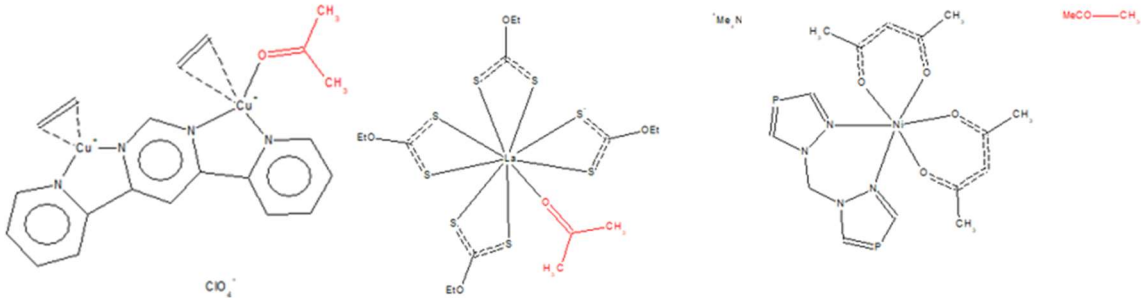

Figure 2- 2. Acetone-metal-ligand search results through CCDC.

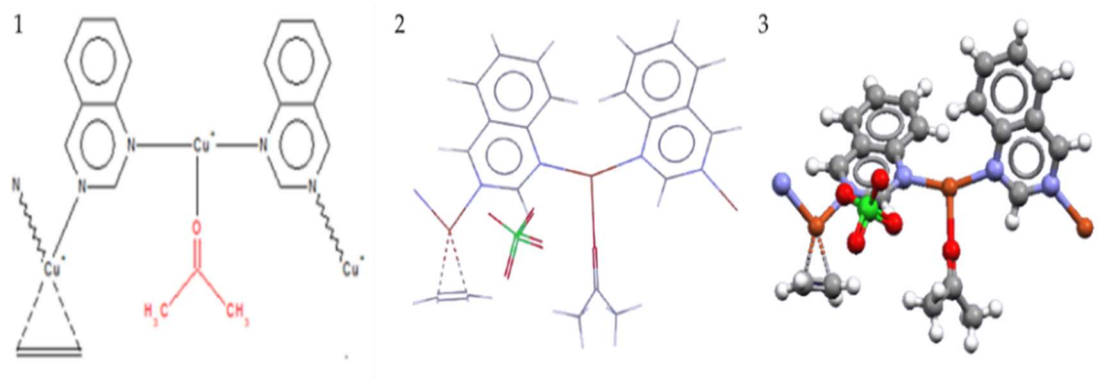

Figure 2- 3. Image of referenced CCDC data (Refcode: HECYUJ, 1: 2D image, 2: 3D image, 3: 3D image).

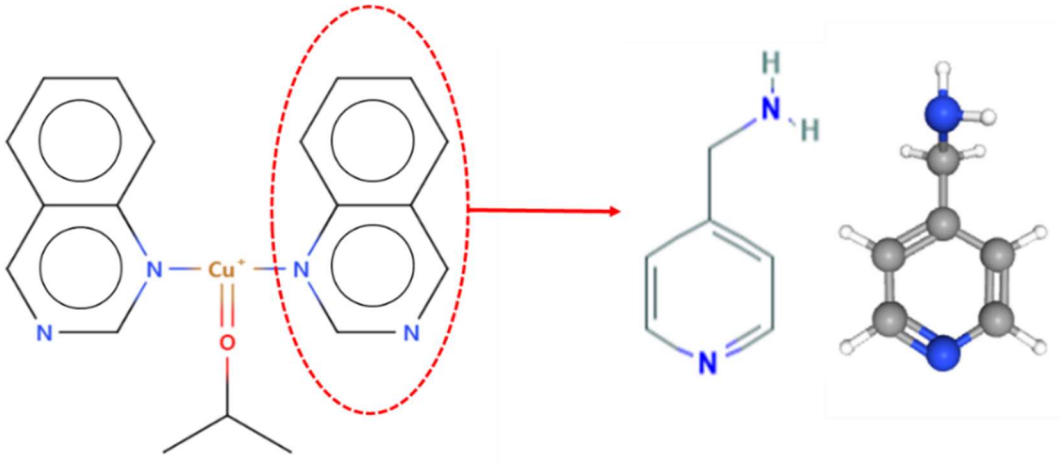

Figure 2- 4. 4-picolylamine's selection process (CCDC Refcode: HECYUJ).

Table 2- 1. Introduction of 4-AMP in the GMA MNWF

Grafting	
Degree of grafting	30~523%
Introduction of 4-picolylamine	
Concentration of 4-picolylamine	1 M
pH	10.5 – 11.5
Reaction temp	353 K
Reaction time	24 h

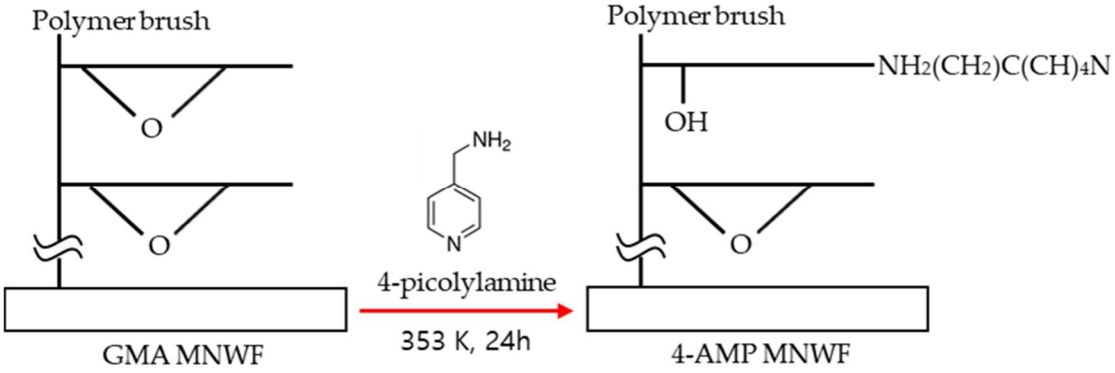

Figure 2- 5. 4-picolylamine introduction process image.

2.2.3. Metal ion immobilization conditions

The experimental method of the study with high copper ion immobilization efficiency was consulted. The referenced research used an iminodiacetate (IDA) group to immobilize copper ions by reacting 0.01 M CuSO4 aqueous solution at 30 °C [22]. The reference study showed the maximum amount of copper immobilization at a reaction time of 2 h. However, the substrate shape and functional group are different from the reference experiment in our case. Therefore, to confirm the maximum copper adsorption amount of GMA MNWF introduced with 4-AMP, the reaction time was changed from 2 hours to 24 hours, and a change in copper adsorption amount over time was observed. The copper ions were adsorbed to 4-AMP MNWF reacted with 1M HCl at a speed of 50 rpm at 25 °C for 2 h, eluted, and then diluted 10 times to measure through ICP-OES. As the reaction time was varied, the change in the amount of copper ion immobilization with time was observed. Table 2 shows the 4-AMP and copper ion immobilization conditions in the GMA-grafted MNWF.

Table 2- 2. Introduction of copper ion immobilization in the GMA MNWF

Copper immobilization condition	
Concentration of $CuSO_4$	0.01 M
Reaction temp	303 K
Reaction time	2-24 h

2.2.4. VOCs gas preparation

Acetone gas is made nitrogen-based. A small amount of acetone solution was inserted into a 50L Tedlar bag filled with nitrogen and vaporized to prepare acetone gas. After acetone evaporated, it was used in the experiment after stabilizing at least 12 h for stabilization. The prepared acetone gas was put together with the sample in a 5 L Tedlar bag, and the concentration change with time was observed through gas chromatography. The VOCs gas used in the experiment was used after giving it a stabilization time of at least 12 h after manufacturing. The concentration of the completed acetone gas was measured through the GASTEC detection tube, and the final concentration of the completed acetone gas was about 40 to 60 ppm. The Acetone absorption experiment was conducted at an average concentration of 50 ppm.

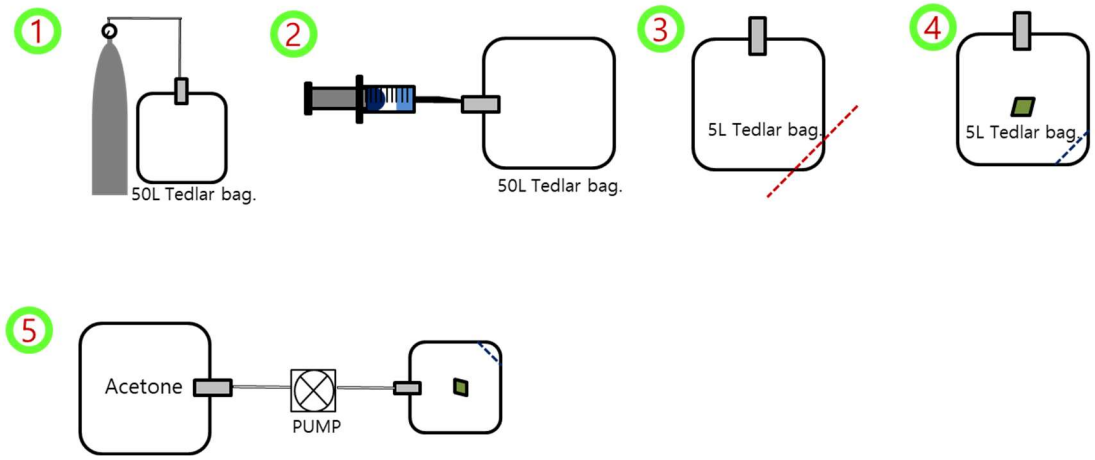

Figure 2- 6. Configuration of acetone gas adsorption experiment using Tedlar bag.

1. Fill the inside with nitrogen (About 40L)
2. Inject the acetone & formalin solution and wait for vaporization. (It gives a stabilization time of at least 12hours.)
3. Cut the corner of the Tedlar bag to create a space where the micriofiber nonwoven fabric can be inserted.
4. After putting the microfiber nonwoven fabric, reseal the cut-out part and make a vacuum state.
5. Use a pump to inject VOCs gas into a 4 L Tedlar bag.

2.2.5. The equation for deriving results

Checking the density of the 4-Picolylamine through the weight of the substrate is called the degree of grafting, and it can be obtained by the following Equation (1). In the case of this experiment, GMA was used as the monomer in all experiments, and the calculation of the amount of GMA introduced into the substrate is described in Equation (2).

$$Degree\ of\ graft\ (dg) = 100(W_1 - W_0)/W_0\ \ [\%] \tag{1}$$

$$Introduced\ GMA = [1000(W_1 - W_0)\ /\ 142.2]\ /\ W_0 \quad [mmol\ /\ g] \tag{2}$$

Here, W0 is the mass of the substrate polymer that has not been treated. W1 is the mass of the polymer after reacting with the GMA monomer. And, the value of 142.2 is the molecular weight of GMA [28].

When an 4-Picolylamine is introduced into the GMA substrate produced through the reaction of the GMA monomer, the 4-Picolylamine is fixed to the epoxy group of the GMA chain. Here, the molar conversion rate or the degree of functionalization of the epoxy group of the GMA chain to the 4-Picolylamine can be obtained from the following Equation (3).

$$Molar\ conversion\ rate = 100[(W_2 - W_1)/108]/[(W_1 - W_0)/142.2]\ [\%] \tag{3}$$

Where W_0 is the mass of the polymer that has not been treated, W_1 is the mass of the polymer after reacting with the GMA monomer. W_2 is the mass of the polymer after introducing an ion-exchange group (functional group) by adding it to the GMA-substrate's epoxy group. The value of 142.2 is the molecular weight of GMA, and the value of 108 is the 4-Picolylamine molecular weight.

The concentration of acetone gas prepared at a concentration of 50 ppm was 0.005%. Using this converted % concentration, it was changed to mg/L unit. Then the number of moles of each VOCs gas used in the experiment was obtained. Calculating the number of moles was converted using Equation (4):

$$Concentration\ of\ acetone\ gas\ [mg/L] = 0.005\left(\frac{M}{22.4}\right)\left(\frac{273}{273+T}\right)\left(\frac{P}{1013}\right) \tag{4}$$

Where 0.005 is a value converted from a unit of 50 ppm of acetone gas to a % unit. M is the molecular weight of acetone, in this case, 58.1. 22.4 is the volume of 1 mole of a molecule at 1 atm, 273 is a Kelvin value, T is the temperature used in the experiment, P is 1—the atmospheric pressure at the measurement point, and 1013 is the hPa value at 1 atmosphere.

Copper, which are metal ions introduced into 4-AMP, were eluted with 1M HCl, and quantitatively measured by ICP-OES. The final ppm value was determined by multiplying the result of ICP-OES by the volume V of the aqueous metal ion solution. The above method follows Equation (5).

$$Final\ metal\ ion\ Conc.\ [ppm] = ICP - OES\ result\ value\ [ppm] * V \quad (5)$$

The ppm value of final metal ion concentration obtained through ICP-OES was converted into [mg/L] and [g/L] through the following Equation (6) to get the [g] value.

$$x\ [ppm] = x\ [mg/L] = \frac{x}{1000}\ [g/L] = \frac{x}{1000000}\ [g] \quad (6)$$

The amount of metal ions converted into [g] values was divided by the molar mass of each metal ion [mol/g] and converted into units of mmol. The above method follows Equation (7).

$$Metal\ ion\ amount\ [mmol] = \frac{x/1000000\ [g]}{Metal\ ion\ molar\ mass\ [\frac{mol}{g}]} * 1000mM/M \quad (7)$$

After confirming the amount of metal ion in the mmol unit, it was divided by W_3, which is the mass of 4-AMP MNWF into which the metal ion was introduced, to finally obtain the value of the metal ion introduced per mass of MNWF. The above method follows Equation (8).

$$Metal\ ion\ introduced\ per\ mass\ of\ MNWF\ [mmol/g] = \frac{x\ [mmol]}{W_3\ [g]} \quad (8)$$

2.3. Results and Discussion

2.3.1. 4-Picolylamine introduction characteristics

A concentration of 1 M of 4-AMP was introduced into GMA MNWF with each degree of grafting, and the introduction characteristics of 4-AMP dependent on the degree of grafting were confirmed. 4-AMP introduced into GMA MNWF was performed through FT-IR peak analysis. Figure 2-7 shows the results of the FT-IR peaks of GMA MNWF and 4-AMP MNWF.

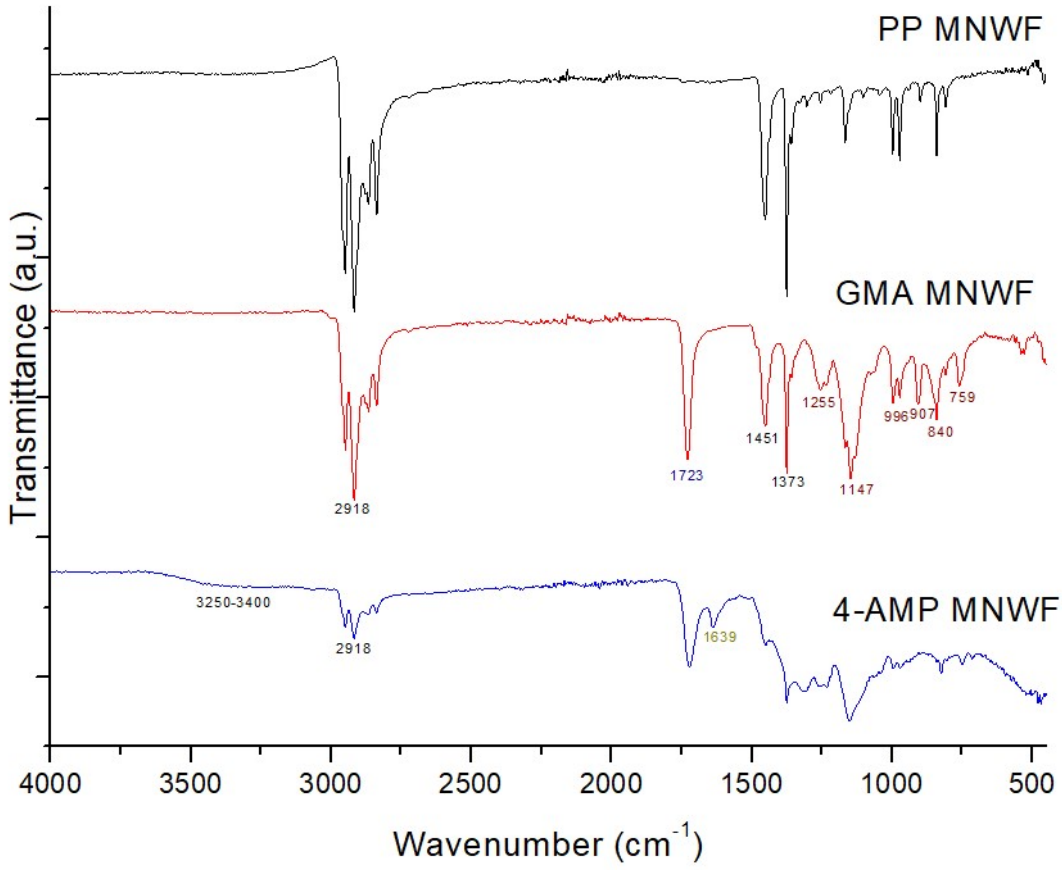

Figure 2- 7. FT-IR characterization of each functional MNWF.

Table 2- 3. Functional group IR peak of each MNWF

Wavenumber (cm^{-1})	Associated functional group	
759 – 1255	Epoxy group, Ester group	[29-34]
1373	-CH_3 vibration	[34-37]
1451	-CH_2 vibration	[37]
1552	Amide II, N-H stretch vibration	[31,38]
1639 - 1636	Amide I, N-H stretch vibration	[29,34,38]
1723-1721	C=O, carboxyl group (COOH) vibration	[31-38]
2918	C-H vibration	[34,36,37]
3250 – 3400	Hydroxyl group (-OH), N-H stretch	[30-37]

When GMA was introduced from the base substrate, PP MNWF, first, the C=O stretching peak of GMA was observed in the range of 1723-1721 cm^{-1} [31-38]. GMA's epoxy and ester groups were also observed at 759, 840, 907, 996, 1147, and 1255 cm^{-1} [29-34]. This confirms the introduction of GMA into the PP MNWF.

In the case of 4-AMP, the peaks of the epoxy and ester groups, which were strong in the peaks of GMA MNWF, are reduced. In addition, since the N-H stretching peak appeared newly at 1639-1636 cm^{-1}[29,34,38], it was confirmed that the introduction of 4-AMP was successful.

After it was confirmed that each functional group was introduced through the confirmation of the FT-IR peak, the amount of 4-AMP introduced depending on the degree of grafting was established. The degree of grafting used in this experiment was 30-523%, and the range was extensive, so it was expected to know the introduction characteristics of 4-AMP in more detail.

In the case of 4-AMP MNWF, a tendency toward the high introduction of 4-AMP was confirmed as the degree of grafting increased. The highest introduced 4-AMP density on MNWF was about 25.7 mmol/g at dg 523%. In general, there is a tendency to draw a saturation curve for materials with a high degree of grafting with a high functional group. However, in the case of 4-AMP, even the MNWF of 523% of the degree of grafting showed a proportionally increasing R-squared value with a

reliability of 0.99. This is presumed to be due to the introduction of 4-AMP, which has a small molecular size, to the characteristics of the newly attempted microfiber nonwoven fabric. Although it is a non-woven fabric, it is judged that many GMA and 4-AMP, which are woven with microfibers and distributed over a large surface area, react and show a continuously increasing trend. These results are shown in Figure 2-8.

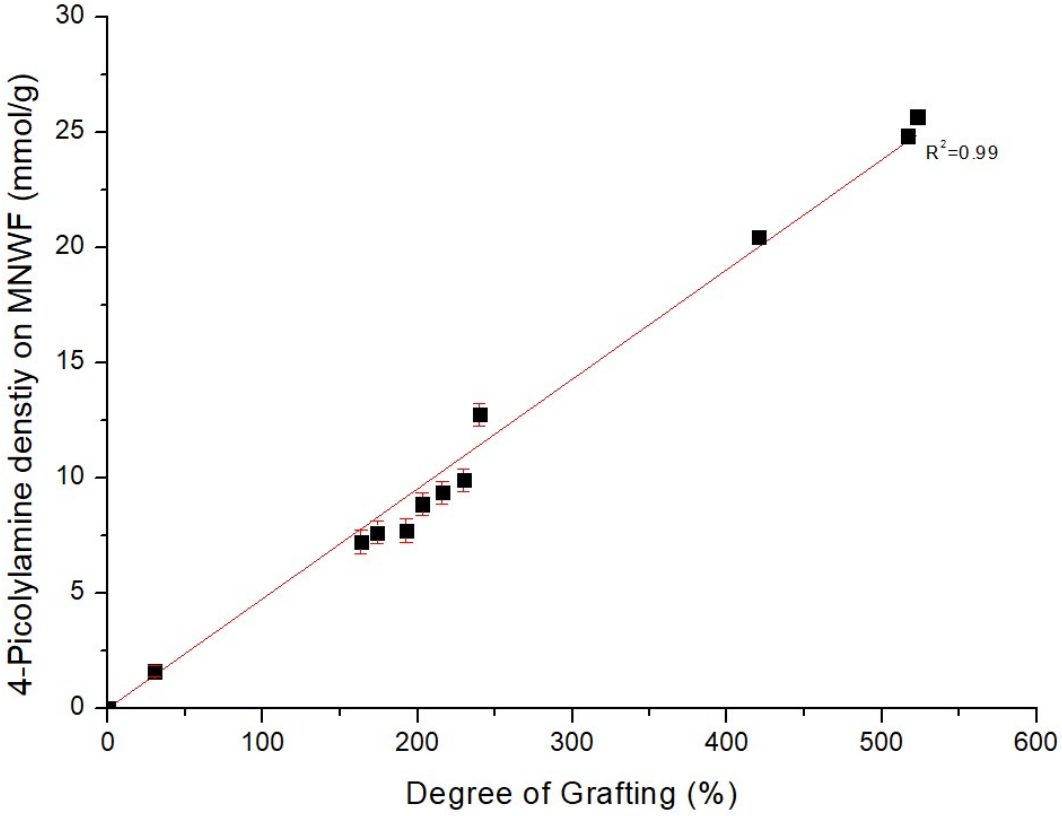

Figure 2- 8. Introduction of 4-AMP on GMA MNWF according to degree of grafting.

From all results, the molar conversion rate of 4-AMP MNWF from GMA-grafted MNWF was around 63% on average, maintaining a high level without significant change.

Also, visually distinguishable color changes were observed as 4-AMP was introduced into MNWF with a higher degree of grafting. The color of the 4-AMP-incorporating MNWF became darker as the degree of grafting increased. In MNWF, which has a range of 30-200% of the degree of grafting, it was possible to observe that the color became darker with the naked eye. And in the case of MWNF, which has a degree of grafting of 200% or more, the difference could not be distinguished with the naked eye. The color change of the MNWF, depending on dg, is shown in Figure 2-9.

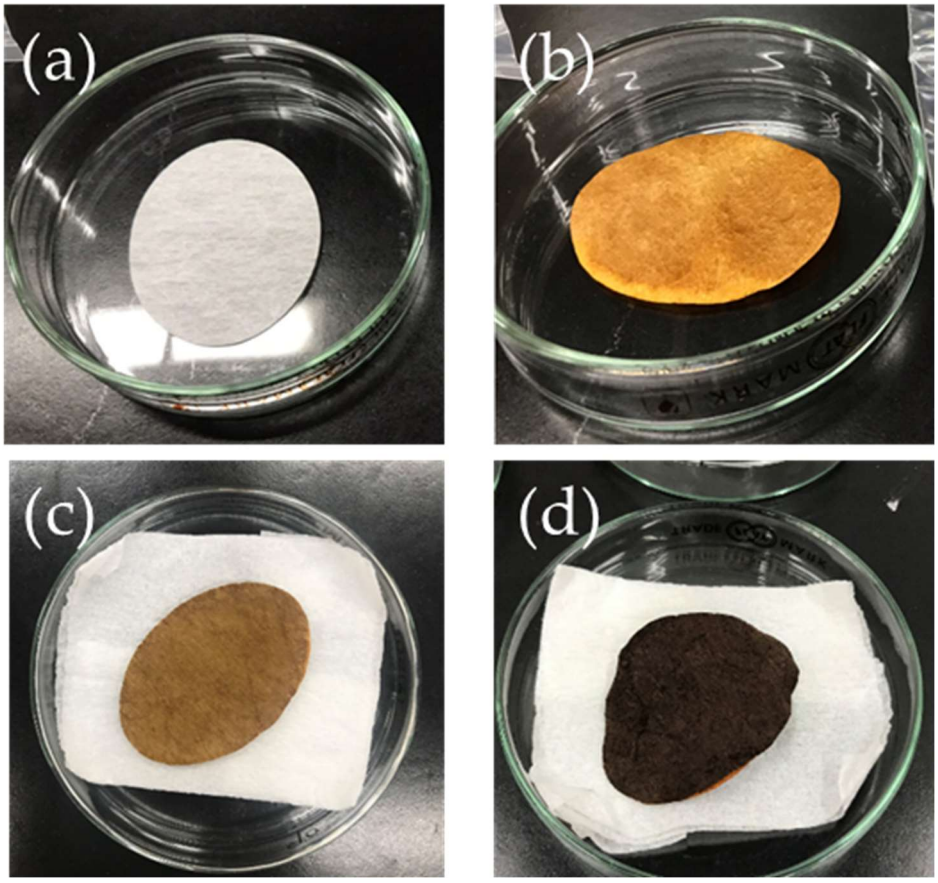

Figure 2- 9. Color change of MNWF depending on the degree of grafting (a): dg 100% GMA MNWF, (b): dg 100% 4-AMP MNWF, (c): dg 170% 4-AMP MNWF, (d): dg 200% 4-AMP MNWF.

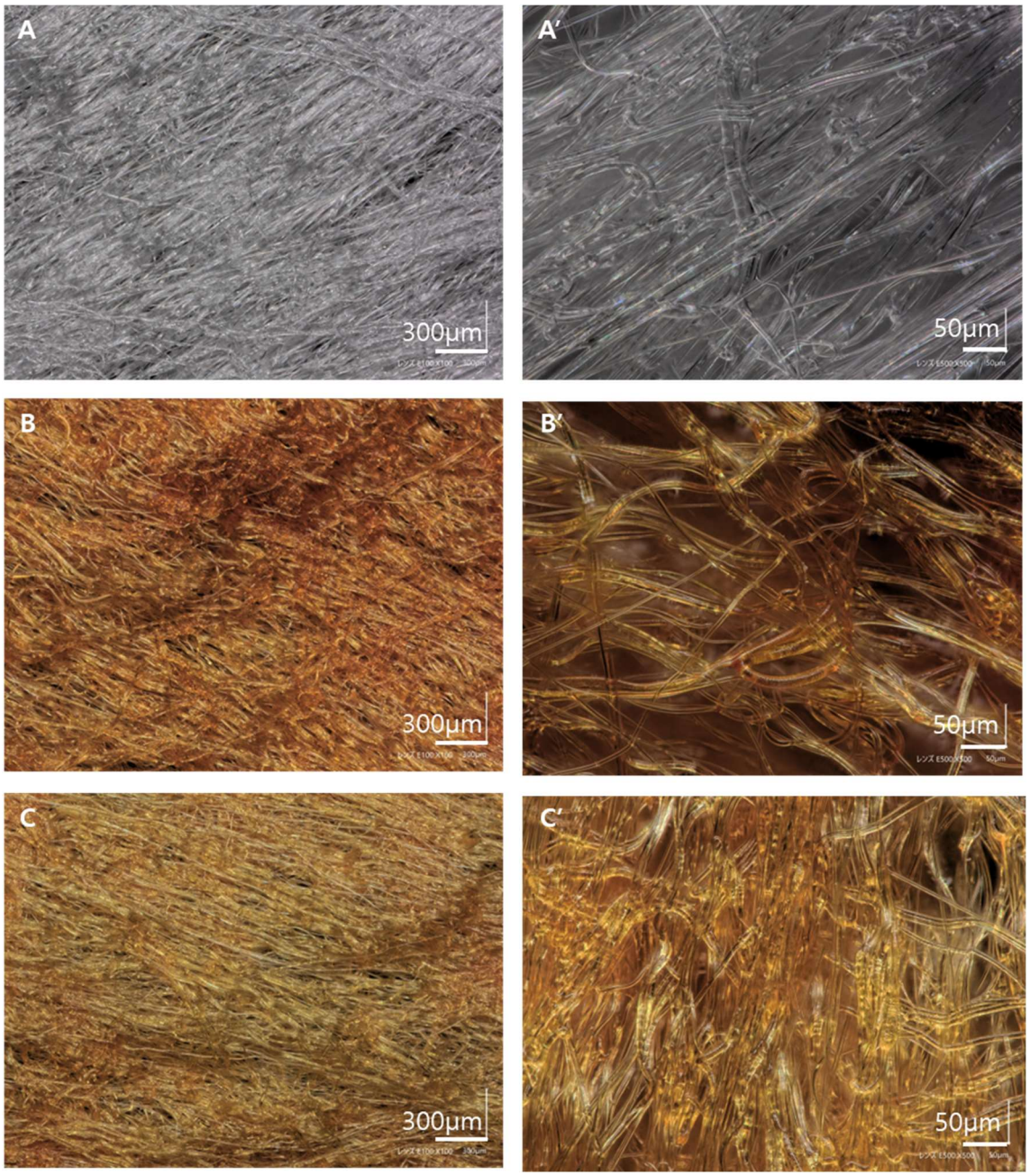

Figure 2- 10. Digital micro scope image of GMA, 4-AMP, 4-AMP-Cu MNWF (Each of MNWF's dg is 90%)

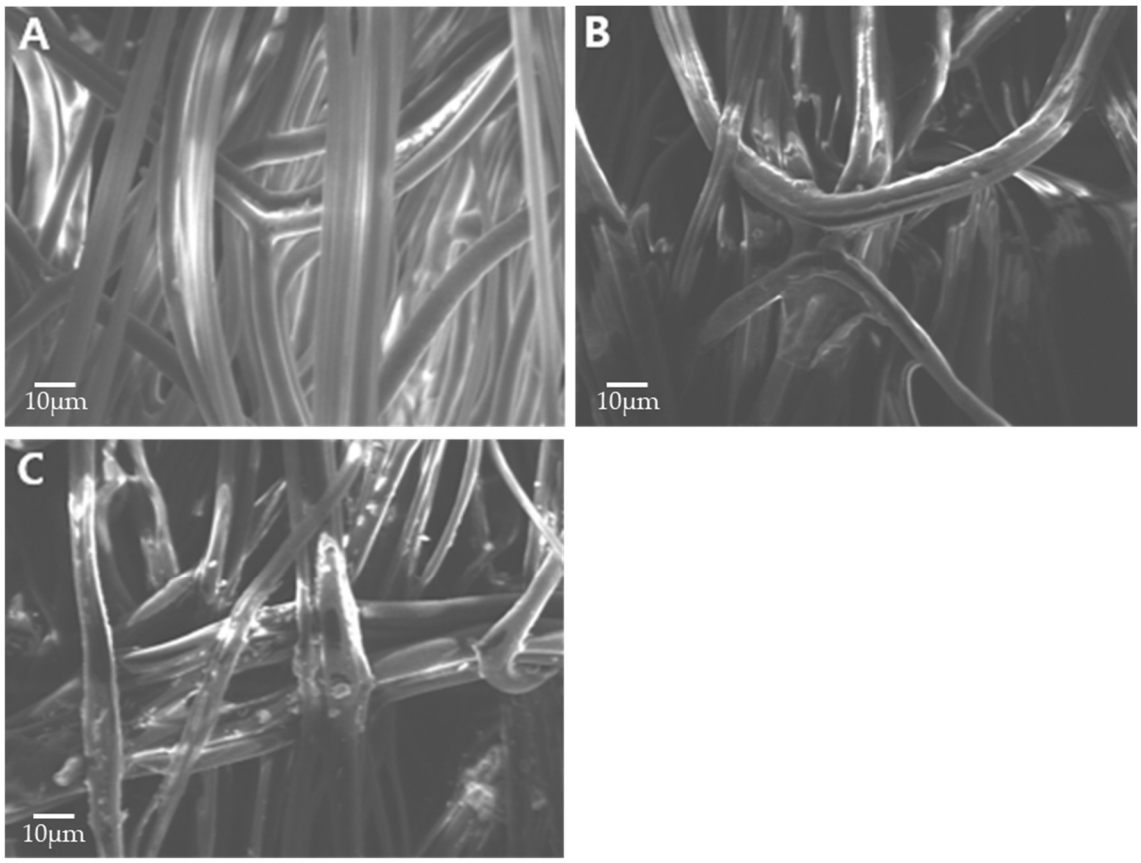

Figure 2- 11. FE-SEM characterization. (A: GMA MNWF, B: 4-AMP MNWF, C: 4-AMP-Cu MNWF. Each of MNWF's dg is 170%).

After observing the appearance, SEM images and digital microscope images of GMA, 4-AMP, 4-AMP with copper (4-AMP-Cu) introduced MNWF, respectively, were observed. After introducing 4-AMP as a functional group, a color change occurred in MNWF, however, no fiber morphology's difference was observed.

As 4-AMP was introduced in GMA MNWF, the weight of MNWF showed a change of about 13-44%, and when copper was introduced in 4-AMP MNWF, a weight change of 0-11% was observed. However, a slight weight increase was observed after each step, but the difference in surface area was not significant.

Figure 2-10 shows Digital microscope images of GMA MNWF, 4-AMP MNWF, and 4-AMP-Cu MNWF. And Figure 2-11 shows each MNWF's SEM images.

2.3.2. Metal ion introduction characteristics

2.3.2.1. Copper

First, the change in copper ion immobilization amount over time is observed and shown in Figure 22. In the copper ion immobilization reaction over time, the 4-AMP MNWF reacted for 24 h can immobilize much more.

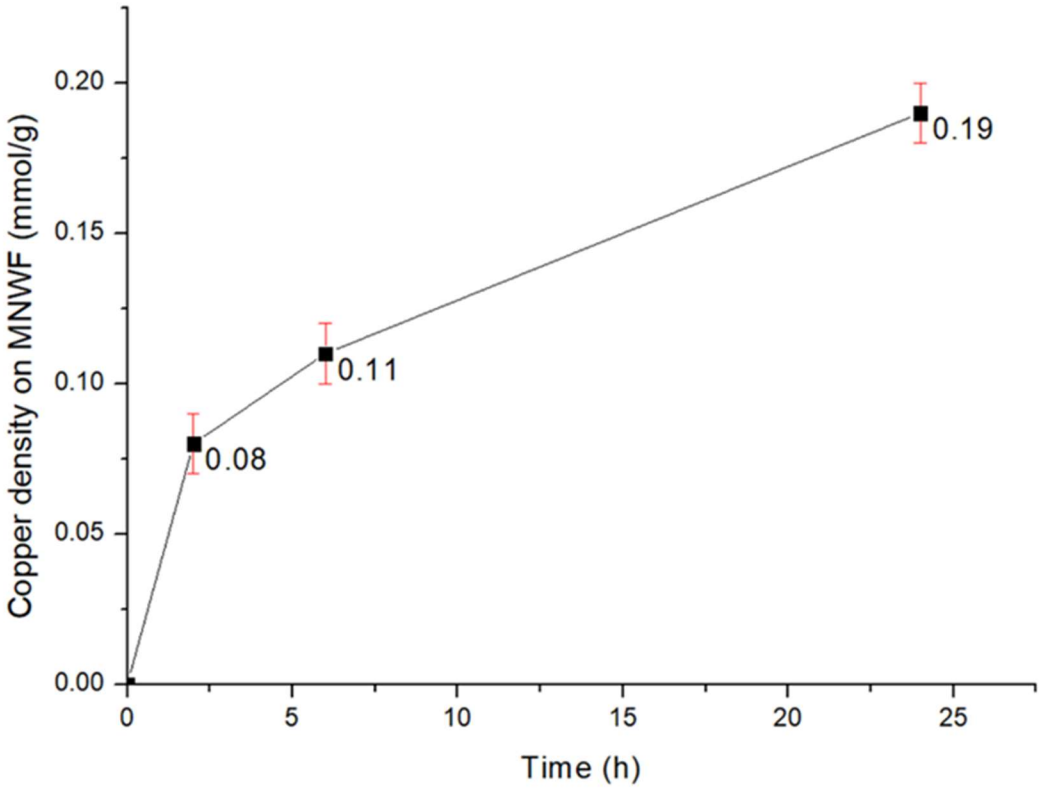

Figure 2- 12. Change in copper ion immobilization amount over time (dg 30% 4-AMP MNWF).

As a result, Figure 2-11 does not confirm whether the amount of copper ion adsorption is in a saturated state; there is a possibility that a higher adsorption amount may appear when it reacts with copper ions for more than 24 h. However, this study is not aimed at observing the maximum adsorption amount of copper ions. In addition, considering that the production process of each functional nonwoven fabric is required in units of 24 h, the adsorption time of copper ions was set to a maximum of 24 h for efficient time distribution.

After fixing the copper reaction time to 24 h, the change in the amount of copper ion adsorption according to the amount of 4-AMP introduced is shown in Figure 2-12.

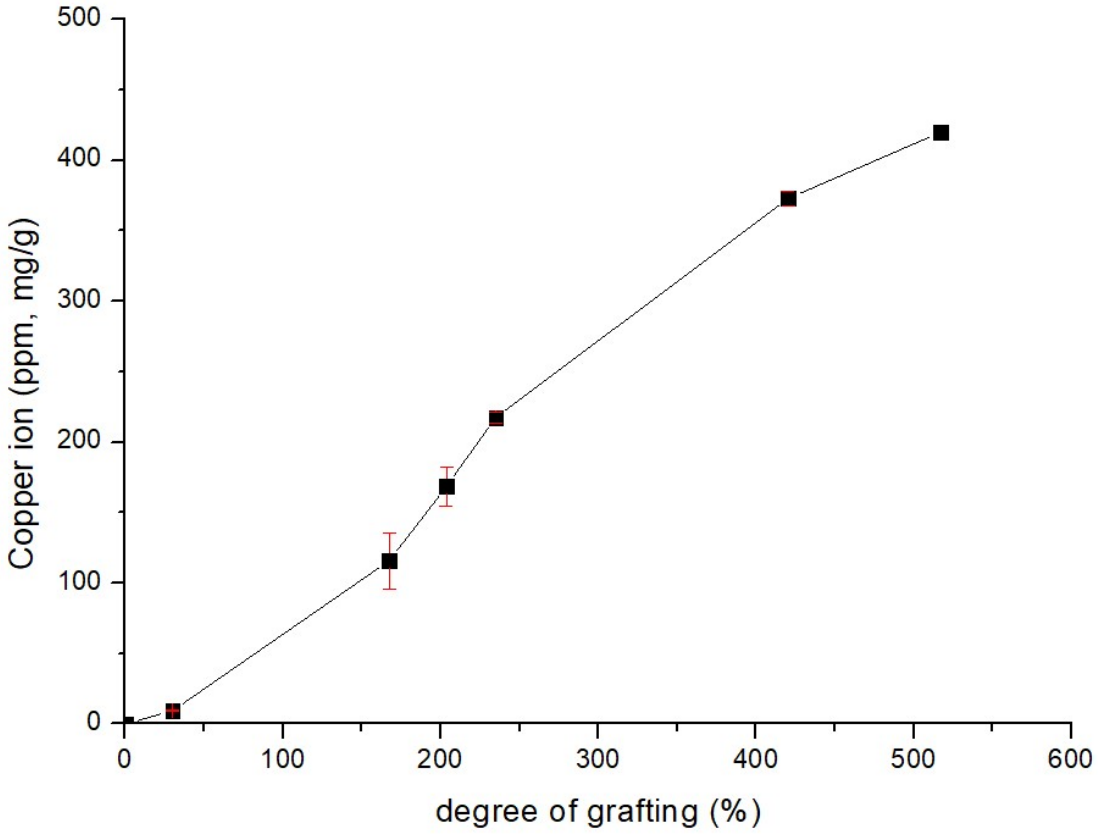

Figure 2- 13. copper ion introduct amount depending on the degree of grafitng

The amount of copper adsorption according to the degree of grafting of 4-AMP MNWF was quantitatively confirmed through ICP-OES. As a result, the copper adsorption amount tended to increase as the degree of grafting increased. These results are shown in Figure 2-13.

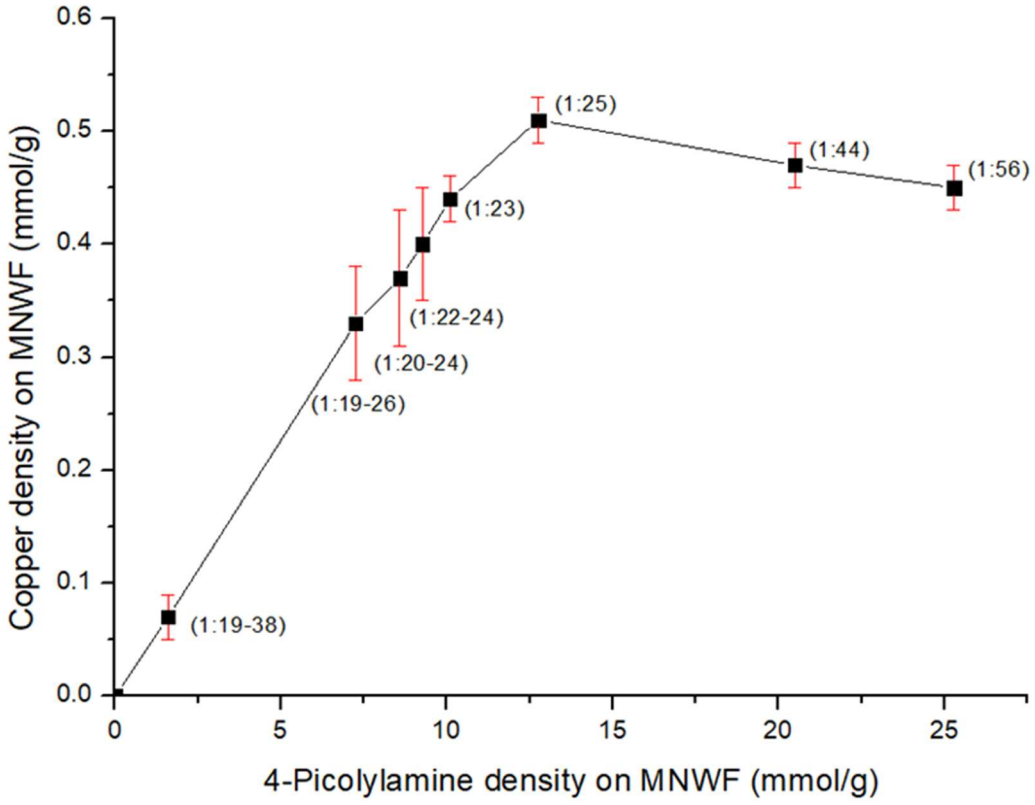

Figure 2- 14. Dependence of copper ion density on 4-AMP density (the content in parentheses is the ratio of Cu mole:4-AMP mole).

Figure 2-14 is a graph with the x-axis changed to 4-picolylamine density, and the y-axis changed to immobilized copper density. Comparing and calculating the ratio number of the copper ions moles depending on the number of moles of 4-AMP, the maximum copper ion immobilization amount was confirmed when the density of the amount of 4-AMP was about 12.75 mmol/g. The highest adsorption was found at dg 240%. At this time, copper ions were immobilized at 0.51 mmol/g. Afterward, the total amount of copper adsorption increases, but the amount of copper introduced does not keep up with the amount of 4-AMP, so it is estimated that a saturation curve appears, as shown in Figures 2-14. According to the reference literature, the copper adsorption amount was 0.42-0.44 mmol/g for IDA-Cu [22] and 0.55 mmol/g for EDA-Cu [40], indicating the copper performance of 4-AMP was satisfactory.

In the case of 4-AMP-Cu MNWF (dg 160–200%), the copper ion immobilization amount was 0.30–0.44 mmol/g, and 4-AMP was 7–10 mmol/g. At this time, the ratio of copper ions to 4-AMP was 1:20–24. The total adsorption amount of copper was lower than dg 240% 4-AMP-Cu MNWF, but the ratio of copper to 4-AMP decreased,

which is thought to have been introduced with the appropriate binding force at the desired level.

A decreasing trend was observed after showing the maximum copper ion immobilization amount in dg 240% 4-AMP MNWF. From the analysis of the results, when each 4-AMP is 21, 25 mmol/g, the immobilized amount of copper ions is 0.44, 0.47 mmol/g, and the ratio of copper ion to 4-AMP is 1:44 and 1:56.

The following assumptions can be made as to the reason for the decrease in the efficiency of the immobilization of copper ions. This appears to be a phenomenon because the increased rate of the copper ion introduced does not keep up with the increased rate of the 4-AMP. It seems that the immobilization of copper ions is somewhat hindered when 4-AMP is present at too high a density. The copper ion density results depend on 4-AMP density; the copper ion immobilization efficiency seems to be the most effective when the ratio is about 1:20–25.

2.3.3. VOCs gas absorption characteristics

MNWF introduced with GMA, 4-AMP, and 4-AMP-metal was put in a 5 L Tedlar bag, and 4 L acetone gas was injected to measure changes over time at room temperature. In the preliminary experiment stage, the acetone gas concentration inside the Tedlar bag tended to decrease to 1 h from the start of the reaction, and since it was confirmed that the acetone gas concentration inside the Tedlar bag increased again after 1 h, the maximum time for the adsorption reaction was set to 1 h. In the case of the change in adsorption amount, 2 mL of acetone gas inside the Tedlar bag was extracted for predetermined times at intervals of 10, 20, 40, and 60 min, and the concentration change was measured by gas chromatography. In the desorption process, the maximum observation time was set equal to 1 h, and the amount of change was checked every 30 min.

2.3.3.1. Acetone

2.3.3.1.1. Each MNWF's acetone gas adsorption

After putting the prepared acetone gas in a 5 L Tedlar bag, the change in the acetone gas concentration in the absence of a functional MNWF was first checked. The acetone gas concentration was changed by about 1–10% in the state where the functional MNWF was not added. For each functional MNWF, GMA, 4-AMP, 4-AMP-Cu and 4-AMP-Zn were used, and the results are shown in Figure 2-15. In the case of the GMA MNWF, there was virtually no adsorption capacity considering the variability (10%) when nothing was added. As for 4-AMP MNWF, the maximum adsorption amount was about 20–30% of the total acetone gas concentration, and the adsorption performance was not excellent. 4-AMP-Cu MNWF could adsorb up to 50% of acetone gas, about two times that of 4-AMP MNWF. Even if the correction value was applied, it was about 40%, which showed higher efficiency than 4-AMP MNWF. Each functional MNWF reached the maximum adsorption amount about 10 min after the acetone gas ad-sorption reaction and then maintained the adsorption level until 1 h after the beginning of the reaction. The above results confirmed that 4-AMP MNWF and 4-AMP-Cu MNWF could adsorb acetone gas at room temperature, and 4-AMP-Cu MNWF has better acetone gas adsorption efficiency.

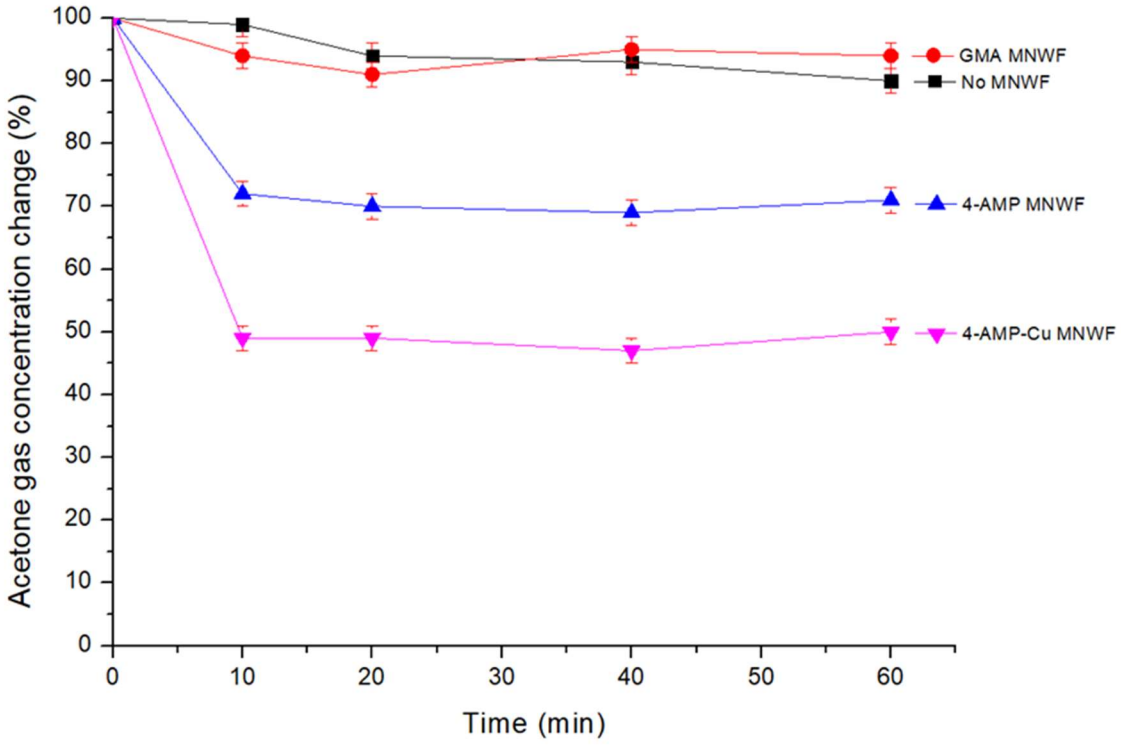

Figure 2- 15. Acetone gas adsorption amount of each MNWF (about 50 ppm, dg 170% MNWF).

The change in acetone gas adsorption amount depending on the dg of copper immobilized MNWF is shown in Figure 2-16. The data used in Figure 2-16 were prepared using those with good ratios of copper and 4-AMP among samples in 4-AMP-Cu MNWF of average dg 40, 100, 170, and 240%. The maximum acetone gas adsorption of 4-AMP-Cu MNWF was observed at dg 170% (Cu:4-AMP, 1:20). In the dg 160–200% 4-AMP-Cu MNWF, which showed the highest efficiency in copper ion adsorption, acetone gas also showed the maximum adsorption amount; after that, it decreased. The hypotheses for the adsorption reduction of acetone gas at 4-AMP-Cu MNWF depending on dg change can be considered follows. The most critical factor in the prepared 4-AMP-Cu MNWF is that acetone is adsorbed to the vacant coordination sites of copper ions immobilized to MNWF. When the dg is too high, too much 4-AMP is introduced, and more 4-AMP is bound to each copper ion, which causes the absence of coordination sites of copper ions. For low dg 4-AMP-Cu MNWF, the copper to 4-AMP ratio sometimes yields similar results to high dg 4-AMP-Cu MNWF. However, since the absolute amount of copper ions immobilized is insufficient, copper ion coordination sites that can bind acetone gas are also lacking. Thus, the 4-AMP-Cu MNWF of too-low dg or too-high dg results is similar to the adsorption amount of 4-AMP MNWF in which copper is not immobilized. Combining

the above assumptions and results, when preparing 4-AMP-Cu MNWF for acetone gas adsorption, the appropriate dg of MNWF is 160–200%, and the immobilized copper ion and the 4-AMP ratio is 1:20 or less.

According to Equation (4), the value of mg/L of acetone inside the Tedlar bag was calculated, and the total amount was confirmed. And, it was confirmed that the concentration of 4L of 50 ppm acetone gas injected into the 5 L Tedlar bag was 0.48 mg/L. The dg 170% 4-AMP-Cu MNWF showed the highest acetone gas adsorption, about 0.04 mmol/g-4-AMP-Cu MNWF, and the ratio of copper ion to adsorbed acetone was 1:10.

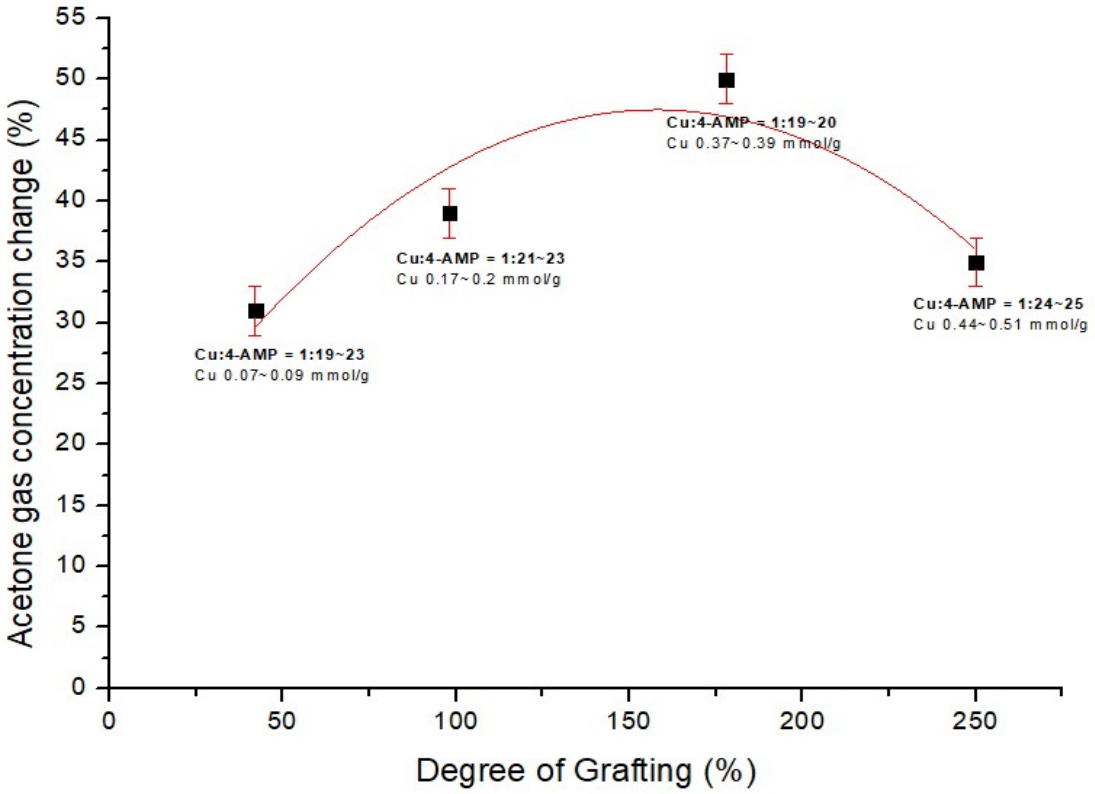

Figure 2- 16. Dependence of acetone gas adsorption on the degree of grafting (about 50 ppm).

2.3.3.1.2. 4-AMP-Cu MNWF's acetone gas desorption

After 1 h of the adsorption experiment, the acetone gas inside the Tedlar bag was re-moved using a vacuum pump, and a vacuum state was created. After that, the change in acetone gas concentration was observed by filling it with fresh air. The desorption process of 4-AMP-Cu MNWF was measured by gas chromatography by extracting 2 mL of gas at 30 and 60 min after the start of the reaction, respectively. The air used in the experiment had an initial acetone gas concentration of about 3% (based on 50 ppm). Additionally, the concentration of acetone gas in the Tedlar bag without functional MNWF fluctuated up to 13%. Therefore, in the experimental stage, it was assumed that about 3 to 13% of acetone gas was already present in the Tedlar bag, and the experiment results were confirmed. 4-AMP-Cu MNWF of dg 170% (Cu: 0.37 mmol/g, 1:20), which showed the best results in the adsorption experiment, was used in the desorption experiment. The time-dependent acetone gas desorption change is shown in Figure 2-17.

In the case of dg 170% 4-AMP-Cu MNWF used in the experiment, it was confirmed that about 43% of gas was desorbed based on a 50 ppm concentration of acetone gas in the desorption process of 1 h. Even excluding the maximum correction value of acetone gas of 13%, which was considered to exist initially, it showed a desorption value of 30%. Since the amount of change in the adsorption and desorption processes was confirmed based on the acetone gas concentration of 50 ppm, the respective results were compared together. Compared to the maximum adsorption amount of acetone gas of 50%, 43/50 (using the correction value, 30/40), or about 86% (using the correction value, 75%) of the adsorption amount was desorbed. The desorption experiment performed at room temperature confirmed that the acetone gas adsorbed to the 4-AMP-Cu MNWF was easily desorbed without a separate separation process. This confirmed that the 4-AMP-Cu MNWF and the ace-tone gas had an appropriate binding level. It is judged that such an appropriate binding level can be advantageous for recycling because additional costs and processes are not required in adsorption and desorption.

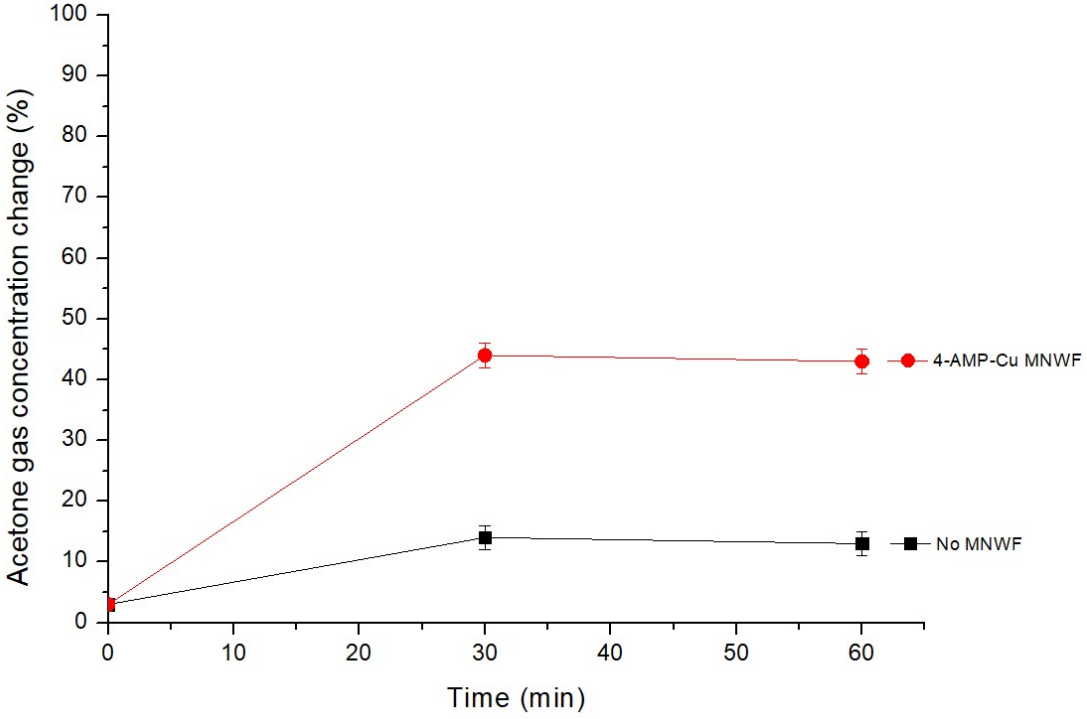

Figure 2- 17. Acetone gas desorption amount of 4-AMP-Cu MNWF (about 50 ppm).

2.3.3.1.3. Reuse experiment of copper immobilized MNWF

Reuse testing was performed using dg 170% 4-AMP-Cu MNWF, which exhibited the highest acetone gas adsorption rate. In each reuse experiment, adsorption and desorption were performed as one process, and this process was repeated three times. In the secondary adsorption, the adsorption rate compared to the total acetone gas concentration de-creased by about 7% compared to the primary adsorption (50% -> 43%). Similarly, in the third experiment, the adsorption amount decreased by about 6% compared to the adsorption in the second experiment (43% -> 37%).

The adsorption amount of acetone gas for each cycle is shown in Figure 2-18.

As the cycle progressed, the adsorption efficiency tended to decrease slightly. The decrease in adsorption efficiency appears to be due to the strong binding of some acetone gases to 4-AMP-Cu MNWF, resulting in limited desorption.

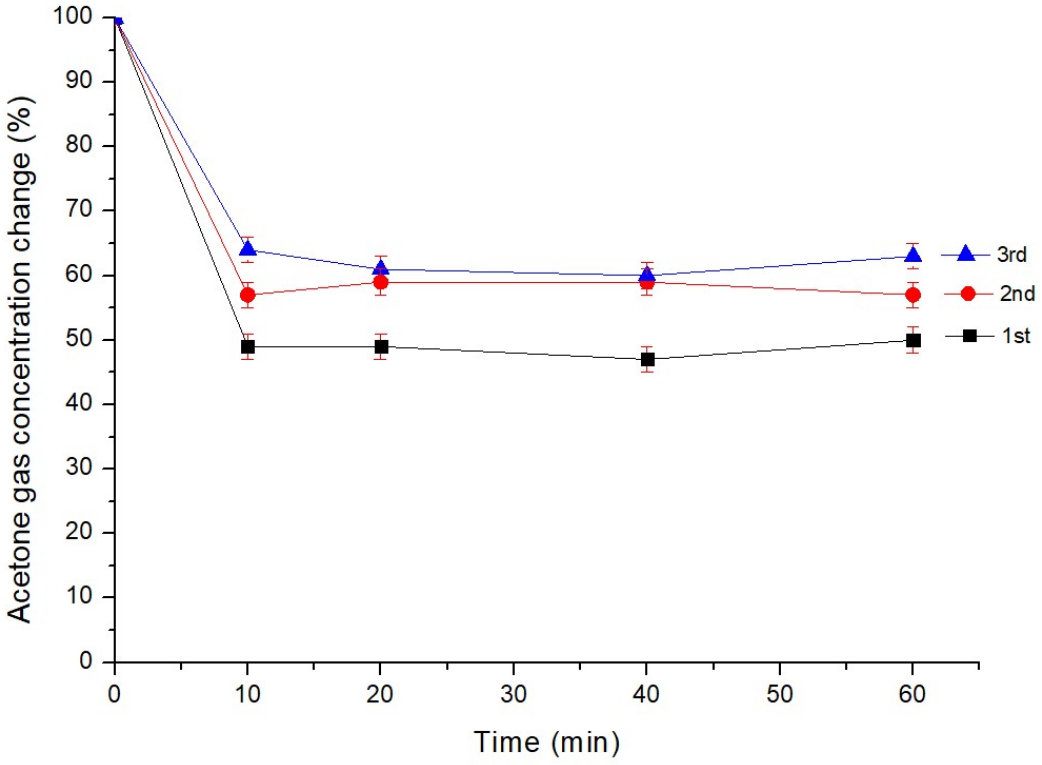

Figure 2- 18. Acetone gas adsorption amount for reuse tests (dg 170% 4-AMP-Cu, 50 ppm).

2.4. Conclusion

This study started from the possibility that VOCs could be efficiently removed and adsorbed by introducing metal ions into microfiber nonwoven fabric, focusing on how metal oxide-based sensors can remove and adsorb VOCs. To be repeatedly used at room temperature, MNWF of polypropylene with good physical durability was used as a base material, and a functional group was estimated to be capable of adsorbing VOCs in a state of immobilized metal ions was selected through the Cambridge Crystal Data Center (CCDC).

In the case of the functional group 4-AMP, selected according to CCDC metal com-plex data, a large amount was introduced while maintaining a high mole conversion rate (avg 63%) even at a high degree of grafting (dg) MNWF. When the ratio of copper ions to 4-AMP was 1:25 at dg 240% 4-AMP-Cu MNWF, the maximum immobilized amount of copper ions was 0.51 mmol/g.

Both adsorption and desorption experiments of acetone gas, one of the volatile organic compounds (VOCs), were conducted at room temperature, and up to 50% of gas could be adsorbed at a concentration of about 50 ppm of acetone gas. The maximum adsorption amount of acetone gas was observed when the dg of 4-AMP-Cu MNWF was 160–200%, and the ratio of copper ions to 4-AMP was 1:20. When the maximum amount of acetone gas adsorption was observed, 4-AMP-Cu MNWF could adsorb about 0.04 mmol/g- 4-AMP-Cu-MNWF at room temperature, and the ratio of copper ions to adsorbed acetone was 1:10. In addition, most adsorption acetone gases are desorbed by about 86% of the adsorption amount just by being exposed to the air, without a separate process.

VOCs gas absorption experiment through the 4-AMP-Cu MNWF is an initial stage of technology development capable of adsorbing and desorbing VOCs using a ligand containing metal ions. However, for 4-AMP-Cu MNWF, more research is needed because it was confirmed that volatile organic compounds could be repeatedly adsorbed and desorbed at room temperature. Optimal 4-AMP introduction conditions must be identified, and studies on selective adsorption with other metal ions or VOCs are also needed.

2.5 Reference

1. Zhu, L.; Shen, D.; Luo, K.H. A critical review on VOCs adsorption by different porous materials: Species, mechanisms and modification methods. J. Hazard. Mater. **2020**, 389, 122102.
2. Li, X.; Zhang, L.; Yang, Z.; Wang, P.; Yan, Y.; Ran, J. Adsorption materials for volatile organic compounds (VOCs) and the key factors for VOCs adsorption process: A review. Sep. Purif. Technol. **2020**, 235, 116213.
3. He, C.; Cheng, J.; Zhang, X.; Douthwaite, M.; Pattisson, S.; Hao, Z. Recent Advances in the Catalytic Oxidation of Volatile Organic Compounds: A Review Based on Pollutant Sorts and Sources. Chem. Rev. **2019**, 119, pp. 4471–4568.
4. Rene, E.R.; Murthy, D.; Swaminathan, T. Performance evaluation of a compost biofilter treating toluene vapours. Process Biochem. **2005**, 40, pp. 2771–2779.
5. Li, Y.; Chang, H.; Yan, H.; Tian, S.; Jessop, P.G. Reversible Absorption of Volatile Organic Compounds by Switcha-ble-Hydrophilicity Solvents: A Case Study of Toluene with N, N-Dimethylcyclohexylamine. ACS Omega **2020**, 6, pp. 253–264.
6. Enesca, A.; Cazan, C. Volatile Organic Compounds (VOCs) Removal from Indoor Air by Heterostruc-tures/Composites/Doped Photocatalysts: A Mini-Review. Nanomaterials **2020**, 10, 1965.
7. Shah, K.W.; Li, W. A Review on Catalytic Nanomaterials for Volatile Organic Compounds VOC Removal and Their Appli-cations for Healthy Buildings. Nanomaterials **2019**, 9, 910.
8. Chi, C.; Chen, W.; Guo, M.; Weng, M.; Yan, G.; Shen, X. Law and features of TVOC and Formaldehyde pollution in urban indoor air. Atmos. Environ. **2016**, 132, pp. 85–90.
9. Kalapos, M.P. Acetone, Encyclopedia of Toxicology, 3rd ed.; Academic Press: Cambridge, MA, USA, **2014**, pp. 36–39.
10. Xu, X.; Chen, Y.; Zhang, G.; Ma, S.; Lu, Y.; Bian, H.; Chen, Q. Highly sensitive VOCs-acetone sensor based on Ag-decorated SnO2 hollow nanofibers. J. Alloy. Compd. **2017**, 703, pp. 572–579.
11. Galassetti, P.R.; Novak, B.; Nemet, D.; Rose-Gottron, C.; Cooper, D.M.; Meinardi, S.; Newcomb, R.; Zaldivar, F.; Blake, D.R. Breath ethanol and acetone as indicators of serum glucose levels: An initial report. Diabetes Technol. Ther. **2005**, 7, pp. 115–123.
12. Wang, Z.; Wang, C. Is breath acetone a biomarker of diabetes? A historical review on breath acetone measurements. J. Breath Res. **2013**, 7, 037109.

13. Wang, C.; Sahay, P. Breath analysis using laser spectroscopic techniques: Breath biomarkers, spectral fingerprints, and de-tection limits. Sensors **2009**, 9, pp. 8230–8262.
14. Marcondes-Braga, F.G.; Gutz, I.G.R.; Batista, G.L.; Saldiva, P.H.N.; Ayub-Ferreira, S.M.; Issa, V.S.; Mangini, S.; Bocchi, E.A.; Bacal, F. Exhaled acetone as a new biomarker of heart failure severity. Chest **2012**, 142, pp. 457–466.
15. Obeidat, Y. The Most Common Methods for Breath Acetone Concentration Detection: A Review. IEEE Sens. J. **2021**, 21, 14540–14558.
16. Kalidoss, R.; Umapathy, S. An overview on the exponential growth of non-invasive diagnosis of diabetes mellitus from exhaled breath by nanostructured metal oxide Chemi-resistive gas sensors and μ-preconcentrator. Biomed. Microdevices **2020**, 22, 2.
17. Lekha. S.; M. Suchetha. Recent Advancements and Future Prospects on E-Nose Sensors Technology and Machine Learning Approaches for Non-Invasive Diabetes Diagnosis: A Review. IEEE Rev. Biomed. Eng. **2021**, 14, pp. 127–138.
18. Martinez, E.P.A.; Osuna, V.; Dominguez, R.B.; Márquez-Lucero, A.; Zaragoza-Contreras, E.A.; Vega-Rios, A. Room Temper-ature Detection of Acetone by a PANI/Cellulose/WO3 Electrochemical Sensor. J. Nanomater. **2018**, 2018, 6519694
19. Dey, A. Semiconductor metal oxide gas sensors: A review. Mater. Sci. Eng. B **2018**, 229, pp. 206–217.
20. Mirzaei, A.; Kim, S.S.; Kim, H.W. Resistance-based H2S gas sensors using metal oxide nanostructures: A review of recent advances. J. Hazard. Mater. **2018**, 357, pp. 314–331.
21. Gardon, M.; Guilemany, J.M. A review on fabrication, sensing mechanisms and performance of metal oxide gas sensors. J. Mater. Sci. Mater. Electron. **2013**, 24, pp. 1410–1421
22. Iwata, H.; Saito, K.; Furusaki, S.; Sugo, T.; Okamoto, J. Adsorption Characteristics of an Immobilized Metal Affinity Mem-brane. Biotechnol. Prog. **1991**, 7, pp. 412–418
23. Munakata, M.; Kuroda-Sowa, T.; Maekawa, M.; Nakamura, M.; Akiyama, S.; Kitagawa, S. Architecture of 2D Sheets with Six-Membered Rings of Coppers Interconnected by 2,1,3-Benzothiadiazoles and a Layered Structure Composed of the 2D Sheets. Inorg. Chem. **1994**, 33, 1284–1291

24. Dong, Z.; Liu, J.; Yuan, W.; Yi, Y.; Zhao, L. Recovery of Au(III) by radiation synthesized aminomethyl pyridine functional-ized adsorbents based on cellulose. Chem. Eng. J. **2016**, 283, pp. 504–513
25. Pal, S. Chapter 5. Pyridine: A Useful Ligand in Transition Metal Complexes; IntechOpen: London, UK, **2018**
26. Shirvan, S.A.; Khazali, F.; Dezfuli, S.H.; Borsalani, A. Synthesis, crystal structure analysis and characterization of mercury(II) complex containing 2-(aminomethyl)pytidine and bromide. J. Chil. Chem. Soc. **2017**, 62, pp. 3350–3353
27. Rahardjo, S.B.; Saraswati, T.E.; Masykur, A.; Finantrena, N.N.F.; Syaima, H. Synthesis and characterization of tetrakis(2-amino-3-methylpyridine)copper(II) sulfate tetrahydrate. IOP Conf. Ser. Mater. Sci. Eng. **2018**, 349, 012056
28. Saito, K.; Fujiwara, K.; Sugo, T. Fundamentals of Radiation-Induced Graft Polymerization. In Innovative Polymeric Adsorbents; Springer: Singapore, **2018**, pp. 1–22.
29. Lee, W.; Furusaki, S.; Saito, K.; Sugo, T. Tailoring a Brush-Type Interface Favorable for Capturing Microbial Cells. J. Colloid Interface Sci. **1998**, 200, pp. 66–73.
30. Bondar, Y.; Kim, H.J.; Yoon, S.H.; Lim, Y.J. Synthesis of cation-exchange adsorbent for anchoring metal ions by modification of poly(glycidyl methacrylate) chains grafted onto polypropylene fabric. React. Funct. Polym. **2004**, 58, pp. 43–51.
31. Zhuang, L.; Chen, S.; Lin, R.; Xu, X. Preparation of a solid amine adsorbent based on polypropylene fiber and its performance for CO2 capture. J. Mater. Res. **2013**, 28, pp. 2881–2889.
32. Nasef, M.M.; Abbasi, A.; Ting, T. New CO2 adsorbent containing aminated poly(glycidyl methacrylate) grafted onto irradiated PE-PP nonwoven sheet. Radiat. Phys. Chem. **2014**, 103, pp. 72–74.
33. Maleki, F.; Gholami, M.; Torkaman, R.; Torab-Mostaedi, M.; Asadollahzadeh, M. Multivariate optimization of removing of cobalt(II) with an efficient aminated-GMA polypropylene adsorbent by induced-grafted polymerization under simultane-ous gamma-ray irradiation. Sci. Rep. **2021**, 11, 18317.
34. Wang, X.; Gillham, J.K. Competitive primary amine/epoxy and secondary amine/epoxy reactions: Effect on the isothermal time-to-vitrify. J. Appl. Polym. Sci. **1991**, 43, pp. 2267–2277.

35. Geng, W.; Nakajima, T.; Takanashi, H.; Ohki, A. Analysis of carboxyl group in coal and coal aromaticity by Fourier transform infrared (FT-IR) spectrometry. Fuel **2009**, 88, pp. 139–144.
36. Chung, C.; Lee, M.; Choe, E.K. Characterization of cotton fabric scouring by FT-IR ATR spectroscopy. Carbohydr. Polym. **2004**, 58, pp. 417–420
37. Gorade, V.G.; Chaudhary, B.U.; Kale, R.D. Moisture management of polypropylene non-woven fabric using microcrystalline cellulose through surface modification. Appl. Surf. Sci. Adv. **2021**, 6, 100151.
38. Xue, Y.; Patel, A.; Sant, V.; Sant, S. Semiquantitative FTIR Analysis of the Crosslinking Density of Poly(ester amide)-Based Thermoset Elastomers. Macromol. Mater. Eng. **2015**, 301, pp. 296–305.

Chapter 3 Sialic acid immobilized polymer brush for lectin in aerosol form

3.1. Introduction

It is no exaggeration to say that viruses accompany the history of humanity. In particular, even now, infectious viruses are a severe problem that affects the economy of the country and the lives of the people. There are countless infectious viruses, but the most representative is the influenza virus, which has been recognized as a big problem from the past to the present. Influenza infection, a usual infectious virus, usually starts in winter, in the eastern or southern hemisphere with high humidity, and then spreads to North America and Europe. In particular, when mutations occur, infectious diseases spread more [1]. In the case of influenza, there is an incubation period of about three days, and during this period, the virus carrier spreads the virus because there are no symptoms. Especially before the 1950s, influenza pandemics killed up to millions to tens of millions of people before influenza was found to be caused by a virus and a vaccine was developed [1,2]. In the modern era of active vaccine development, dying from influenza is lower than before. However, deaths are still occurring. Infectious viruses are still very deadly and dangerous because they evolve with mutants. Vaccine research is active however, influenza viruses are constantly mutating, and the most effective treatment is vaccination and isolation from the source of infection.

In general, the route of infection of infectious viruses can be divided into infection by droplet and infection by contact [3,4]. Infection by contact occurs when the mucous membrane is touched with the part of the body that has come into contact with the virus, and the best way to prevent this is to keep the body clean. However, since infection by droplets is invisible, it is difficult for both carriers and those around them to notice the risk of infection, and it is even more dangerous. Both droplet and contact infections occur when the virus binds to cells in the human body, and hemagglutinin (HA) [3,5–7] and neuraminidase (NA) are known to be involved in the primary infection routes of the infectious virus. HA is one of the antigenic projections, a type of glycoprotein that causes red blood cells to be aggregate, and NA is one of the enzymes that are antigenic determinants found on the surface of influenza viruses in various organisms. Among them, HA is a direct factor in the infection process as it causes the antigenic projections it possesses to attach to the cells of animals and plants directly. Influenza viruses (80-120 nm) [8] are known to cause infection by binding to sialic acid [6, 7, 9], a type of sugar on the cell surface. Sialic acid present on the surface of animal and plant cells generally exists in the form of a sugar chain. Sugar chains refer to monosaccharides that combine in

various formats to form a chain shape. In general, the interaction between a single sugar chain and a single protein is weak because weak forces such as hydrogen bonding and hydrophobic interactions mainly occur. Compensating for these shortcomings is the sugar cluster effect or sugar chain polyvalent effect [10-14].

In other words, proteins or glycolipids do not spread into cells but concentrate in some areas as needed to form sugar clusters, increasing the binding force. This sugar cluster effect has become the primary design guideline for developing antibodies, antivirals, and toxin inhibitors in immunology.

We decided to mimic the sugar chain cluster effect to develop material for adsorbing the influenza virus, and MNWF prepared by radiation-induced graft polymerization was selected as the substrate. Substrates made through radiation-induced graft polymerization have the advantage of controlling the length or density of polymer brushes created by controlling the amount of radiation or monomer concentration [15]. And glycidyl methacrylate (GMA) was selected as the monomer used for radiation-induced graft polymerization, and in this case, the polymer contains an epoxy group and has hydrophilicity [16-18]. We expected that if sialic acid could be introduced into the polymer brushes of the substrate prepared by this radiation graft polymerization method, it would be possible to mimic the effect of sugar chain clusters by controlling the density of the polymer brushes. In general, the average length of polymer brushes extending to the substrate is known to be 35 nm [16], which is a sufficient size to bind HA (13.5 nm) [5,6] present on the surface of the influenza virus.

However, we did not use it directly because of the risk of infection when handling the influenza virus as an early step in influenza virus adsorption experiments. Instead, an experiment was performed by selecting a lectin with a similar binding reaction through a specific recognition with sialic acid. Therefore, the efficiency of lectin binding was checked by introducing sialic acid into MNWF with various polymer brush concentrations. Scheme 1 shows a projected image of the MNWF attempting influenza virus adsorption with sialic acid introduced into a polymer brush.

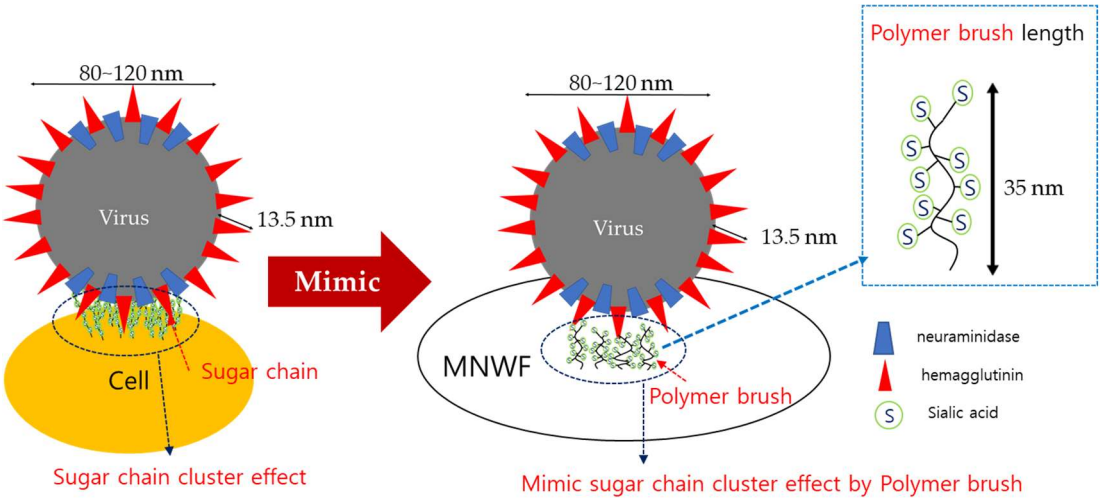

Scheme 3- 1. A design concept that mimics the sugar chain cluster effect with sialic acid introduced into the functional microfiber nonwoven fabric.

3.2. Experimental

3.2.1. Materials

disodium iminodiacetate monohydrate (98%, WAKO Chemical Co., Ltd., Odawara, Japan), microfiber nonwoven fabric (polypropylene, dg 38~183%, ENEOS Corporation, Tokyo, Ja-pan), 1-(3-dimethylaminopropyl)-3-ethylcarbodiimide hydrochloride (98%, Tokyo chemical industry Co., Ltd., Tokyo, Japan), N-acetylneuraminic acid (Nacalai tesque, INC, Kyoto, Japan), WGA-Biotin (J220, J-chemical, INC, Tokyo, Japan), sodium dodecyl sulfate (95%, WAKO Chemical Co., Ltd., Odawara, Japan), BCA Protein Assay Kit (T9300A, Takara, Kusatsu, Japan), Synergy HT Multimode Microplate Readers (Biotek, Winooski, VT, USA), Spectrum Two FT-IR Spectrometer (Perkin Elmer, Waltham, MA, USA), wheat germ ag-glutinin, Triticum vulgaris, FITC Conjugate (FL-1021, Vector Laboratories, Burlingame, CA, USA), Olympus IX81 fluorescence microscope (Olympus Optical Co. Ltd., Tokyo, Japan), and FE-SEM-EDS (JSM-7800f, Jeol, Tokyo, Japan), Digital micro scope(VHX-8000, Keyence, Osaka, Japan).

3.2.2. Selection of functional group

It has already been demonstrated in several studies whether an artificial enzyme can function as a catalyst by immobilizing it on a polymer brush [16,19,20]. Thus, it was expected that the introduction of sialic acid by selecting an appropriate functional group could be efficiently used for lectin binding. The selection of functional groups was considered from various perspectives, and the functional group used in this experiment was determined to be disodium iminodiacetate monohydrate (IDA). The IDA group is a functional group [21–25] widely used in protein adsorption, enzyme purification and fixation, and metal ion adsorption. In particular, IDA is judged to be more efficient when introducing sialic acid because there are two places where sialic acid can be introduced. However, in this experiment, to increase the efficiency of introducing sialic acid, it was finally decided to use the IDA-EDC functional group made through coupling with 1-(3-dimethylaminopropyl)-3-ethylcarbodiimide hydrochloride (EDC) instead of using IDA alone. The coupling process of IDA-EDC is shown in Figure 3-1. In general, EDC is a substance used to covalently bond carboxylate (–COOH) or phosphate ($–PO_4$) sulfide with an amine group ($–NH_2$). EDC has the disadvantage of being self-polymerized in some target biomolecules (e.g., peptides) containing both carboxylates and amine groups, however, it is water-soluble, so it is easy to handle and efficiently reacts with amine compounds [26].

IDA was used at a concentration of 0.125 mol, and since IDA has two sites that can react with sialic acid, EDC was used at a concentration of 0.25 mol, twice the concentration of IDA, to prepare an IDA-EDC complex. In the case of the IDA-EDC complex, a coupling reaction was performed at 25 °C for 72 h before being introduced into MNWF and used. Similarly, N-acetylneuraminic acid (NANA, sialic acid) was also introduced at a concentration of 0.25 mol, twice the concentration of IDA. The process of introducing IDA-EDC and NANA into the GMA MNWF is shown in Figure 3-2.

Table 3- 1. IDA-EDC introduction condition

IDA-EDC Coupling	
IDA Concentration	0.125 M
EDC Concentration	0.25 M
Reaction temperature	298 K
Reaction time	72 h
Introduction of IDA-EDC	
Reaction temperature	353 K
Reaction time	24 h
Introduction of NANA	
NANA Concentration	0.25 M
Reaction temperature	298 K
Reaction time	24 h

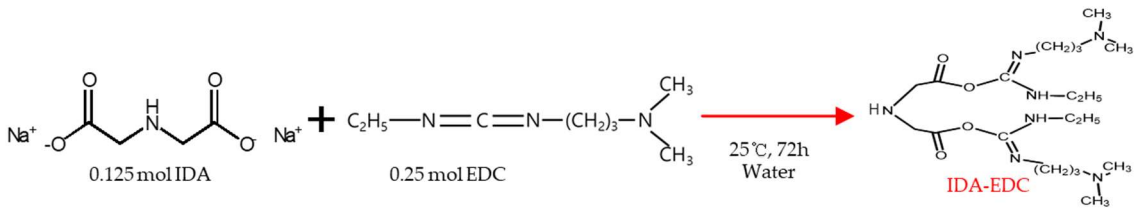

Figure 3- 1. Introduction diagram of the IDA-EDC coupling reaction

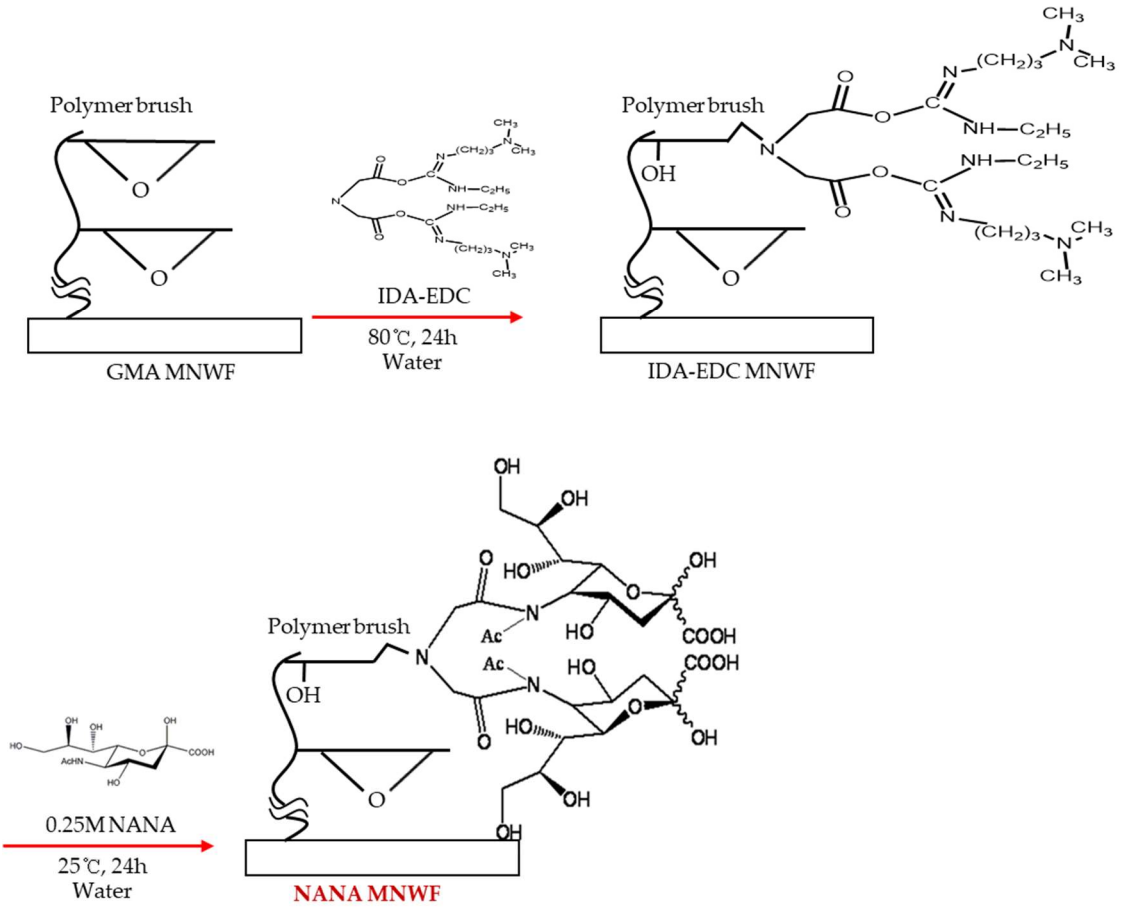

Figure 3- 2 Introduction image of IDA-EDC & NANA on GMA MNWF.

3.2.3. Lectin absorption procedure

3.2.3.1. Adsorption in aerosol form

Several methods have been devised to adsorb lectin onto NANA MNWF. Experiments for the development of adsorbents have traditionally used batch methods. When using the batch method, it was thought that the maximum lectin adsorption characteristics of NANA MNWF could be confirmed. However, since influenza viruses are generally infected in droplets, it was judged that the experimental method through the batch meth-od was not appropriate. Therefore, we decided to aerosolize lectin and try adsorption to NANA MNWF. A lectin adsorption experiment was prepared similarly to studies in [27,28] that adsorbed aerosols onto nonwoven samples. Figure 3-3 shows the device form of lectin aerosolization and adsorption to NANA MNWF used in the experiment.

For the aerosol adsorption experiment, a WGA lectin solution was prepared at a 2000 μg/mL concentration, and 0.1 mL of the WGA solution was put into the nebulizer. Therefore, 0.1 mL of WGA lectin solution was considered to contain up to 200 μg of WGA. The nebulizer was operated using a pump, and the aerosolized WGA solution was permeated through the NANA MNWF for about 1 min. After the adsorption process finished, NANA MNWF was washed with ionized water to remove lectins that may remain on the surface of NANA MNWF without being adsorbed.

The nebulizer was operated using a pump, and the aerosolized WGA solution was permeated through the NANA MNWF for about 1 min. After the adsorption process finished, NANA MNWF was washed with ionized water to remove lectins that may remain on the surface of NANA MNWF without being adsorbed.

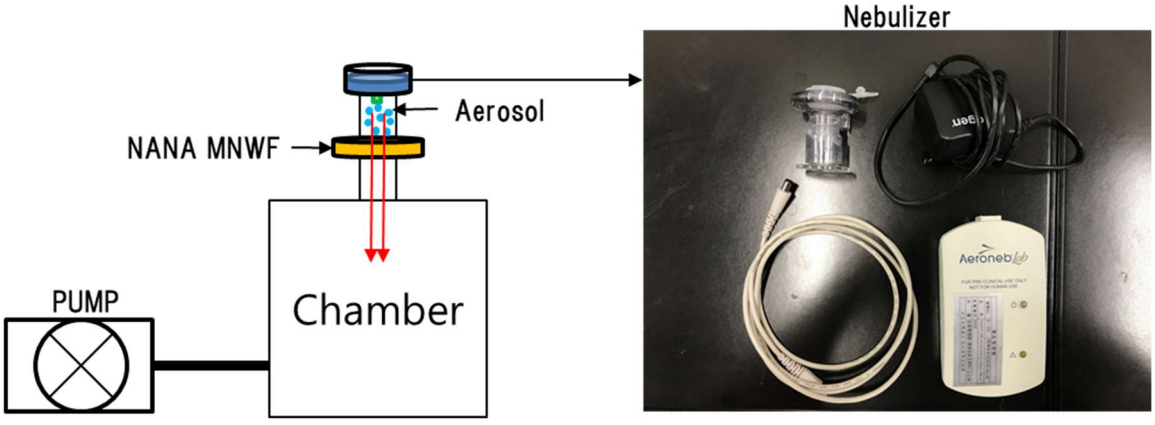

Figure 3- 3. Lectin aerosolization device image

3.2.3.2. BCA Method

Lectins adsorbed to NANA MNWF were separated by 0.2 wt% sodium dodecyl sulfate (SDS) solution [29–32]. Lectins isolated by SDS were treated with the bicinchoninic acid (BCA) method [32–35] and then measured using a spectrophotometer for quantitative measurement.

3.2.3.3. Fluorescence labeling experiment

The adsorption of the lectin was checked by using the fluorescently labeled lectin on the functional nonwoven fabric of each step. To confirm the adsorption of the lectin, the lectin fluorescently labeled with Fluorescein isothiocyanate [36–38] was adsorbed and eluted in the form of an aerosol. Fluorescence images were identified at a 4 magnification using an Olympus IX81 model.

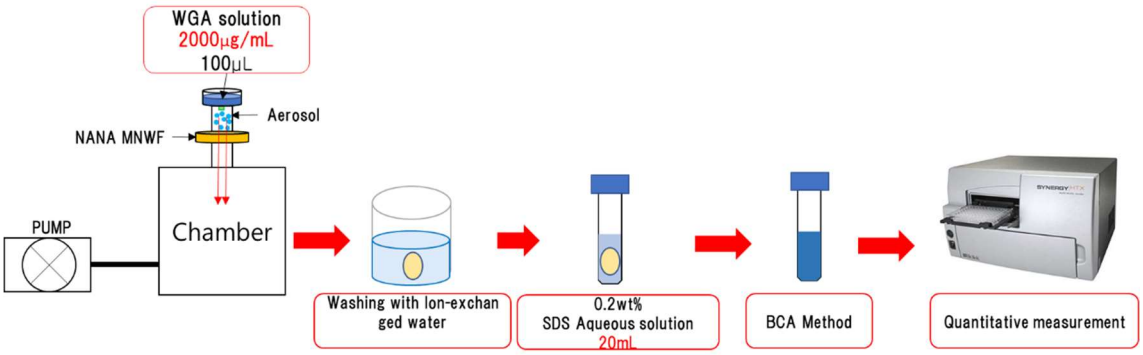

Figure 3- 4. Lectin adsorption quantity quantitative measurement procedure by BCA method

3.2.4. The equation for deriving results

Checking the density of the 4-Picolylamine through the weight of the substrate is called the degree of grafting, and it can be obtained by the following Equation (1). In the case of this experiment, GMA was used as the monomer in all experiments, and the calculation of the amount of GMA introduced into the substrate is described in Equation (2).

$$Degree\ of\ graft\ (dg) = 100(W_1 - W_0)/W_0\ \ [\%] \tag{1}$$

$$Introduced\ GMA = [1000(W_1 - W_0)\ /\ 142.2]\ /\ W_0 \quad [mmol\ /\ g] \tag{2}$$

Here, W0 is the mass of the substrate polymer that has not been treated. W1 is the mass of the polymer after reacting with the GMA monomer. And, the value of 142.2 is the molecular weight of GMA [15].

When a 4-Picolylamine is introduced into the GMA substrate produced through the reaction of the GMA monomer, the 4-Picolylamine is fixed to the epoxy group of the GMA chain. Here, the molar conversion rate or the degree of functionalization of the epoxy group of the GMA chain to the 4-Picolylamine can be obtained from the following Equation (3).

$$Molar\ conversion\ rate = 100[(W_2 - W_1)/514.5]/[(\ W_1 - W_0)/142.2]\ [\%] \tag{3}$$

Where W_0 is the mass of the polymer that has not been treated, W_1 is the mass of the polymer after reacting with the GMA monomer. W_2 is the mass of the polymer after introducing an ion-exchange group (functional group) by adding it to the GMA-substrate's epoxy group. The value of 142.2 is the molecular weight of GMA, and the value of 514.5 is the IDA and two EDC's molecular weights.

3.3. Results and Discussion

3.3.1. IDA-EDC and NANA introduction characteristics

The spectrum of FT-IR was measured to confirm the introduction of a functional group in MNWF for each step. The spectral results of FT-IR are shown in Figure 3-4, and the interpretation of each peak is shown in Table 3-2.

For the GMA on PP MNWF, peaks in epoxy and ester groups were found at 747, 841, 972, 1053, 1166, and 1238 cm^{-1}, and peaks of C=O were found at 1726 cm^{-1} [39–46].

In the case of IDA-EDC MNWF, the peaks of epoxy and ester groups were reduced compared to GMA MNWF, and it was confirmed that new peaks of N-H were generated at peaks of 1554–1564 [41,48] and 1659–1662 cm^{-1} [39,44,48]. In addition, new peaks of the hydroxyl group (-OH) and N-H were generated at 3250–3400 cm^{-1} [40–47], confirming the introduction of IDA-EDC.

In the case of NANA MNWF, the peak indicating C=O and the carboxyl group (COOH) was observed at 1726 cm^{-1} [39–46], significantly increased, and the hydroxyl group of 3250–3400 cm^{-1} [40–47] was also increased when compared with the peak of IDA-EDC MNWF. The introduction of NANA was confirmed by increasing the peak size of the carboxyl group and the hydroxyl group.

Table 3- 2. Functional group IR peak of each MNWF

Wavenumber (cm^{-1})	Associated functional group	
747–1238	Epoxy group, Ester group	[39–46]
1376	–CH_3 vibration	[44–47]
1451	–CH_2 vibration	[47]
1564–1554	Amide II, N–H stretch vibration	[41,48]
1662–1659	Amide I, N–H stretch vibration	[39,44,48]
1726	C=O, carboxyl group (COOH) vibration	[39–46]
2950	C–H vibration	[44,46,47]
3250–3400	Hydroxyl group (–OH), N–H stretch	[40–47]

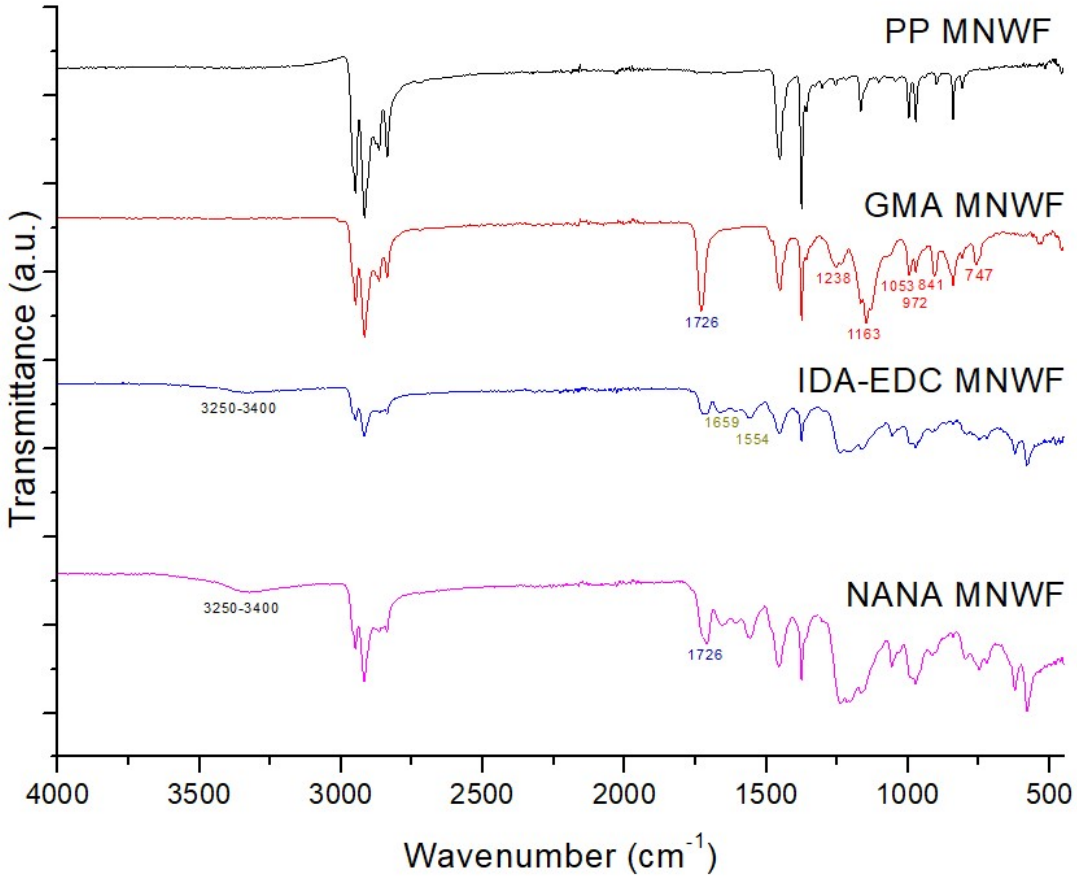

Figure 3- 5. FT-IR characterization of each functional MNWF

IDA-EDC was introduced into GMA MNWF according to the degree of grafting (dg), and the characteristics of IDA-EDC introduction according to the dg were confirmed. These results are shown in Figure 3-5. The amount of IDA-EDC introduced into GMA MNWF was confirmed using Equations (2) and (3).

In the case of IDA-EDC MNWF, it was confirmed that the higher the degree of grafting, the more IDA-EDC was introduced. In this experiment, the highest density of IDA-EDC introduced in GMA MNWF was about 8.4 mmol/g at 173% dg. This seems to be because as the dg increases, the GMA content increases so that IDA-EDC reacts with more GMA. A 40-150% weight change was found when IDA-EDC was introduced into the GMA MNWF at dg 38-183%. From all results, the molar conversion rate of IDA-EDC MNWF from MNWF grafted with GMA was confirmed to be about 47% on average.

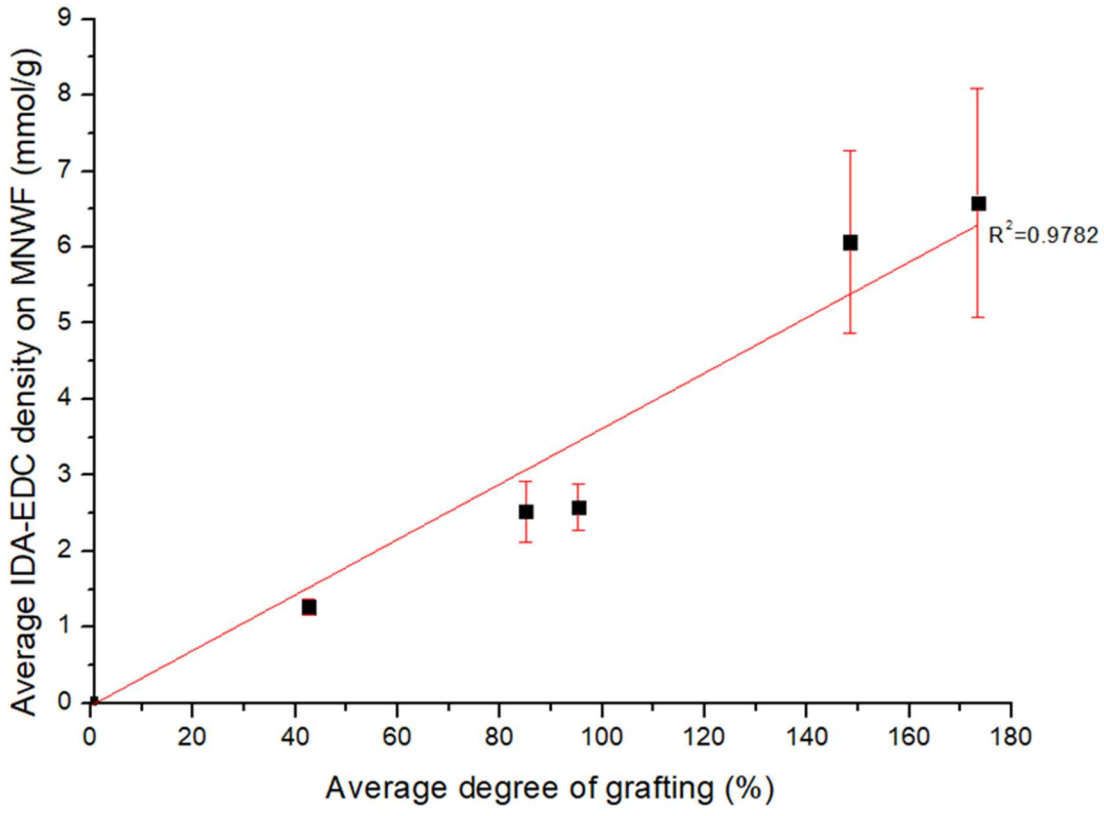

Figure 3- 6. Introduction of IDA-EDC on GMA MNWF according to degree of grafting.

In MNWF supplemented with IDA-EDC, the surface state of MNWF was significantly changed as the dg increased. In the case of IDA-EDC MNWF with a dg of 100% or less, the edges of the MNWF were slightly curled, and in the case of IDA-MNWF with a dg of 100% or more, the MNWF was severely bent. It seems that the durability of MNWF cannot be sustained when IDA-EDC is introduced in too large a quantity.

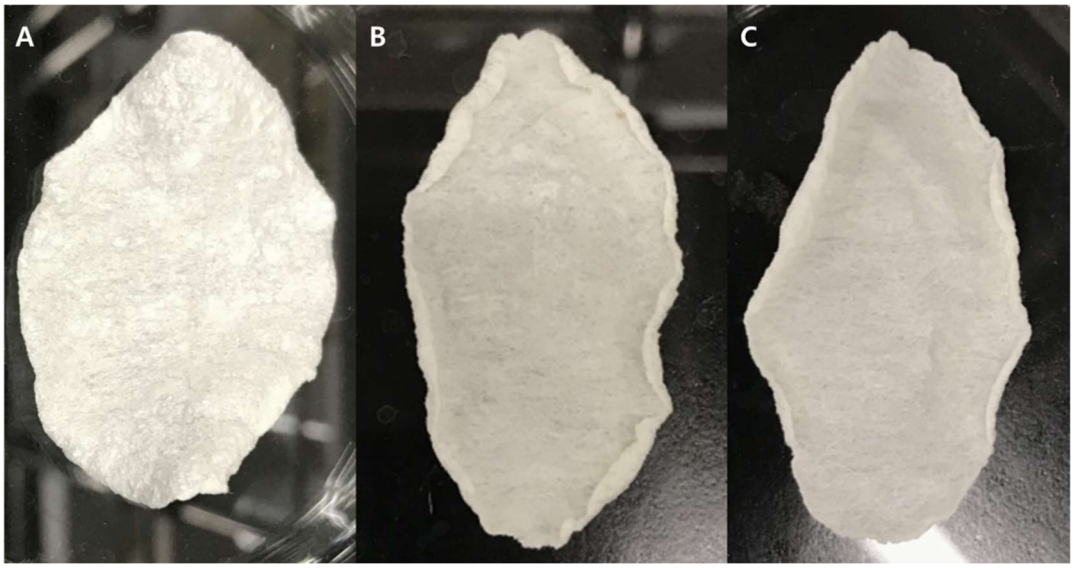

Figure 3- 7. Surface change depending on degree of grafting (Each nonwoven is all IDA-EDC MNWF, A: dg 105%, B: dg 149%, C: dg 181%).

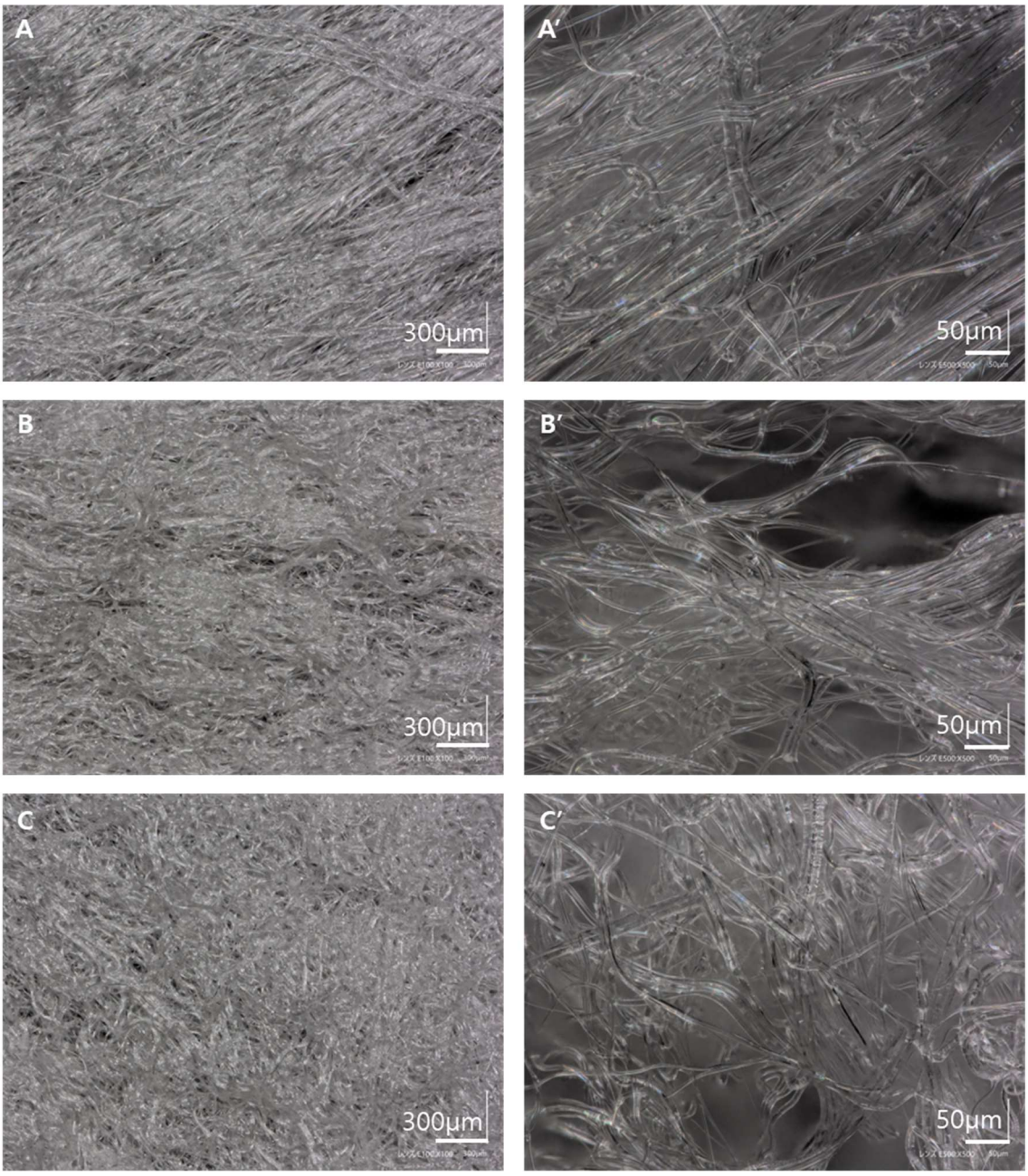

Figure 3- 8 Digital micro scope image of GMA, IDA-EDC, NANA MNWF

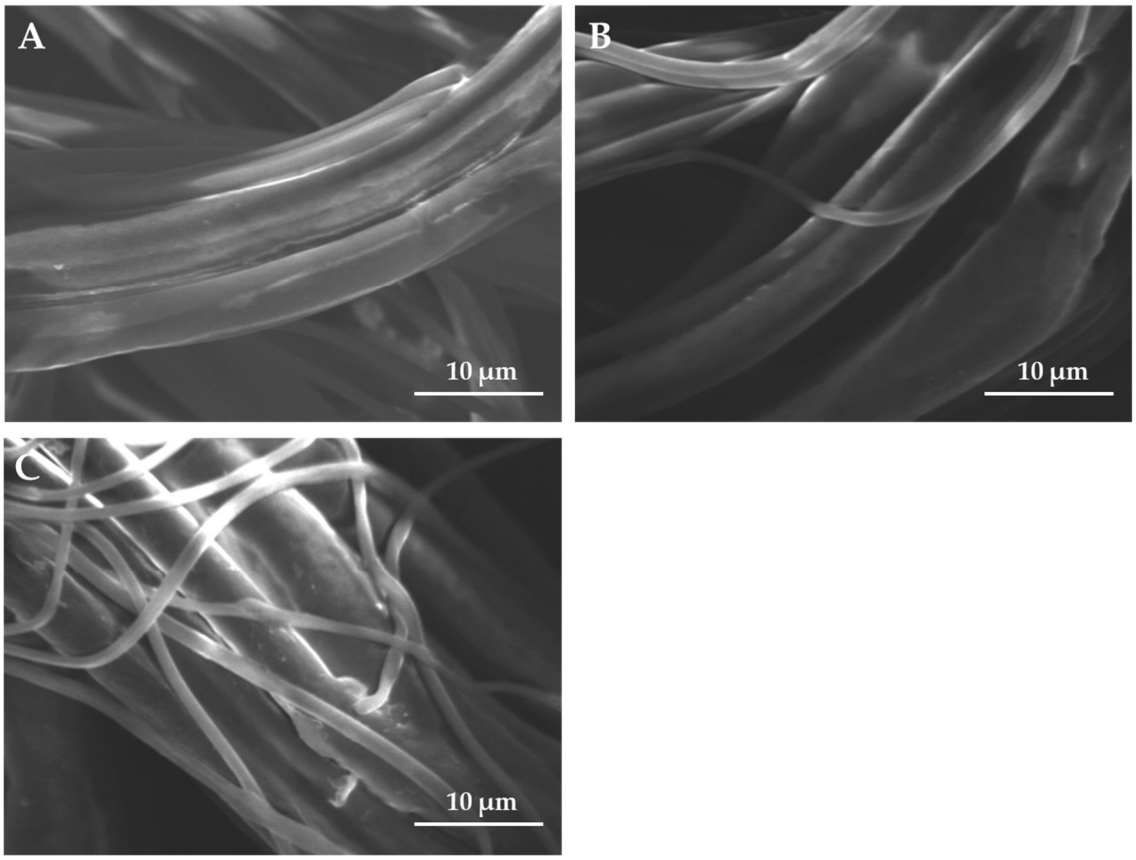

Figure 3- 9. FE-SEM characterization (A: GMA MNWF, B: IDA-EDC MNWF, C: NANA MNWF, Each MNWF's dg is 90%).

The SEM and digital microscope images were confirmed to observe the change of the surface of the MNWF into which each functional group was introduced. The digital microscope image in which each functional group was introduced is shown in Figure 3-7, SEM image is shown in Figure 3-8. After GMA was first introduced as a monomer, no significant difference was observed on the surface of MNWF while the functional group IDA-EDC or the primary adsorption target NANA were introduced, respectively. However, it was confirmed that the weight of MNWF increased in each process, and the surface area of the nonwoven fabric was increased accordingly.

3.3.2. Lectin absorption characteristics

3.3.2.1. Fluorescence labeling experiment

As a result of confirming GMA MNWF through a fluorescence microscope, it was confirmed that almost no lectin was adsorbed. The fluorescence image could confirm a slight luminescence, but similar results were obtained even after lectin elution with 0.2 wt.% SDS solution. Therefore, it is thought that non-selective adsorption of lectin by GMA MNWF occurred.

The IDA-EDC MNWF confirmed that the lectin was adsorbed to some extent through a slight light emission. Similarly, it was confirmed that a small amount of fluorescent material remained after the elution of the lectin.

NANA MNWF showed the most robust luminescence image, confirming the most effective lectin adsorption. In the case of NANA MNWF, it was also confirmed that a small amount of fluorescent material also remained even after lectin was extracted with SDS solution. Through fluorescence microscopy analysis, NANA MNWF showed the most robust luminescence image.

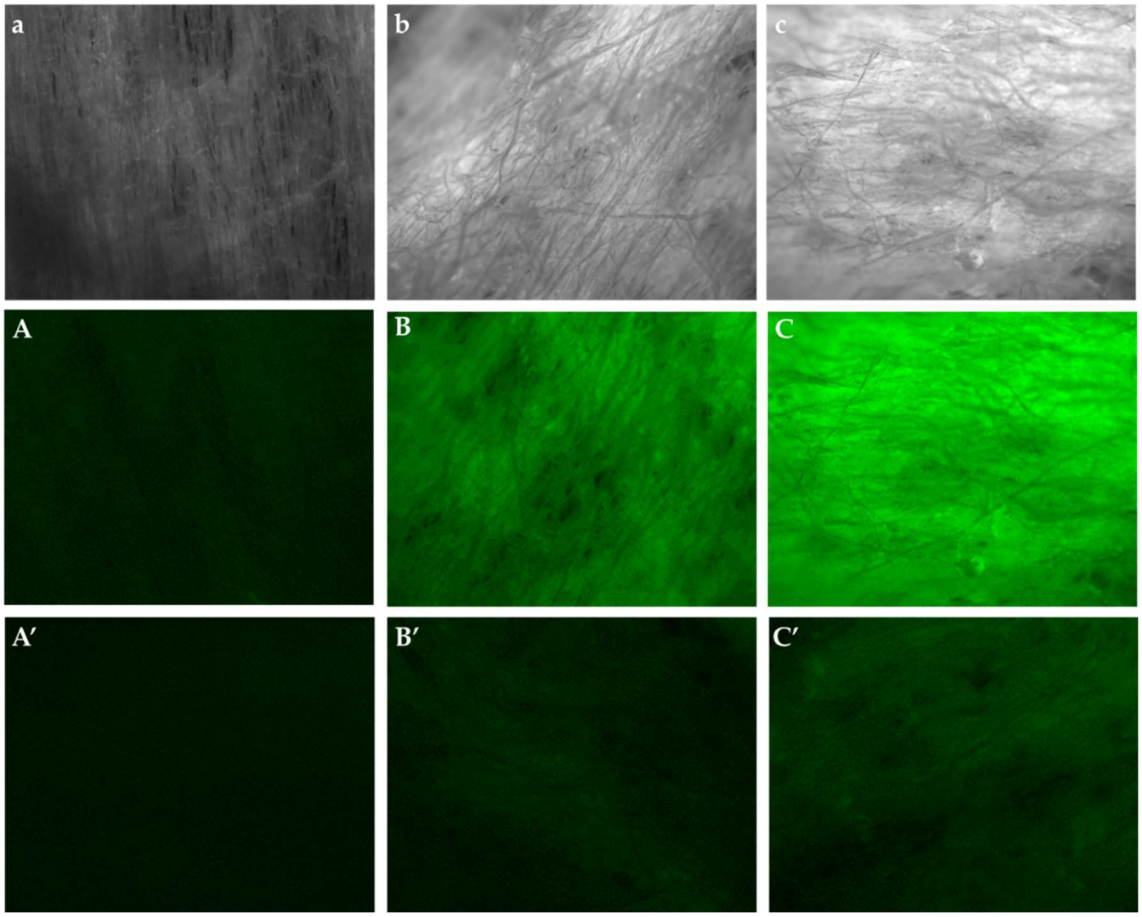

Figure 3- 10. Fluorescent marker lectin adsorption image of functional MNWF at each stage. (a–c) GMA, IDA-EDC, and NANA MNWF, respectively. (A–C) GMA, IDA-EDC, and NANA MNWF after fluorescence-labeled lectin adsorption, respectively. (A'–C') GMA, IDA-EDC, and NANA MNWF after eluting fluorescently labeled lectin with 0.2 wt.% SDS solution, respectively. Each MNWF's dg is 50%.

3.3.2.2. Aerosol Adsorption

3.3.3.2.1. Adsorption characteristics of each functional MNWF

Since GMA and IDA-EDC MNWF were also capable of adsorption of lectins, the amount of lectin adsorption of MNWF into which each functional group was introduced was quantitatively confirmed. Figure 3-9 shows the lectin adsorption amount of GMA, IDA-EDC, and NANA MNWF at an average dg of 90%. As demonstrated by the fluorescence image, it was confirmed that a small amount of non-selective lectin adsorption occurred in GMA MNWF. In the case of IDA-EDC, lectin adsorption was possible to some extent. However, it was shown at the half level of NANA MNWF's result, confirming that the sialic acid was introduced adequately into NANA MNWF with these results.

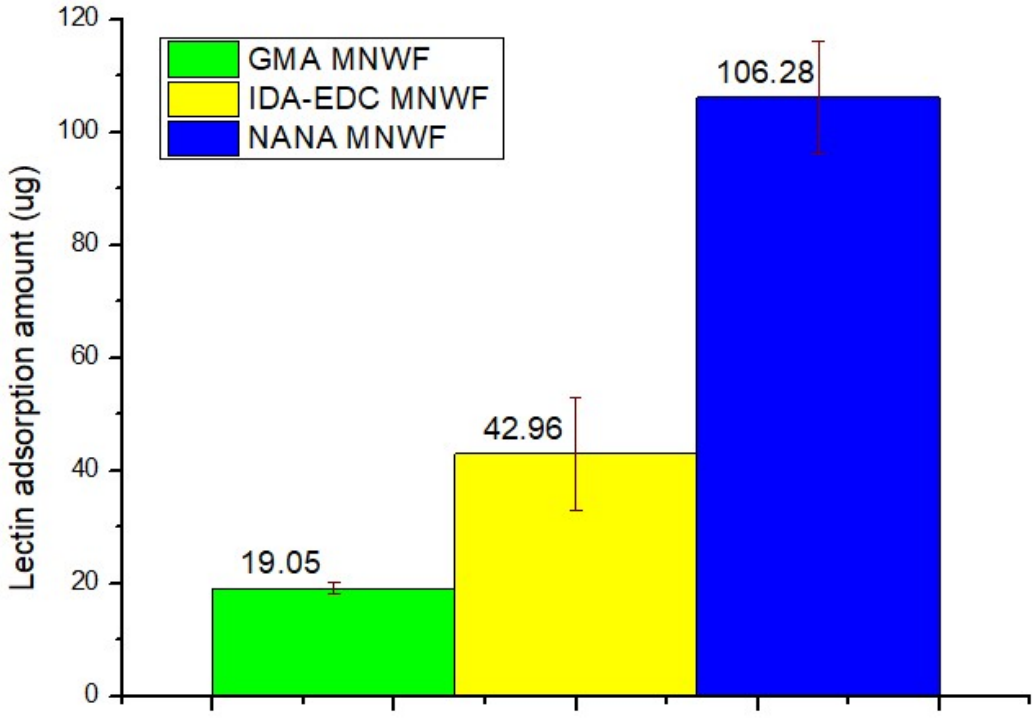

Figure 3- 11. Lectin adsorption amount difference in each functional nonwoven fabric (each used functional MNWF's average dg is 90%).

3.3.3.2.2. Adsorption characteristics according to change of degree of grafting

As NANA MNWF showed utility for lectin adsorption, the lectin adsorption amount change of NANA MNWF according to the dg was compared. The difference in the amount of lectin adsorption according to the dg is shown in Figure 3-10.

The maximum lectin adsorption amount was 59.1% in dg 87% NANA MNWF. This results from adsorption of 118.2 out of 200 μg of lectin. The maximum adsorption was observed at dg 87%. However, the lectin adsorption results of NANA MNWF at dg 40–100% were very similar. NANA MNWF with the lowest dg of 38% used in this experiment adsorbed 109.7 μg out of a total of 200 μg, showing an adsorption efficiency of 54.9%. The dg 30–100% results were similar, but it was confirmed that the adsorption amount decreased in the case of NANA MNWF with a high dg.

These results are similar to studies that attempted to immobilize enzymes on membranes prepared through radiation-induced graft polymerization [16].

According to the effects of [16], it can be confirmed that the results of the dg 50% membrane had higher adsorption efficiency when the enzyme was immobilized on the dg 50% membrane and the dg 100% membrane. This is thought to impede rather than induce more adsorption about the target if the density of the polymer brush is too high.

In reference [16] details a membrane experiment with a large usable surface area to volume ratio. The membrane is a material with many advantages, but the disadvantage is that the pores are easily clogged, so it is thought that the maximum efficiency was observed at dg 50%. In our study, since MNWF was used, similar results were observed at a higher dg because the advantage of MNWF is that the pores are not easily clogged.

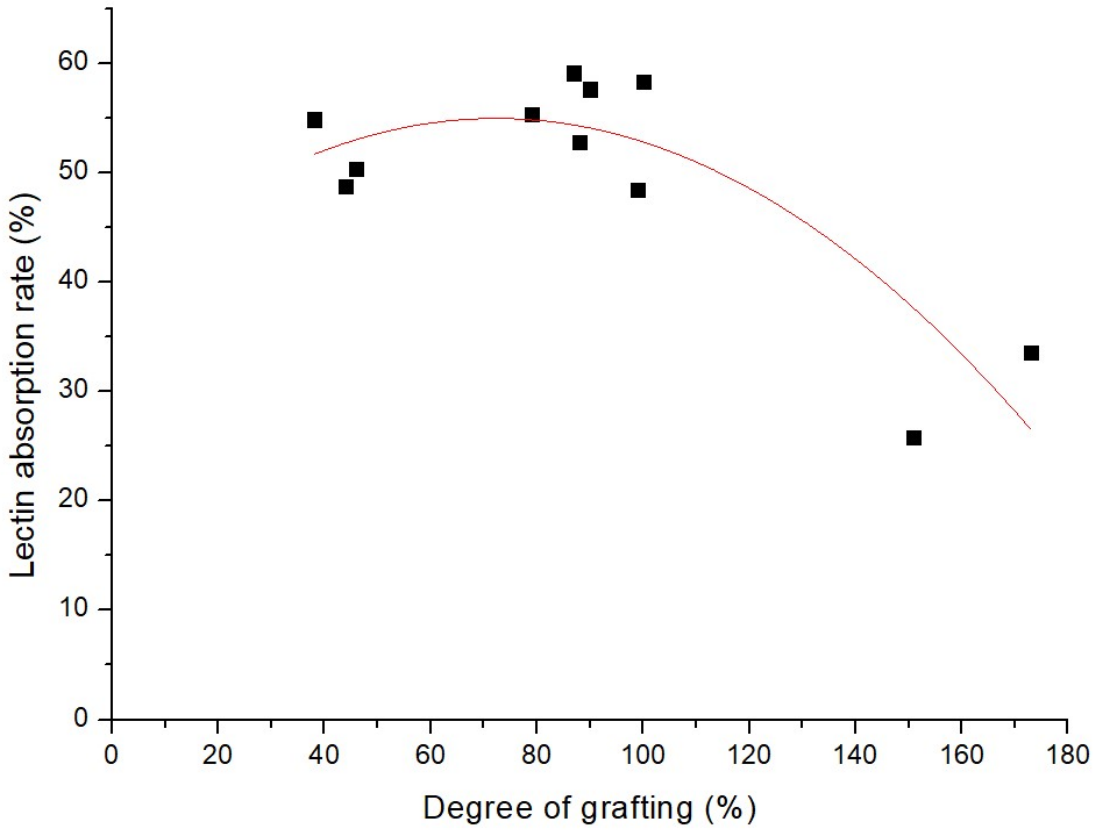

Figure 3- 12. Dependence of lectin absorption rate on the degree of grafting.

3.3.3.2.3. Effect of GMA concentration used in the manufacture.

In addition, according to [16], it was confirmed that when the GMA concentration was changed when the membranes with the same dg were prepared, the length of the polymer brushes of the membranes prepared at lower GMA concentrations increased. Therefore, our research selected NANA MNWF with the same dg but different GMA concentrations during preparation, and the results were compared.

Among the samples used in the lectin adsorption experiment, adsorption efficiency was compared to the average dg 89% NANA MNWF (manufactured GMA concentration 4.5%) and the average dg 96% NANA MNWF (manufactured GMA concentration 7%). There was a 5% difference in average dg. However, this difference was minimal, and it was judged that the effect on the results would be negligible. This result is shown in Figure 3-11. Similar to the results in reference [16], in the case of NANA MNWF manufactured at a GMA concentration of 4.5%, the average lectin adsorption was about 10 μg higher, which is a difference in adsorption rate of about 5%. Therefore, in the case of the NANA MNWF proposed here, it can be said that the use of the MNWF produced at a concentration of 4.5% GMA with a dg of 40–100% showed the best efficiency.

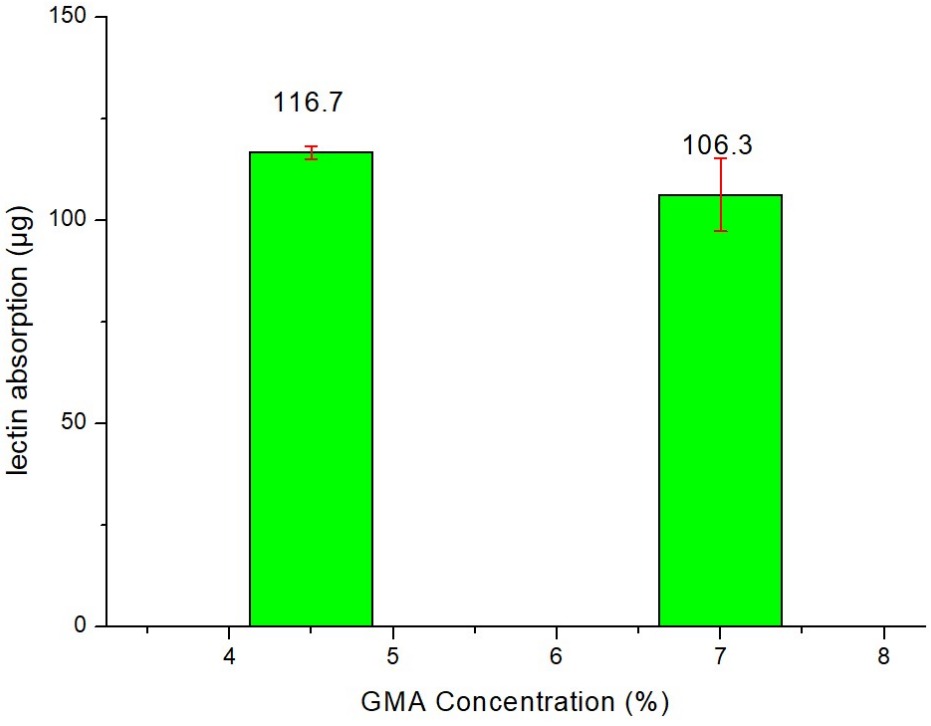

Figure 3- 13. Dependence of average lectin absorption amount on GMA concentration used in the preparation.

3.4. Conclusion

In this research, NANA was introduced into MNWF by mimicking the effect of sugar chain clusters, which are densely present to increase the binding force in the process of virus adsorption to cells, and an adsorbent that successfully interacts with lectins was developed. As a functional group for introducing NANA, IDA-EDC was prepared and used. The introduction of IDA-EDC and NANA was confirmed through FT-IR peak analysis and SEM images in the MNWF of each step. In addition, to ensure the lectin adsorption performance in MNWF at each stage, the emission image of the fluorescently labeled lectin was checked, and the amount of lectin eluted with the SDS solution was compared. As a result, in the case of NANA MNWF, it was confirmed that the lectin was efficiently adsorbed. As for the maximum adsorption amount of lectin, 118.2 of 200 μg of lectin was adsorbed in dg 87% NANA MNWF, showing an adsorption efficiency of 59.1%. In addition, similar to the reference [16], MNWF, which has an identical dg but has a low GMA concentration at the time of production, showed a better lectin adsorption performance. This seems to be affected by the length of the polymer brush.

We confirmed the usefulness of a polymer brush containing sialic acid in this experiment. However, at the same time, we faced several limits. The first thing that should be given priority is the discovery of the optimal introduction conditions for IDA-EDC and the accurate analysis of the amount of introduction. In this experiment, we assumed that IDA-EDC reacted 100% with each other through the coupling reaction before proceeding with the experiment. The molar conversion rate of IDA-EDC was also calculated under this assumption. Therefore, it is necessary to find a way to calculate the IDA-EDC coupling result accurately. If this process can be preceded, I think it will be possible to confirm the amount of sialic acid introduced quantitatively.

3.5 Reference

1. Potter, C.W. A history of influenza. J. Appl. Microbiol. **2001**, 9, pp. 572–579.
2. Palese, P. Influenza: Old and new threats. Nat. Med. **2004**, 10, pp. 582–587.
3. Chilamakuri, R.; Agarwal, S. COVID-19: Characteristics and Therapeutics. Cells **2021**, 10, 206.
4. Brankston, G.; Gitterman, L.; Hirji, Z.; Lemieux, C.; Gardam, M. Transmission of influenza A in human beings. Lancet. Infect. Dis. 2007, 7, pp. 257–265.
5. Webster, R.G.; Laver, W.G. The origin of pandemic influenza. Bull World Health Organ. **1972**, 47, pp. 449–452.
6. Boonstra, S.; Blijleven, J.S.; Roos, W.H.; Onck, P.R.; van der Giessen, E.; van Oijen, A.M. Hemagglutinin-Mediated Membrane Fusion: A Biophysical Perspective. Annu. Rev. Biophys. **2018**, 47, pp. 153–173.
7. Kuchipudi, S.; Nelli, R.; Gontu, A.; Satyakumar, R.; Nair, M.S.; Subbiah, M. Sialic Acid Receptors: The Key to Solving the Enigma of Zoonotic Virus Spillover. Viruses **2021**, 13, 262.
8. Vajda, J.; Weber, D.; Brekel, D.; Hundt, B.; Müller, E. Size distribution analysis of influenza virus particles using size exclusion chromatography. J. Chromatogr. A **2016**, 1465, pp. 117–125
9. Nicholls, J.M.; Chan, R.W.; Russell, R.J.; Air, G.M.; Peiris, J.M. Evolving complexities of influenza virus and its receptors. Trends Microbiol. **2008**, 16, pp. 149–157.
10. Monsigny, M.; Mayer, R.; Roche, A.C. Sugar-lectin interactions: Sugar clusters, lectin multivalency and avidity. Carbohydr. Lett. **2000**, 4, pp. 33–52.
11. Carlescu, Irina; Scutaru, Dan; Popa, Marcel; Uglea, Constantin V. Synthetic sialic-acid-containing polyvalent antiviral inhibitors. Medicinal Chemistry Research **2008**, 18, 6, pp. 477-494
12. Nagao M; Fujiwara Y; Matsubara T; Hoshino Y; Sato T;Miura Y. Design of Glycopolymers Carrying Sialyl Oligosaccharides for Controlling the Interaction with the Influenza Virus. Biomacromolecules **2017**, 18, 12, pp. 4385-4392
13. Hai-Peng Liu; Xin Meng; Qun Yu; Yun-Chang Tao; Fei Xu; Yun He; Peng Yu; Yang Yang. Synthesis of S-sialyl polymers as efficient polyvalent influenza inhibitors and capturers. Journal of carbohydrate chemistry **2018**, 37, 1, pp. 18-29
14. Nagao, Masanori; Kurebayashi, Yuuki; Seto, Hirokazu; Tanaka, Tomonari; Takahashi, Tadanobu; Suzuki, Takashi; Hoshino, Yu; Miura, Yoshiko.

Synthesis of well-controlled glycopolymers bearing oligosaccharides and their interactions with influenza viruses. Polymer Journal **2016**, 48, pp. 745-749

15. Saito, K.; Fujiwara, K.; Sugo, T. Fundamentals of Radiation-Induced Graft Polymerization. In Innovative Polymeric Adsorbents; Springer: Singapore, **2018**, pp. 1–22.
16. Okobira, T.; Matsuo, A.; Matsumoto, H.; Tanaka, T.; Kai, K.; Minari, C.; Goto, M.; Kawakita, H.; Uezu, K. Enhancement of immobilized lipase activity by design of polymer brushes on a hollow fiber membrane. J. Biosci. Bioeng. **2015**, 120, pp. 257–262.
17. Kiyohara, S.; Kim, M.; Toida, Y.; Saito, K.; Sugita, K.; Sugo, T. Selection of a precursor monomer for the introduction of affinity ligands onto a porous membrane by radiation-induced graft polymerization. J. Chromatogr. A **1997**, 758, pp. 209–215
18. Kim, M.; Saito, K. Preparation of silver-ion-loaded nonwoven fabric by radiation-induced graft polymerization. React. Funct. Polym. **1999**, 40, pp. 275–279.
19. Goto, M.; Kawakita, H.; Uezu, K.; Tsuneda, S.; Saito, K.; Goto, M.; Tamada, M.; Sugo, T. Esterification of lauric acid using lipase immobilized in the micropores of a hollow-fiber membrane. J. Am. Oil Chem. Soc. **2006**, 83, pp. 209–213
20. Choi, S.H.; Lee, K.P.; Kang, H.D.; Park, H.G. Radiolytic immobilization of lipase on poly(glycidyl methacrylate)-grafted polyethylenicrobeads. Macromol. Res. **2004**, 12, pp. 586–594.
21. Mhapatra, S.; Pal, D.; Ghosh, S.K.; Pramanik, P. Design of superparamagnetic iron oxide nanoparticle for purification of re-combinant proteins. J. Nanosci. Nanotechnol. **2007**, 7, pp. 3193–3199.
22. Zhang, Y.; Yang, Y.; Ma, W.; Guo, J.; Lin, Y.; Wang, C. Uniform Magnetic Core/Shell Microspheres Functionalized with Ni2+–Iminodiacetic Acid for One Step Purification and Immobilization of His-Tagged Enzymes. ACS Appl. Mater. Interfaces **2013**, 5, pp. 2626–2633.
23. Jian, G.; Liu, Y.; He, X.; Chen, L.; Zhang, Y. Click chemistry: A new facile and efficient strategy for the preparation of Fe3O4 nanoparticles covalently functionalized with IDA-Cu and their application in thepletion of abundant protein in blood sam-ples. Nanoscale **2012**, 4, pp. 6336–6342.

24. Kráčalíková, K.; Tishchenko, G.; Bleha, M. Effect of the matrix structure and concentration of polymer-immobilized Ni2+–iminodiacetic acid complexes on retention of IgG1. J. Biochem. Biophys. Methods **2006**, 67, pp. 7–25.
25. Jiang, L.; Ye, L. Nanoparticle-supported temperature responsive polymer brushes for affinity separation of histidine-tagged recombinant proteins. Acta Biomater. **2019**, 94, pp. 447–458.
26. Rao, S.S.; Winter, J.O. Adhesion molecule-modified biomaterials for neural tissue engineering. Front. Neuroeng. **2009**, 2, 6
27. Shimasaki, N.; Okaue, A.; Kikuno, R.; Shinohara, K. Comparison of the Filter Efficiency of Medical Nonwoven Fabrics against Three Different Microbe Aerosols. Biocontrol Sci. **2018**, 23, pp. 61–69.
28. Zuo, Z.; de Abin, M.; Chander, Y.; Kuehn, T.H.; Goyal, S.M.; Pui, D.Y. Comparison of spike and aerosol challenge tests for the recovery of viable influenza virus from non-woven fabrics. Influenza Other Respir. Viruses **2013**, 7, pp. 637–644.
29. Tan, S.C.; Yiap, B.C. DNA, RNA, and protein extraction: The past and the present. J. Biomed. Biotechnol. 2009, 2009, 574398.
30. Kushnirov, V.V. Rapid and reliable protein extraction from yeast. Yeast **2000**, 16, pp. 857–860.
31. Wang, L.; Li, T.; Sun, D.; Tang, M.; Sun, Z.; Chen, L.; Luo, X.; Li, Y.; Wang, R.; Li, Y.; et al. Effect of electron beam irradiation on the functional properties and antioxidant activity of wheat germ protein hydrolysates. Innov. Food Sci. Emerg. Technol. **2018**, 54, pp. 192–199.
32. Byun, M.-W.; Kim, J.-H.; Lee, J.-W.; Park, J.-W.; Hong, C.-S.; Kang, I.-J. Effects of Gamma Radiation on the Conformational and Antigenic Properties of a Heat-Stable Major Allergen in Brown Shrimp. J. Food Prot. **2000**, 63, pp. 940–944.
33. Chang, S.K.C, Zhang, Y. Chapter 18 Protein analysis. In Food Analysis; Nielsen, S.S., Ed.; Springer: Singapore, **2017**; pp. 315–331.
34. Cortés-Ríos, J.; Zárate, A.M.; Figueroa, J.D.; Medina, J.; Lemus, E.F.; Rodríguez-Fernández, M.; Aliaga, M.; López-Alarcón, C. Protein quantification by bicinchoninic acid (BCA) assay follows complex kinetics and can be performed at short incubation times. Anal. Biochem. **2020**, 608, 113904.
35. Walker, J.M. Thicinchoninic acid (BCA) assay for protein quantitation. Methods Mol. Biol. **1994**, 32, pp. 5–8

36. Che, A.F.; Huang, X.J.; Xu, Z.K. Polyacrylonitrile-based nanofibrouembrane with glycosylated surface for lectin affinity adsorption. J. Membr. Sci. **2011**, 366, pp. 272–277.
37. Fang, Y.; He, T.; Gao, H.; Fan, L.; Liu, J.; Li, B.; Zhang, H.; Bai, H. Polymer Membrane with Glycosylated Surface by a Chemo-Enzymatic Strategy for Protein Affinity Adsorption. Catalysts **2020**, 10, 415
38. Hama, Y.; Urano, Y.; Koyama, Y.; Kamiya, M.; Bernardo, M.; Paik, R.S.; Krishna, M.C.; Choyke, P.L.; Kobayashi, H. In Vivo Spectral Fluorescence Imaging of Submillimeter Peritoneal Cancer Implants Using a Lectin-Targeted Optical Agent. Neo-plasia **2006**, 8, 607–IN2
39. Lee, W.; Furusaki, S.; Saito, K.; Sugo, T. Tailoring a Brush-Type Interface Favorable for Capturing Microbial Cells. J. Colloid Interface Sci. **1998**, 200, pp. 66–73.
40. Bondar, Y.; Kim, H.J.; Yoon, S.H.; Lim, Y.J. Synthesis of cation-exchange adsorbent for anchoring metal ions by modification of poly(glycidyl methacrylate) chains grafted onto polypropylene fabric. React. Funct. Polym. **2004**, 58, pp. 43–51.
41. Zhuang, L.; Chen, S.; Lin, R.; Xu, X. Preparation of a solid amine adsorbent based on polypropylene fiber and its performance for CO2 capture. J. Mater. Res. **2013**, 28, pp. 2881–2889.
42. Nasef, M.M.; Abbasi, A.; Ting, T. New CO2 adsorbent containing aminated poly(glycidyl methacrylate) grafted onto irradi-ated PE-PP nonwoven sheet. Radiat. Phys. Chem. **2014**, 103, pp. 72–74.
43. Maleki, F.; Gholami, M.; Torkaman, R.; Torab-Mostaedi, M.; Asadollahzadeh, M. Multivariate optimization of removing of cobalt(II) with an efficient aminated-GMA polypropylene adsorbent by induced-grafted polymerization under simultaneous gamma-ray irradiation. Sci. Rep. **2021**, 11, 18317.
44. Wang, X.; Gillham, J.K. Competitive primary amine/epoxy and secondary amine/epoxy reactions: Effect on the isothermal time-to-vitrify. J. Appl. Polym. Sci. **1991**, 43, pp. 2267–2277.
45. Geng, W.; Nakajima, T.; Takanashi, H.; Ohki, A. Analysis of carboxyl group in coal and coal aromaticity by Fourier transform infrared (FT-IR) spectrometry. Fuel **2009**, 88, pp. 139–144.
46. Chung, C.; Lee, M.; Choe, E.K. Characterization of cotton fabric scouring by FT-IR ATR spectroscopy. Carbohydr. Polym. **2004**, 58, pp. 417–420.

47. Gorade, V.G.; Chaudhary, B.U.; Kale, R.D. Moisture management of polypropylene non-woven fabric using microcrystalline cellulose through surface modification. Appl. Surf. Sci. Adv. 2021, 6, 100151.
48. Xue, Y.; Patel, A.; Sant, V.; Sant, S. Semiquantitative FTIR Analysis of the Crosslinking Density of Poly(ester amide)-Based Thermoset Elastomers. Macromol. Mater. Eng. **2015**, 301, pp. 296–305.

Chapter 4. Summary and Final conclusion.

This thesis studied a new method of imparting functionality to polymer brushes made of microfiber nonwoven fabrics (MNWF) manufactured by reacting with GMA monomer. Adsorption of the final target through the polymer brush is usually attempted right after the functional groups are introduced. However, this time, we attempted to improve the adsorption performance of the final target by introducing additional adsorption materials (primary adsorption target) after introducing functional groups into the polymer brush. The functional groups' selection was based on the association of the primary and final adsorption targets. The summaries and conclusion in each chapter are followed below:

Chapter 2 attempted to detect and absorb volatile organic compounds through a polymer brush with immobilized metal ions, inspired by recently trending research on detecting and removing volatile organic compounds through metal oxides. The functional groups to be introduced in the polymer brush were required to be in a form that could bind to metal ions and VOCs. We found and selected ligands capable of binding to metal ions and VOCs through the Cambridge Crystallographic Data Center (CCDC) to solve this problem. The 4-Picolylamine (4-AMP) ligand selected through CCDC was introduced into a polymer brush at a high molar conversion rate of 63% on average in the range of 30 to 523% of the degree of grafting. In the case of copper ions, which are the primary adsorption targets for additional functionality, the maximum adsorption amount was confirmed to be 0.51 mmol/g. This is judged to have shown excellent performance considering that the maximum adsorption of iminodiacetate functional groups and copper is 0.42-0.44mmol/g and the maximum adsorption of ethylenediamine functional groups copper is 0.55mmol/g in another study aimed at copper adsorption. GMA, 4-AMP, 4-AMP-Cu MNWF was used to compare the adsorption performance of acetone, which is the final adsorption target. 4-AMP-Cu MNWF performed better from each result than MNWF introduced with other functionalities. In the case of 4-AMP-Cu MNWF, which introduced copper as additional functionality, when the final target, acetone, was at a concentration of 50 ppm, 50% of the removal was possible after 10 minutes of reaction. If this is converted into acetone adsorption amount per weight of adsorbent, the calculation is 0.04 mmol/g- 4-AMP-Cu-MNWF. This result demonstrates that the results can be better when the polymer brush is added with additional functionality (primary adsorption target, copper) than when only functional groups are provided alone.

Chapter 3, in order to adsorb the influenza virus, a representative infectious virus, there was an attempt to mimic the way cells bind to the influenza virus. In general, influenza infection is achieved by binding to sialic acid present in the cell. The reaction between a single sialic acid and influenza has a weak binding force, and sialic acid exists in a dense form to supplement the binding force. Existing in this form is called a sugar chain cluster or a sugar chain polyvalent effect. We tried to reproduce this dense sialic acid form with a polymer brush. In general, when polymer brushes are manufactured, polymer brushes' density and length can be controlled through monomer concentration and reaction time. Therefore, it was estimated that binding to the influenza virus would be possible if a functional group was introduced into the polymer brush and sialic acid was introduced. An iminodiacetate group (IDA) with two sites capable of adsorbing targets was selected as a functional group. Afterward, through coupling with 1-(3-dimethylaminopropyl)-3-ethylcarbodiimide hydrochloride (EDC), the adsorption performance with substances with amine groups was maximized, which was called IDA-EDC. N-acetylneuraminic acid (NANA, sialic acid) was introduced into IDA-EDC, and the confirmation of NANA introduction was made by comparing luminescence images upon adsorption fluorescence-treated lectin and quantitative adsorption amount of lectin. The confirmation of Lectin adsorption amount confirmed that NANA introduced showed better adsorption, indicating that polymer brushes with additional functions (primary adsorption targets, sialic acid) showed better adsorption performance than when the only functional group was introduced alone into polymer brushes.

From the results of each chapter, we suggested that to adsorb the final target, adding additional functionality through an additional adsorption procedure can give better results than trying adsorption using only functional groups.

Chapter 5. Improvement plan and future plan.

Nonwoven fabric, the basic material used in this experiment, is often used as a basic material in many fields due to its various advantages. Still, it is also one of the materials with clear limitations. As mentioned in reference [1], regardless of the type of materials used in the past, if the degree of graft has more than 150%, the durability of the material is limited, and the performance as an adsorbent often fails. However, with the advancement of science, there have been many changes in the way materials are made, and the microfiber is woven non-woven fabric used this time is one such material. The GMA microfiber nonwoven fabric manufactured by ENEOS is introduced with a GMA polymer brush without significant deformation up to about 500% of the graft. After introducing the polymer brush, a substantial change in weight and increased surface area were confirmed. Still, the appearance was maintained without major deformation even after adsorption of the ion exchanger and the primary adsorption target, and the performance as an adsorbent was maintained. In this experiment, non-woven fabric was used as the most popular adsorbent material, however, I think it will be valuable to experiment with other materials.

From Chapter 2, it was confirmed that acetone gas adsorption performance was better when metal ions were immobilized in an ion exchanger in the development of adsorption and detection materials for volatile organic compounds. In addition, the possibility of using it as a detection material was in mind because it has the characteristic of re-emitting the naturally bound acetone gas. However, since the adsorbent is not conductive, it has been confirmed that the possibility of its use as a detection material is low. Of course, there is still room for improvement in how the 4-picolylamine functional group is introduced. However, the optimal introduction condition of functional groups cannot solve the conductivity problem of the adsorbent. We believe that these issues can be facilitated by changing the base material of the adsorbent. Recent research in the field of materials is showing improved materials than previously existing materials through the interaction between nanomaterials and polymer materials. The material properties of the improved material can have better mechanical strength, solubility, electrical conductivity, optical properties, scratch resistance, thermal stability, and flame retardancy [2]. Although improved base materials are being developed for various purposes, electrical conductivity is recognized as a very important issue in the bio, battery industry,

and chemical sensor fields, and work to improve it is continuing [2-6]. We think that through the preparation of these materials and the improvement of functionality through the polymer brush, the problem of electrical conductivity, which was regrettable in this experiment, can be solved. In subsequent experiments, it is essential to determine the optimal conditions for introducing 4-picolylamine and confirm the selectivity in introducing metal ions. Similarly, since acetone was selected as the initial target for VOCs and its potential was confirmed with satisfactory performance, it is also necessary to confirm the adsorption properties of other VOCs. As a subsequent procedure, we plan first to check the adsorption properties of other VOCs. Adsorption of acetone, a ketone, has been confirmed, but adsorption of aldehyde groups has not been confirmed yet. Therefore, as a future goal, we plan to check the adsorption properties of formaldehyde, a representative VOCs. If the optimal functional group introduction conditions, metal ion immobilization selectivity, and VOCs adsorption selectivity are confirmed, the experiment will proceed based on a material with electrical conductivity rather than a microfiber nonwoven fabric. In this case, it seems that the manufactured material can also be expected to function as a sensor.

From Chapter 3, we could confirm the introduction of sialic acid through the amount of lectin adsorption. However, in the case of the functional group produced by the coupling reaction, it wasn't easy to quantitatively measure the amount introduced. In this experiment, we conducted this experiment under the assumption that IDA and EDC reacted 100% through the 72h coupling reaction of IDA-EDC. However, there is still no evidence that a 100% reaction was achieved. Therefore, first, it is necessary to check whether all changes in IDA-EDC have occurred through the coupling reaction. First, as EDC was introduced to better react with sialic acid, it is necessary to compare the amount of NANA introduced with IDA-EDC and IDA. After that, it is thought that the optimal coupling reaction time of IDA-EDC and accurate measurement of the introduction amount will be possible to some extent by changing the coupling reaction time of IDA-EDC and conducting the experiment. In addition, since WGA lectin was used as a substitute for the influenza virus in this experiment, the adsorption potential of the influenza virus is very high. Still, it is difficult to determine the exact adsorption level of the influenza virus. Therefore, it is necessary to try to adsorb the influenza virus directly. In addition to these points,

as mentioned above, it is seemed that possible to increase efficiency by using a more improved base material.

Experiments on granting functionality through polymer brushes are among the oldest research fields. However, in line with the development of science, its usage and application methods are also continuously developing. Our study is an example of how to use a polymer brush application, and we believe that it has provided an appropriate guide as to how to apply it. In addition to the methods presented by us, numerous applications are being proposed in the field of sensors [7-10] and virus adsorption [11-13].

References

1. Saito, K.; Fujiwara, K.; Sugo, T. Fundamentals of Radiation-Induced Graft Polymerization. In Innovative Polymeric Adsorbents. Springer: Singapore **2018**, pp. 1–22.
2. Umar Ali; Khairil Juhanni Bt. Abd Karima; Nor Aziah Buang. A Review of the Properties and Applications of Poly (Methyl Methacrylate) (PMMA). Polymers reviews **2015**, 55, 4, pp. 678-705
3. Huang Y; Kormakov S; He X; Gao X; Zheng X; Liu Y; Sun J; Wu D. Conductive Polymer Composites from Renewable Resources: An Overview of Preparation, Properties, and Applications. Polymers **2019**, 11, 2, 187
4. Oluwaseun Ayotunde Alo; Iyiola Olatunji Otunniyi. Electrical conductivity of polyethylene/epoxy/graphite/carbon black composites: synergy of blend immiscibility and hybrid filler. Polymer-Plastics Technology and Materials **2021**, 60, 18, pp. 2075-2088
5. Nguyen M.H.T; Sugartseren N; Kim B.Y; Jeon S.I; Cho Y-.Y; Kim T.W; Oh E.S. Enhancing the electrochemical performance of lithium ion battery anodes by poly(acrylonitrile–butyl acrylate)/graphene nanoplatelet composite binder. Journal of Applied Electrochemistry **2019**, 49, 4, pp. 389-398
6. Beladi-Mousavi SM; Sadaf S; Mahmood AM; Walder L. High Performance Poly(viologen)-Graphene Nanocomposite Battery Materials with Puff Paste Architecture. ACS nano **2017**, 11, 9, pp. 8730-8740
7. Kim S; Kwak DH; Choi I; Hwang J; Kwon B; Lee E; Ye J; Lim H; Cho K; Chung HJ; Lee WH. Enhanced Gas Sensing Properties of Graphene Transistor by Reduced Doping with Hydrophobic Polymer Brush as a Surface Modification Layer. ACS applied materials & interfaces **2020**, 12, 49, pp. 55493-55500
8. Fortin N; Klok HA. Glucose monitoring using a polymer brush modified polypropylene hollow fiber-based hydraulic flow sensor. ACS applied materials & interfaces **2015**, 7, 8, pp. 4631-4640.
9. Reimhult E; Höök F. Design of surface modifications for nanoscale sensor applications. Sensors **2015**, 15, 1, pp. 1635-1675.
10. Buzzacchera I; Vorobii M; Kostina NY; de Los Santos Pereira A; Riedel T; Bruns M; Ogieglo W; Möller M; Wilson CJ; Rodriguez-Emmenegger C.

Polymer Brush-Functionalized Chitosan Hydrogels as Antifouling Implant Coatings. Biomacromolecules **2017**, 18, 6, pp. 1983-1992.

11. Michala F; Alina P; Ivana V; Jakub K; N.Scott L; Petr Y; Jakub D; Vaclav H; Martin P; Hana M; Filip D; Jan S; Marketa V; Judita A; Monika S; Chao-ping T; An-Suei Y; Alexandr D; Hana V.L. Biosensor for rapid detection of SARS-CoV-2 in real-world samples. IEEE SENSORS **2021**, pp. 1-4.
12. Delaveris CS; Webster ER; Banik SM; Boxer SG; Bertozzi CR. Membrane-tethered mucin-like polypeptides sterically inhibit binding and slow fusion kinetics of influenza A virus. Proceedings of the National Academy of Sciences of the United States of America **2020**, 117, 23, pp. 12643-12650.
13. Chen Z; Liang X; Yang R; Yang M; Tan T; Cao H. Construction of Ordered Multienzyme Systems using Multifunctional Polymer Brush-Grafted Magnetic Nanoparticles as Scaffolds. Colloids and Surface A **2019**, 583, 123920